[redacted]

Copy 44
RM SL58G28

NACA

RESEARCH MEMORANDUM

for the

U. S. Air Force

LONGITUDINAL AND LATERAL STABILITY AND CONTROL CHARACTERISTICS AND VERTICAL-TAIL-LOAD MEASUREMENTS FOR A 0.03-SCALE MODEL OF THE AVRO CF-105 AIRPLANE AT MACH NUMBERS OF 1.60, 1.80, AND 2.00

By H. Norman Silvers, Roger H. Fournier, and
Jane S. Wills

Langley Aeronautical Laboratory
Langley Field, Va.

NATIONAL ADVISORY COMMITTEE
FOR AERONAUTICS

WASHINGTON

[redacted]

NATIONAL ADVISORY COMMITTEE FOR AERONAUTICS

RESEARCH MEMORANDUM

for the

U. S. Air Force

LONGITUDINAL AND LATERAL STABILITY AND CONTROL CHARACTERISTICS AND VERTICAL-TAIL-LOAD MEASUREMENTS FOR A 0.03-SCALE MODEL OF THE AVRO CF-105 AIRPLANE AT MACH NUMBERS OF 1.60, 1.80, AND 2.00*

By H. Norman Silvers, Roger H. Fournier, and
Jane S. Wills

SUMMARY

An investigation has been made in the Langley Unitary Plan wind tunnel at Mach numbers of 1.60, 1.80, and 2.00 to determine the aerodynamic characteristics of a 0.03-scale model of the Avro CF-105 airplane. The investigation included the determination of the static longitudinal and lateral stability, the control and the hinge-moment characteristics of the elevator, rudder, and aileron, as well as the vertical-tail-load characteristics.

Although the data are presented without analysis, a limited inspection of the longitudinal control results indicates a loss in maximum lift-drag ratio due to trimming of about 1.8 because of the large static margin. A reduction in static margin would be expected to improve the trim lift-drag ratio but would also reduce the directional stability. With the existing static margin, the configuration is directionally unstable at angles of attack above about 6° or 8°.

INTRODUCTION

At the request of the United States Air Force, an investigation of the aerodynamic characteristics of a 0.03-scale model of the Avro CF-105 airplane has been made in the Langley Unitary Plan wind tunnel.

*Title, Confidential.

The airplane is a twin-jet-propelled tailless fighter design having a cambered 61.4° delta wing with a thickness ratio of 3.5 percent. The inner wing leading edge is drooped 8°, and the outer wing leading edge is extended 10 percent of the wing chord and drooped 4°. A leading-edge notch is located between the inboard and outboard leading-edge sections. Inlets are located on the sides of the fuselage forward of the wing leading edge. A swept vertical tail is used to provide directional stability. Longitudinal, lateral, and directional control are provided by conventional flap-type surfaces.

An investigation of this model has been made at a Mach number of 1.41 in the Langley 4- by 4-foot supersonic pressure tunnel and the results are presented in reference 1. The purpose of the present paper is to present the results of an investigation of the 0.03-scale model of the Avro CF-105 at Mach numbers of 1.60, 1.80, and 2.00 in the Langley Unitary Plan wind tunnel. In addition to six-component force and moment results for the model, three-component force and moment results were obtained on the vertical tail. Elevator, rudder, and aileron hinge moments were also measured. Total pressures were measured at two spanwise stations on the vertical tail near the tip.

The results of this investigation are presented without analysis.

COEFFICIENTS AND SYMBOLS

The systems of axes used are shown in figure 1. All data are referred to the body axis system except for the lift and drag coefficients which are presented about the stability axis system. Moment coefficients are referred to a point in the wing chord plane which is located at the 28-percent chord of the wing mean aerodynamic chord.

B_V panel bending moment, in-lb

b span, in.

$\bar{c}$ mean aerodynamic chord, in.

C_L lift coefficient, $\frac{\text{Lift}}{qS}$

C_D drag coefficient, $\frac{\text{Drag}}{qS}$

$C_{D,i}$ internal drag coefficient, $\frac{\text{Internal drag}}{qS}$

[redacted]

$C_{D,b}$ base drag coefficient, $\frac{\text{Base drag}}{qS}$

C_m pitching-moment coefficient, $\frac{M_Y}{qS\bar{c}}$

C_l rolling-moment coefficient, $\frac{M_X}{qSb}$

$C_{l_{\delta_a}}$ aileron-control effectiveness parameter, $\frac{\partial C_l}{\partial \delta_a}$

C_n yawing-moment coefficient, $\frac{M_Z}{qSb}$

$C_{n_{\delta_r}}$ rudder-control effectiveness parameter, $\frac{\partial C_n}{\partial \delta_r}$

C_Y side-force coefficient, $\frac{Y}{qS}$

$C_{h,e}$ elevator hinge-moment coefficient, $\frac{H_e}{qS_e\bar{c}_e}$

$C_{h,r}$ rudder hinge-moment coefficient, $\frac{H_r}{qS_r\bar{c}_r}$

$C_{h,a}$ aileron hinge-moment coefficient, $\frac{H_a}{qS_a\bar{c}_a}$

C_p pressure coefficient, $\frac{p_l - p_\infty}{q}$

$C_{b,v}$ root-bending-moment coefficient of vertical tail about vertical-tail root chord (0.96 in. above fuselage reference line), $\frac{B_v}{qS_v b_v}$

$C_{n,v}$ yawing-moment coefficient of vertical tail about a vertical axis through the leading-edge point of the vertical-tail root chord, $\frac{n_v}{qS_v\bar{c}_v}$

$C_{Y,v}$ side-force coefficient of vertical tail, based on wing area, $\frac{Y_v}{qS}$

$C_{m_{C_L}}$ pitching-moment-curve slope $\left(C_L = 0\right)$, $\frac{\partial C_m}{\partial C_L}$

C_{L_α} lift-curve slope $\left(\alpha = 0^\circ\right)$, $\frac{\partial C_L}{\partial \alpha}$

C_{l_β} effective-dihedral parameter $\left(\beta = 0^\circ\right)$, $\frac{\partial C_l}{\partial \beta}$

C_{n_β} directional-stability parameter $\left(\beta = 0^\circ\right)$, $\frac{\partial C_n}{\partial \beta}$

C_{Y_β} side-force parameter $\left(\beta = 0^\circ\right)$, $\frac{\partial C_Y}{\partial \beta}$

H hinge moment, in-lb

M free-stream Mach number

M_X moment about X-axis, in-lb

M_Y moment about Y-axis, in-lb

M_Z moment about Z-axis, in-lb

n_v panel yawing moment, in-lb

p_l local total pressure

p_∞ free-stream total pressure

q free-stream dynamic pressure, lb/sq ft

S wing area including body intercept, sq ft

Y force along Y-axis, lb

Y_v panel side force, lb

α angle of attack referred to body reference line, deg

β angle of sideslip referred to model plane of symmetry, deg

δ_e elevator deflection perpendicular to hinge line, deg

δ_r rudder deflection perpendicular to hinge line, deg

δ_a aileron deflection perpendicular to hinge line, deg

δ_f deflection of wing nose flap, deg

Subscripts:

a aileron

e elevator

0 denotes value of parameter at zero lift coefficient

r rudder

v vertical-tail panel

APPARATUS

Wind Tunnel

The tests were conducted in the low Mach number test section of the Langley Unitary Plan wind tunnel, which is a variable pressure, return-flow type of tunnel. The test section is 4 feet square and approximately 7 feet in length. The nozzle leading to the test section is of the asymmetric sliding-block type, which permits a continuous variation of Mach number from approximately 1.56 to 2.80.

Support System

Forces and moments for the model were measured by means of a six-component internal strain-gage balance. This balance was attached by means of a sting to the tunnel central support system. Included in the model support system was a remotely operated adjustable angle coupling that permitted tests to be made at variable angles of attack concurrently with variations in angle of sideslip.

Model

Details of the model are shown in figure 2, and its geometric characteristics are given in table I. Photographs of the model are presented in figure 3.

The model had a modified delta wing with a leading-edge sweep of 61.4°, and aspect ratio of 2.04, a taper ratio of 0.089, and was composed of 3.5-percent-thick cambered airfoil sections. The outer wing leading edge was extended 10 percent of the chord and drooped 4°. The inner wing leading edge was drooped 8°. A leading-edge notch was located between the inner and outer portion of the wing leading-edge sections at about the midsemispan point.

The fuselage of the model had a conical nose with an included angle of 30°. The external lines of the model fuselage were altered slightly from those of the airplane in that a portion of the afterbody on the underside of the fuselage was enlarged to accommodate the sting support.

The model was equipped with inlets on the fuselage sides that were ducted to a single exit around the sting at the base of the model. For most of the investigation, the inlets were open to permit air flow through the model. In addition, for one test, faired plugs (see fig. 2(a)) were used to close the inlets so that some results might be obtained without flow through the ducts. The model was equipped with a rudder, two elevators, and a single aileron on the right wing. These controls were manually adjustable and were equipped with strain-gage beams. The vertical tail was equipped with a three-component strain-gage balance designed to to measure the side force on the tail, the root bending moment of the tail, and the tail yawing moment.

TESTS

Tests were made through an angle-of-attack range from approximately -4° to 18° at about -4°, 0°, and 4° angles of sideslip. To obtain the lateral stability parameters throughout the angle-of-attack range, the incremental differences were taken between the lateral coefficient results obtained at sideslip angles of -4° and 4° and divided by the increment in the angle of sideslip. At nominal angles of attack of 1.5°, 6°, 10°, and 17°, tests were made from angles of sideslip of -4° to 18° to illustrate the linearity of the lateral characteristics with change in sideslip angle.

Tests were made over an angle-of-attack range from approximately -4° to 18° with various deflections of each control surface (elevator, rudder,

and aileron) to determine control effectiveness. The right aileron only was deflected for the aileron effectiveness runs.

The test conditions are listed in the following table:

Mach number	Stagnation pressure, psia	Dynamic pressure, psf	Reynolds number
1.60	11.7	710	2.82×10^6
1.80	11.7	665	2.65
2.00	11.7	602	2.44

Tests were conducted at a stagnation temperature of 125° F. Reynolds number is based on the mean aerodynamic chord of the wing.

CORRECTIONS AND ACCURACY

No corrections have been applied to the data for stream angularity or buoyancy. The longitudinal pressure gradients are small and produce negligible effects on the model. Preliminary indications from the tunnel calibration are that some flow angularity exists. The flow angularity is in a direction to increase the angles of attack presented and is of the order of 0.3°, 0.5°, and 0.7° at the test Mach numbers of 1.60, 1.80, and 2.00, respectively. The changes in the model angles of attack resulting from flow angularity will have an effect on the drag coefficients presented. The effects are of most significance at the smaller angles of attack when the drag coefficients based on corrected angles will be larger for positive angles and smaller for negative angles. This change in the model drag coefficients is not included in the quoted accuracy of drag in the listing of accuracy that follows.

The maximum deviation of local Mach number in the portion of the tunnel occupied by the model was ±0.015 from the average values listed in the preceding section.

The angles of attack and sideslip have been corrected for the deflection of the support system under load. The angles of the control surfaces (elevator, rudder, and aileron) have not been corrected for deflection under load. The control-surface angles presented are the static values measured during pretest calibration.

The internal drag coefficients were determined for the model with undeflected controls by use of a ring choke at the exit of the duct. The pressure differential between the measured total pressure ahead of the normal shock at the choke and free-stream total pressure was used to calculate the internal drag coefficient. The pressures on the annulus of the base of the fuselage were measured with the inlet open and with the inlet faired. With the inlet faired, the annulus area is equal to the total base area. The pressures in the chamber housing the strain-gage balance were also measured for both the open and faired conditions of the inlet. However, it was found that the chamber was not pressure sealed from the ducts, so that with the inlets open an unreliable value of chamber pressure was measured. Hence, no chamber drag coefficients are presented for the model with the inlets open. The measured chamber pressures have been combined with the measured base pressures for the model with the faired inlets and are included in the base drag coefficients presented for the model with faired inlets. The values of base drag coefficients presented refer the measured pressures to the level of free-stream static pressure at the base of the model. The model drag ccefficients presented are not corrected for either the internal drag or the base drag. A correction of the drag coefficients can be made for the faired inlet model by a subtraction of the base drag coefficients from the presented model drag coefficients. It is not possible, however, to obtain net external drag coefficients for the open-inlet model because the chamber pressure drag could not be evaluated.

The estimated accuracy of the individual measured coefficients of forces and moments and angles is within the following limits:

C_L	±0.008
C_D	±0.0013
C_m	±0.003
C_l	±0.0008
C_n	±0.0008
C_Y	±0.0038
$C_{h,e}$	±0.0072
$C_{h,r}$	±0.0026
$C_{h,a}$	±0.0066
$C_{b,v}$	±0.0013
$C_{n,v}$	±0.0016
$C_{Y,v}$	±0.0010
α, deg	±0.1
β, deg	±0.1
δ_e, deg	±0.3
δ_r, deg	±0.3
δ_a, deg	±0.4

It should be remembered that flow angularity exists in the test section. The results presented are not corrected for this condition. The accuracy values quoted for angle of attack represent the positioning accuracy of the model in the test section and do not include test-section flow angularity.

RESULTS

The results of this investigation are presented in the following figures:

	Figure
Base and internal drag coefficients, inlets open	4
Base drag coefficients, inlets faired	5
Schlieren photographs of 0.03-scale model of Avro CF-105 airplane tested in Unitary Plan wind tunnel	6
Effect of elevator deflection on longitudinal aerodynamic characteristics of test model; $\delta_r = \delta_a = 0^\circ$	7
Effect of deflection of outboard wing-leading-edge flap on longitudinal aerodynamic characteristics of test model; $\delta_e = \delta_r = \delta_a = 0^\circ$	8
Effect of aileron deflection on longitudinal aerodynamic characteristics of test model; $\delta_e = -9.8^\circ$ and $\delta_r = 0^\circ$	9
Effect of inlet fairing on longitudinal aerodynamic characteristics of test model; $\delta_e = \delta_r = \delta_a = 0^\circ$	10
Variation of lateral stability characteristics of test model with angle of sideslip; $\delta_e = \delta_a = 0^\circ$	11
Variation of lateral stability characteristics of test model with angle of attack; $\delta_e = \delta_r = \delta_a = 0^\circ$	12
Variation of lateral stability characteristics of test model, vertical tail off, with angle of attack; $\delta_e = \delta_a = 0^\circ$	13
Effect of rudder deflection on lateral aerodynamic characterisitcs of test model; $\delta_e = \delta_a = 0^\circ$	14
Effect of aileron and elevator deflection on lateral aerodynamic characteristics of test model; $\delta_r = 0^\circ$	15
Variation of elevator hinge-moment coefficient with angle of attack	16
Variation of elevator hinge-moment coefficient with lift coefficient	17
Variation of rudder hinge-moment coefficient with angle of attack	18
Variation of aileron hinge-moment coefficient with angle of attack	19

Figure

Variation of pressure coefficient with angle of attack for probes at tip of vertical tail 20
Variation of vertical tail loads of test model with angle of attack; $\delta_e = \delta_r = \delta_a = 0^\circ$ 21
Variation of aerodynamic characteristics of vertical-tail loads with angle of sideslip. 22
Effect of rudder deflection on aerodynamic characteristics of vertical-tail loads 23
Summary of longitudinal stability characteristics of test model 24
Summary of longitudinal control effectiveness of test model 25
Summary of aileron control characteristics of test model 26
Summary of rudder control characteristics of test model 27
Summary of lateral stability parameters with variation of angle of attack of test model 28
Summary of lateral stability parameters with variation of Mach number of test model 29

CONCLUDING REMARKS

Although the drag coefficients of the model are not corrected for either internal and base pressure effects or angularity of the airstream, a valid indication of the increment in drag due to trimming the model can be obtained from the results. In terms of the maximum lift-drag ratio, it is estimated that trimming the model reduces the maximum lift-drag ratio about 1.8 from that for the untrimmed model with undeflected controls. This is in part due to the large static margin employed.

A reduced static margin would of course reduce the loss in lift-drag ratio due to trimming, but it would also reduce the directional stability of the configuration. With the existing static margin, the model becomes directionally unstable at angles of attack greater than 6° or 8° which is well within the operational angle-of-attack range of this configuration at supersonic speeds.

Langley Aeronautical Laboratory,
National Advisory Committee for Aeronautics,
Langley Field, Va., July 15, 1958.

REFERENCE

1. Spearman, M. Leroy, Robinson, Ross B., and Driver Cornelius: Longitudinal and Lateral Stability, Control Characteristics, and Vertical-Tail Load Measurements for 0.03-Scale Model of the Avro CF-105 Airplane at Mach Number 1.41. NACA RM SL56H27, U. S. Air Force, 1956.

TABLE I.- GEOMETRIC CHARACTERISTICS OF MODEL

Wing:	
Area, sq ft	1.1025
Span (projected), in.	18.000
Mean geometric chord, in.	10.878
Sweep of quarter-chord line, deg	55
Sweep of leading edge, deg	61.4
Aspect ratio	2.04
Taper ratio	0.089
Dihedral, deg	-4
Incidence, deg	0
Thickness ratio, percent	3.5
Vertical tail (theoretical, with root station 0.96 inch above fuselage reference line):	
Area, sq ft	0.143
Span, in.	4.635
Mean geometric chord, in.	4.872
Sweep of leading edge, deg	59.3
Aspect ratio (panel)	1.04
Taper ratio	0.298
Elevator:	
Area, sq ft	0.048
Span, in.	3.665
Mean geometric chord, in.	1.89
Rudder:	
Area, sq ft	0.0343
Span, in.	3.615
Mean geometric chord, in.	1.422
Aileron:	
Area, sq ft	0.030
Span, in.	3.605
Mean geometric chord, in.	1.261

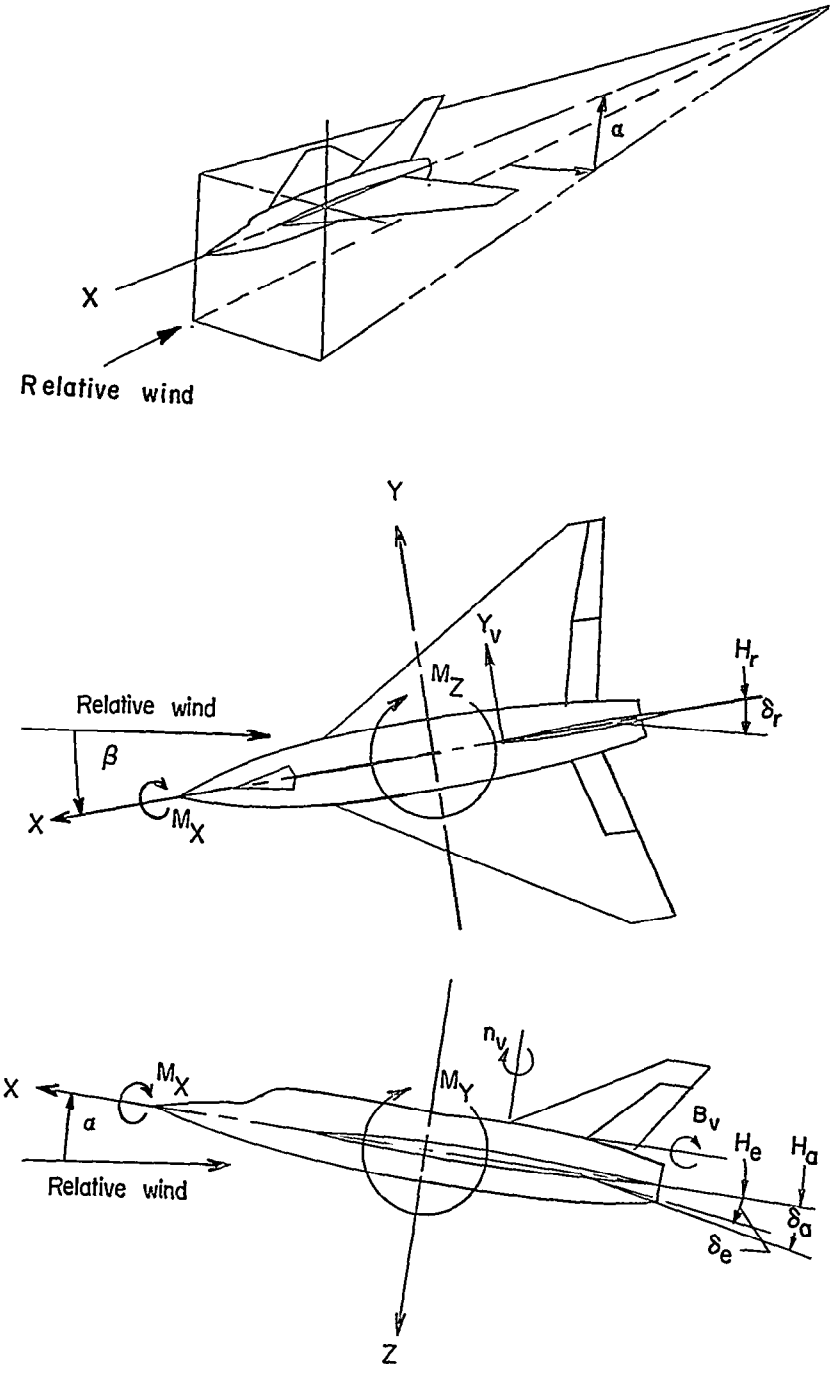

(a) Body axes.

Figure 1.- Axis systems. Arrows indicate positive directions.

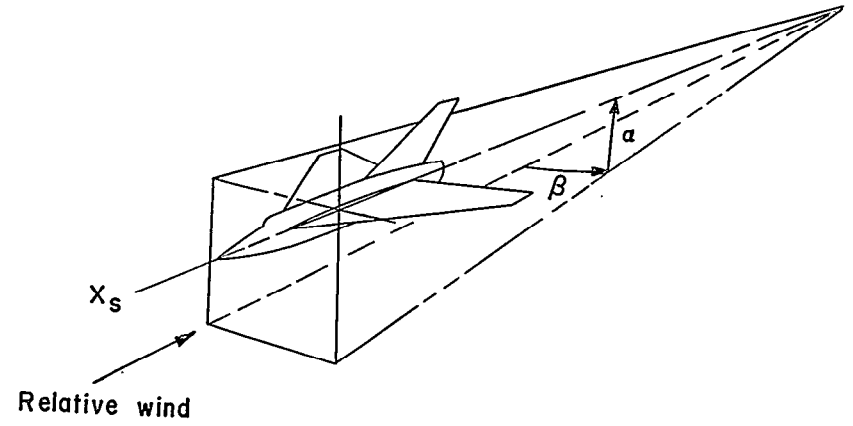

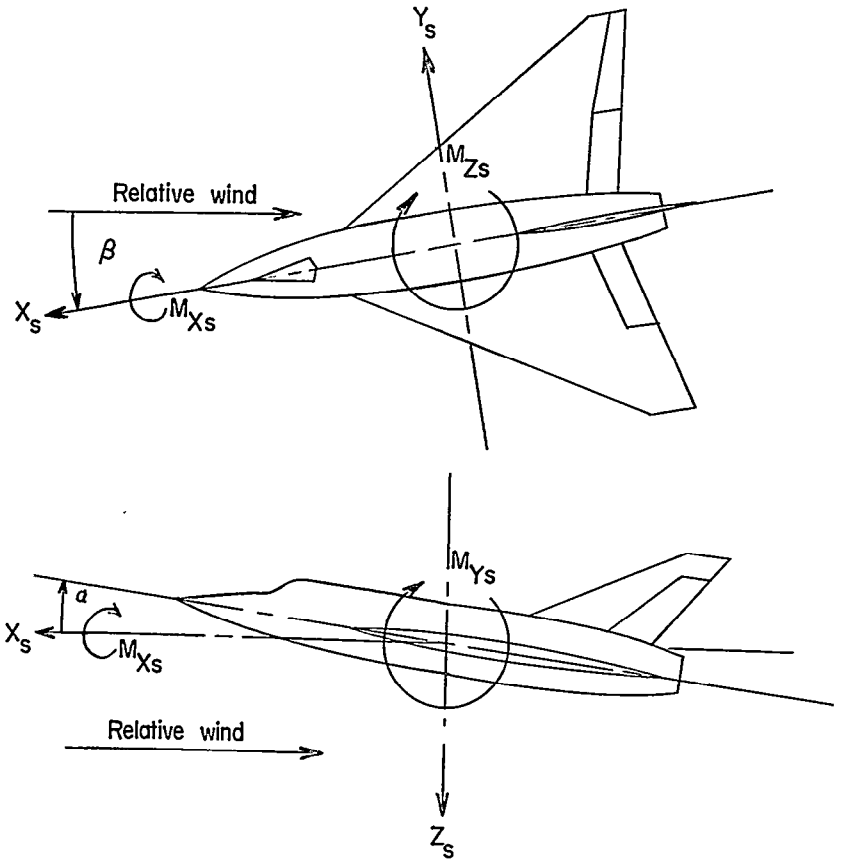

(b) Stability axes.

Figure 1.- Concluded.

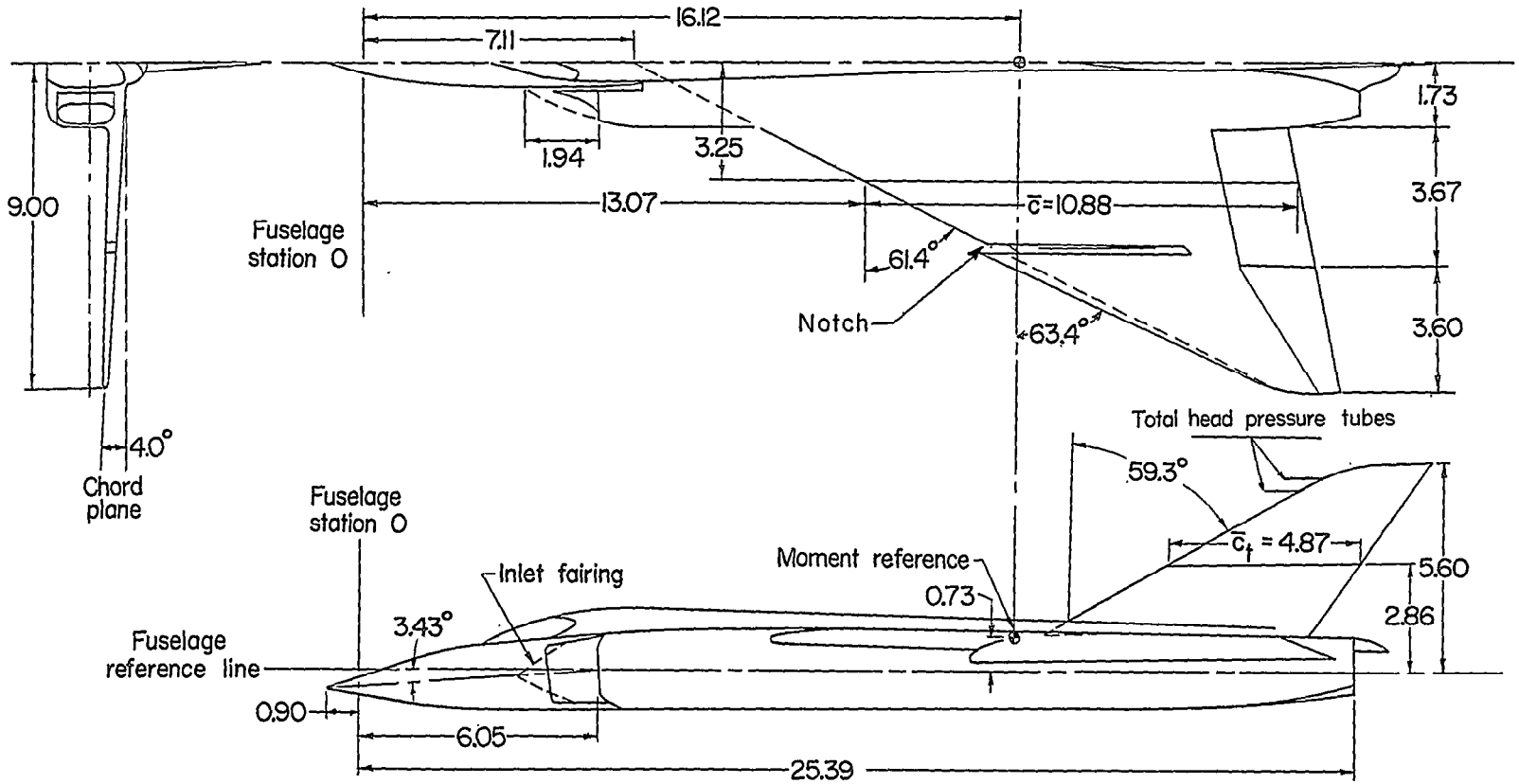

(a) Three-view drawing of model.

Figure 2.- Details of model. All dimensions in inches unless otherwise noted.

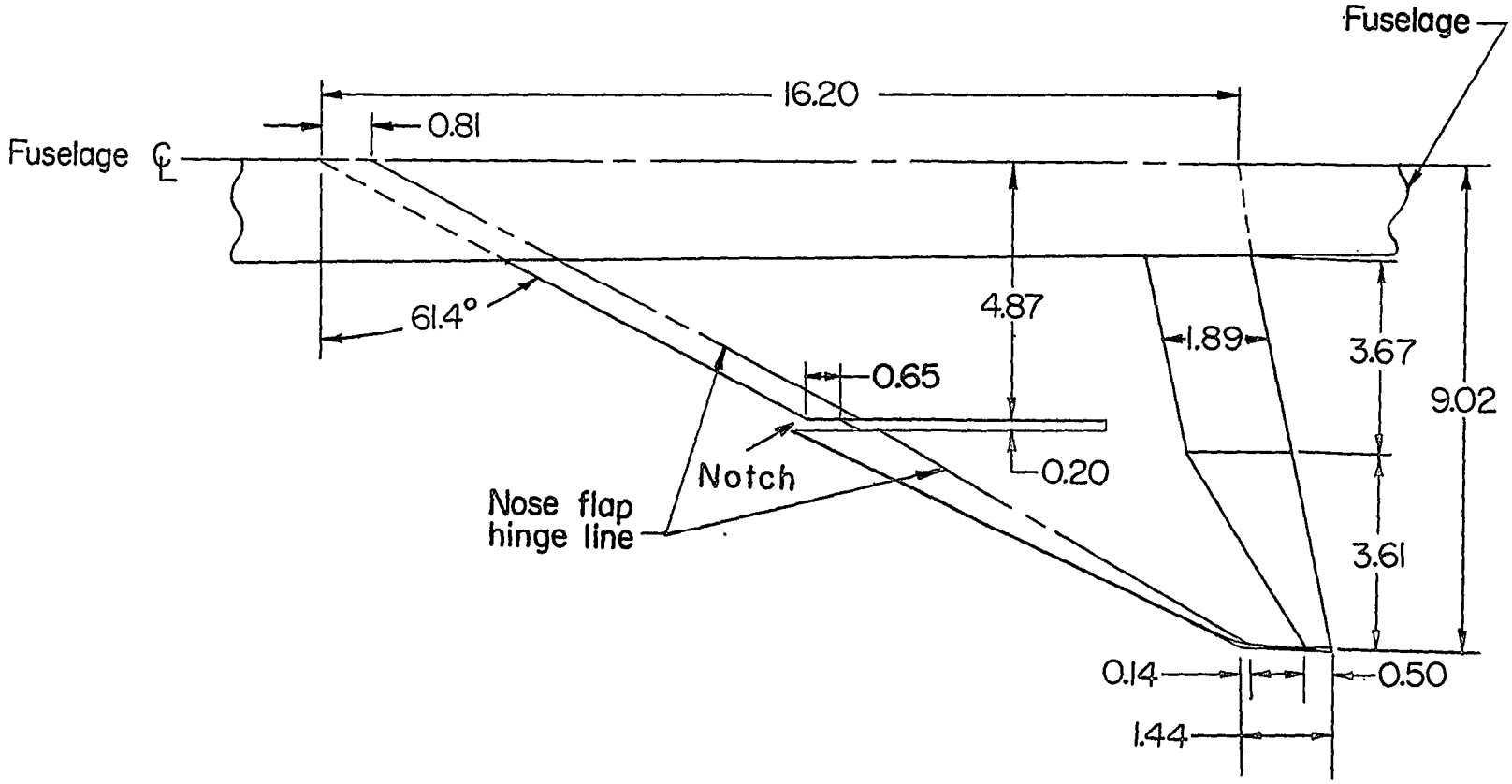

(b) Details of wing.

Figure 2.- Continued.

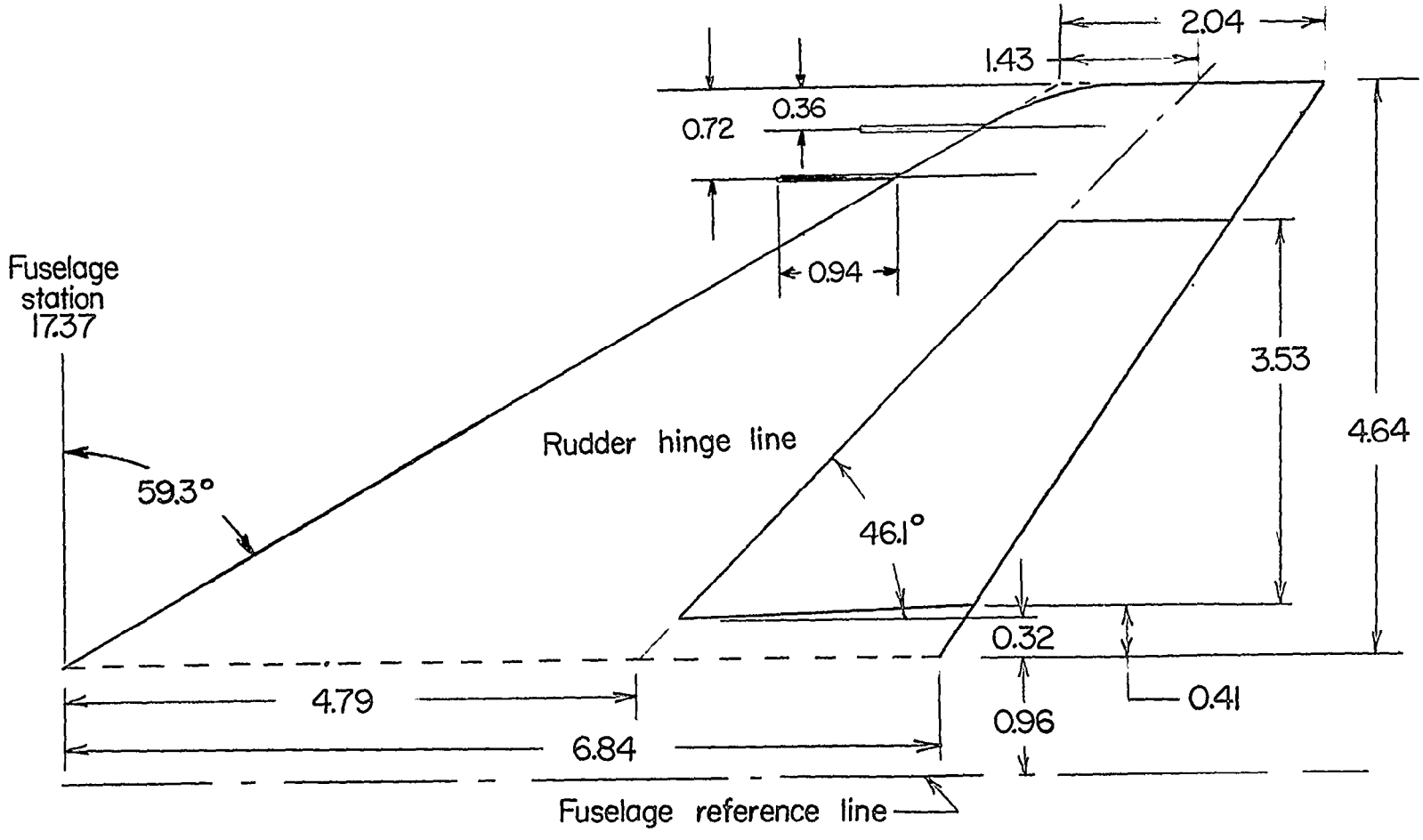

(c) Details of vertical tail.

Figure 2.- Concluded.

(a) Side view. L-95126

Figure 3.- Photographs of a 0.03-scale model of the Avro CF-105 airplane.

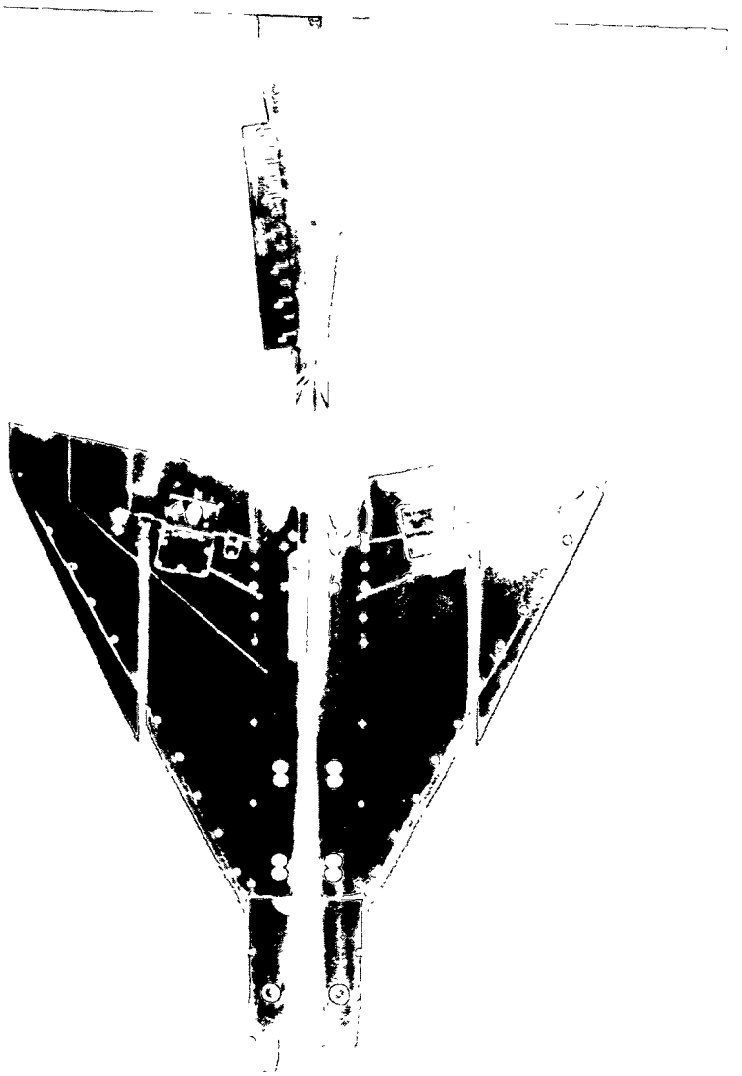

L-95127

(b) Top view.

Figure 3.- Continued.

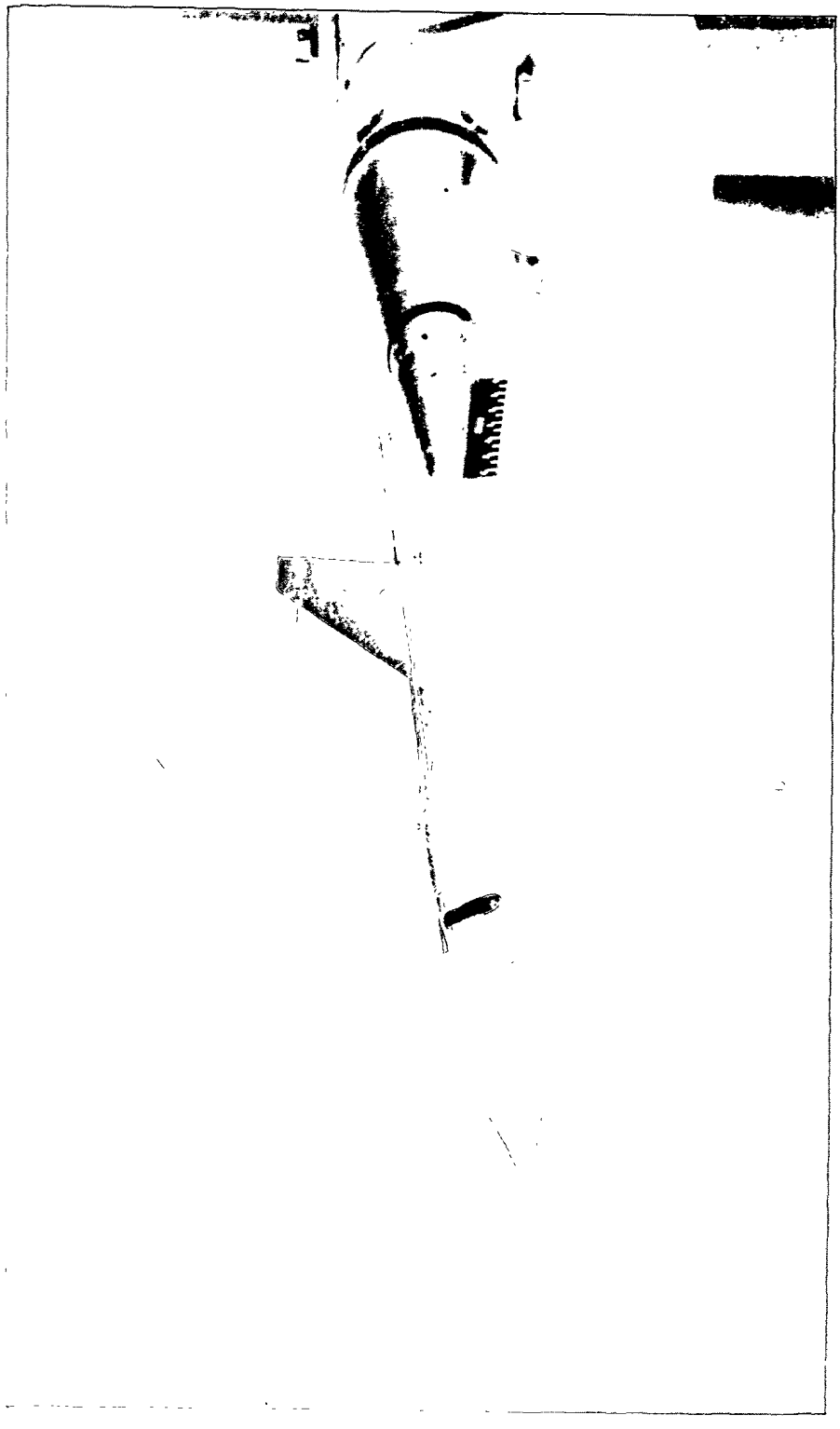

L-95128

(c) Three-quarter front view.

Figure 3.- Continued.

L-95129

(d) Bottom view.

Figure 3.- Concluded.

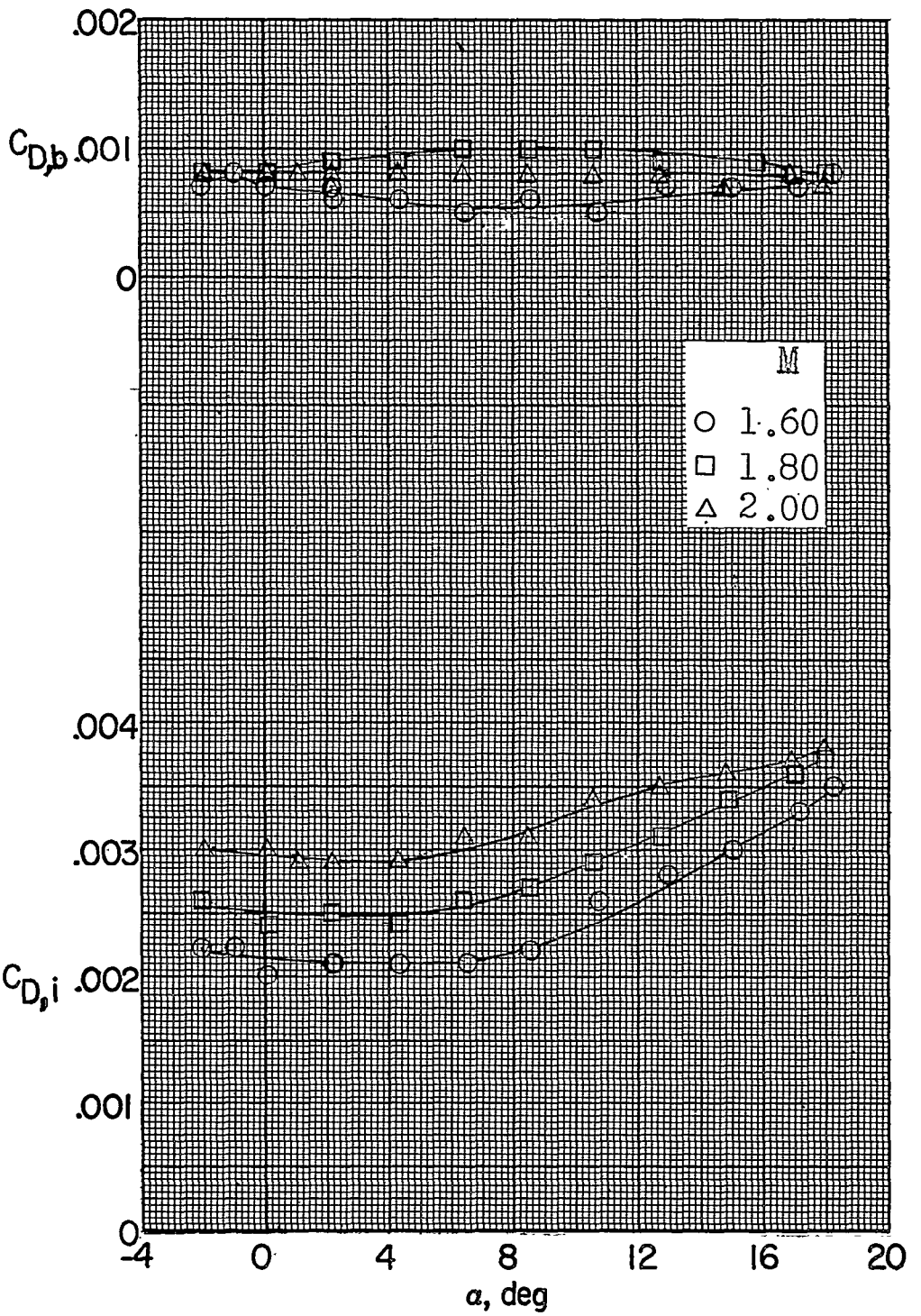

Figure 4.- Variation of base drag coefficient and internal drag coefficient with angle of attack with the inlets open.

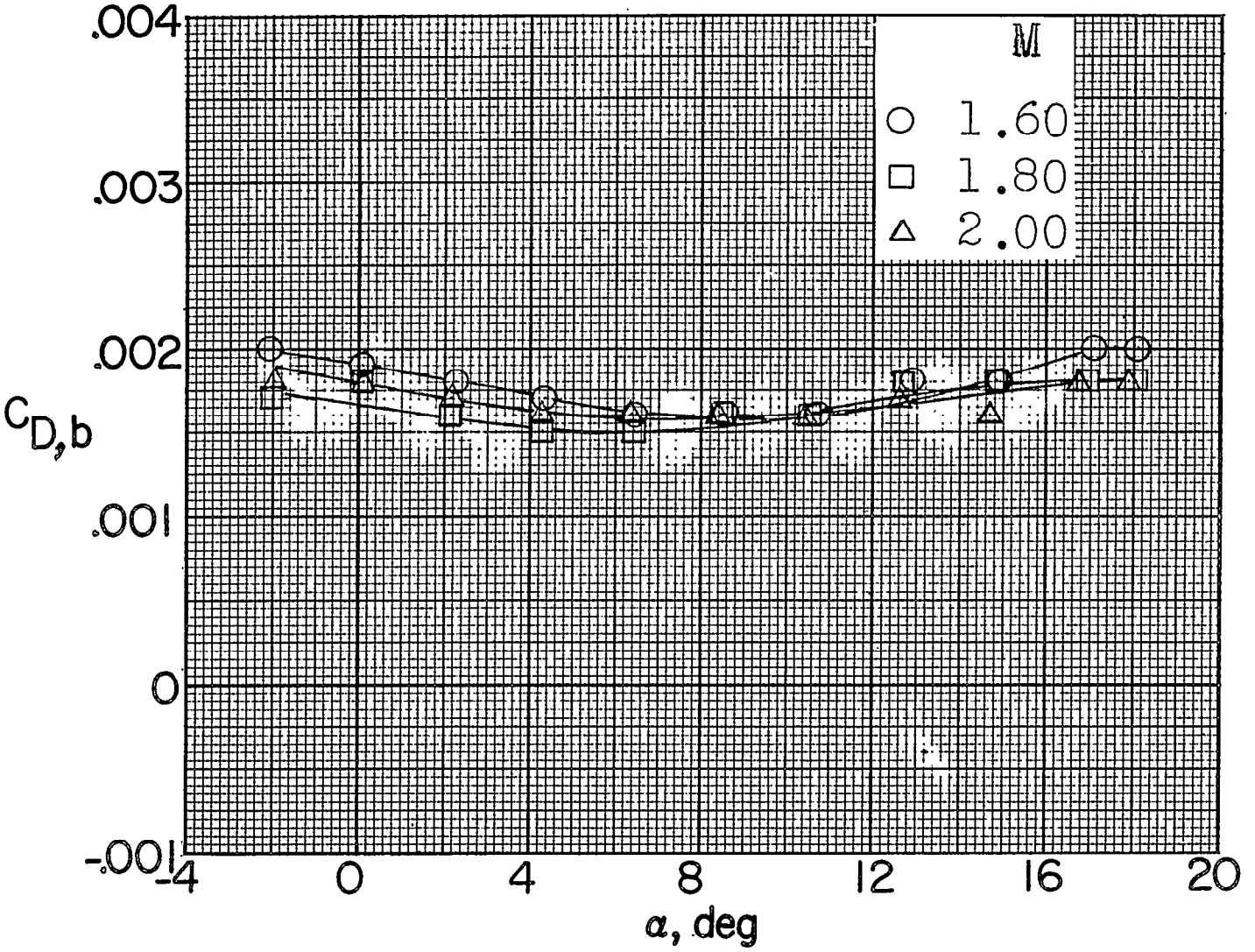

Figure 5.- Variation of base drag coefficient with angle of attack with the inlets faired.

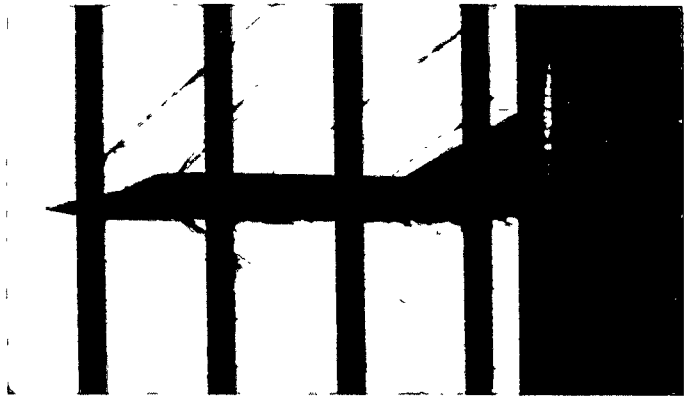

$\alpha = 0.1°$

$\alpha = 4.3°$

$\alpha = 12.9°$

$\alpha = 15.0°$

(a) M = 1.60.

L-58-2513

Figure 6.- Schlieren photographs of a 0.003-scale model of the Avro CF-105 airplane.

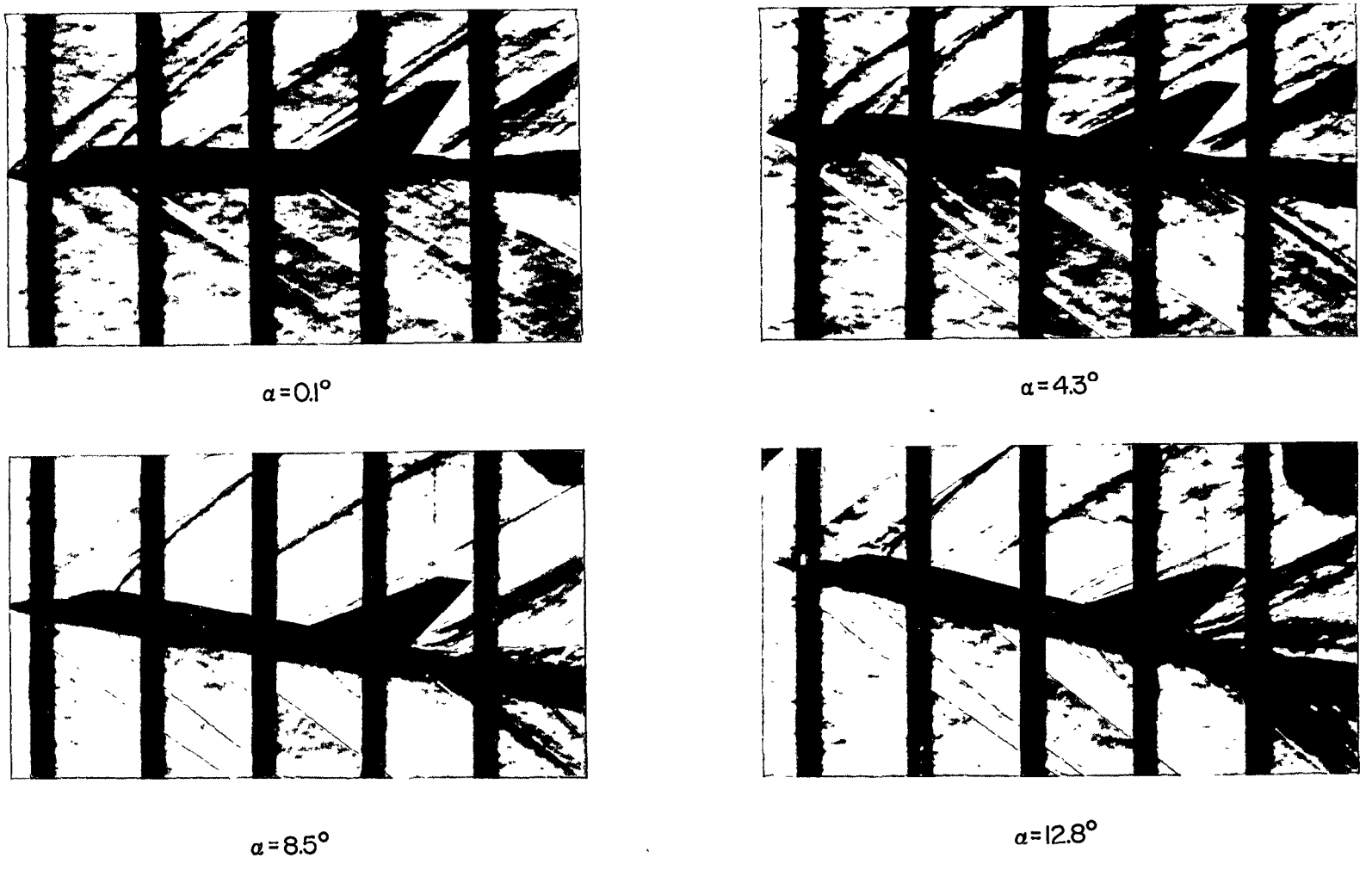

(b) M = 1.80. L-58-2514

Figure 6.- Continued.

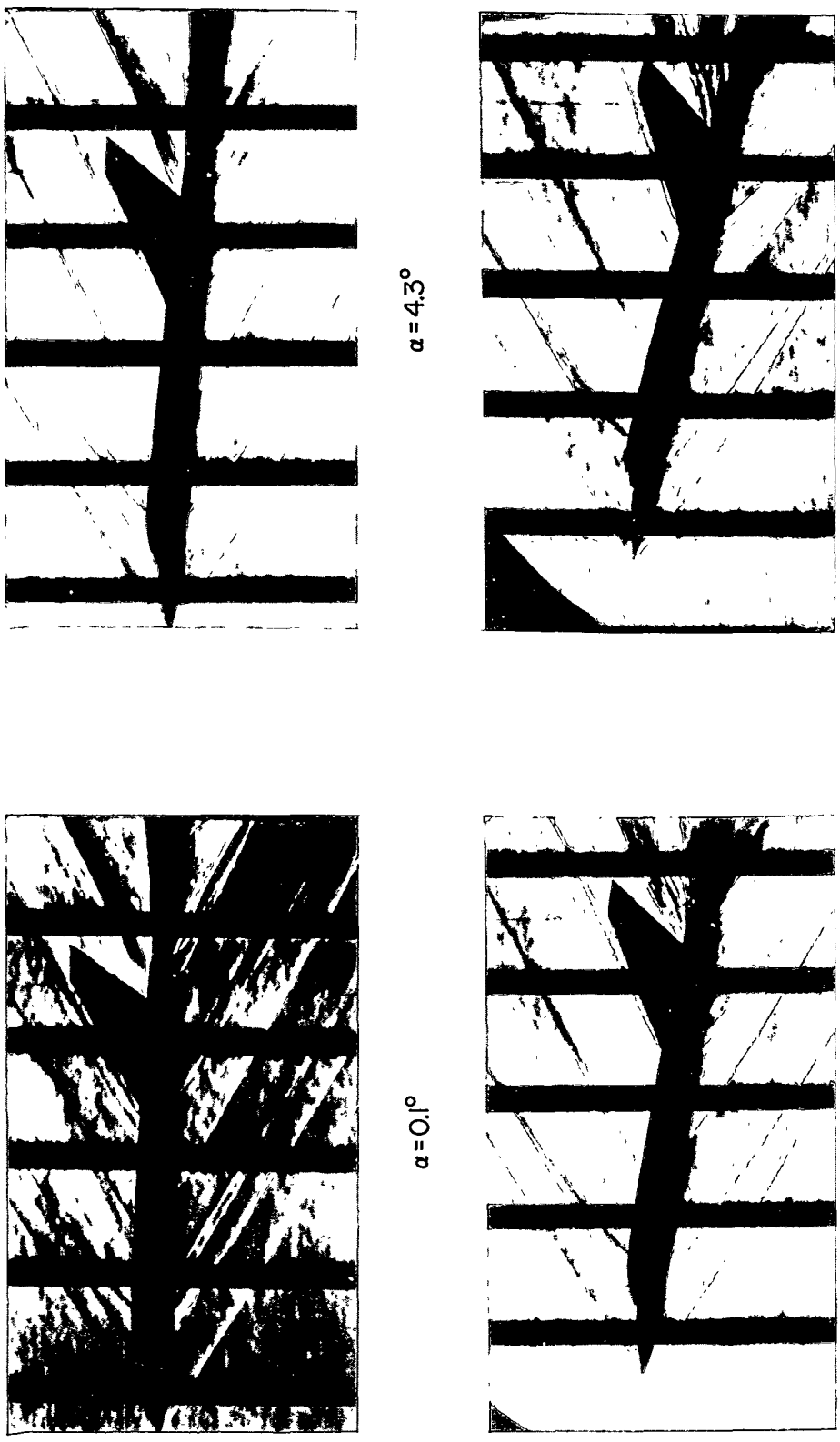

(c) M = 2.00.

Figure 6.- Concluded.

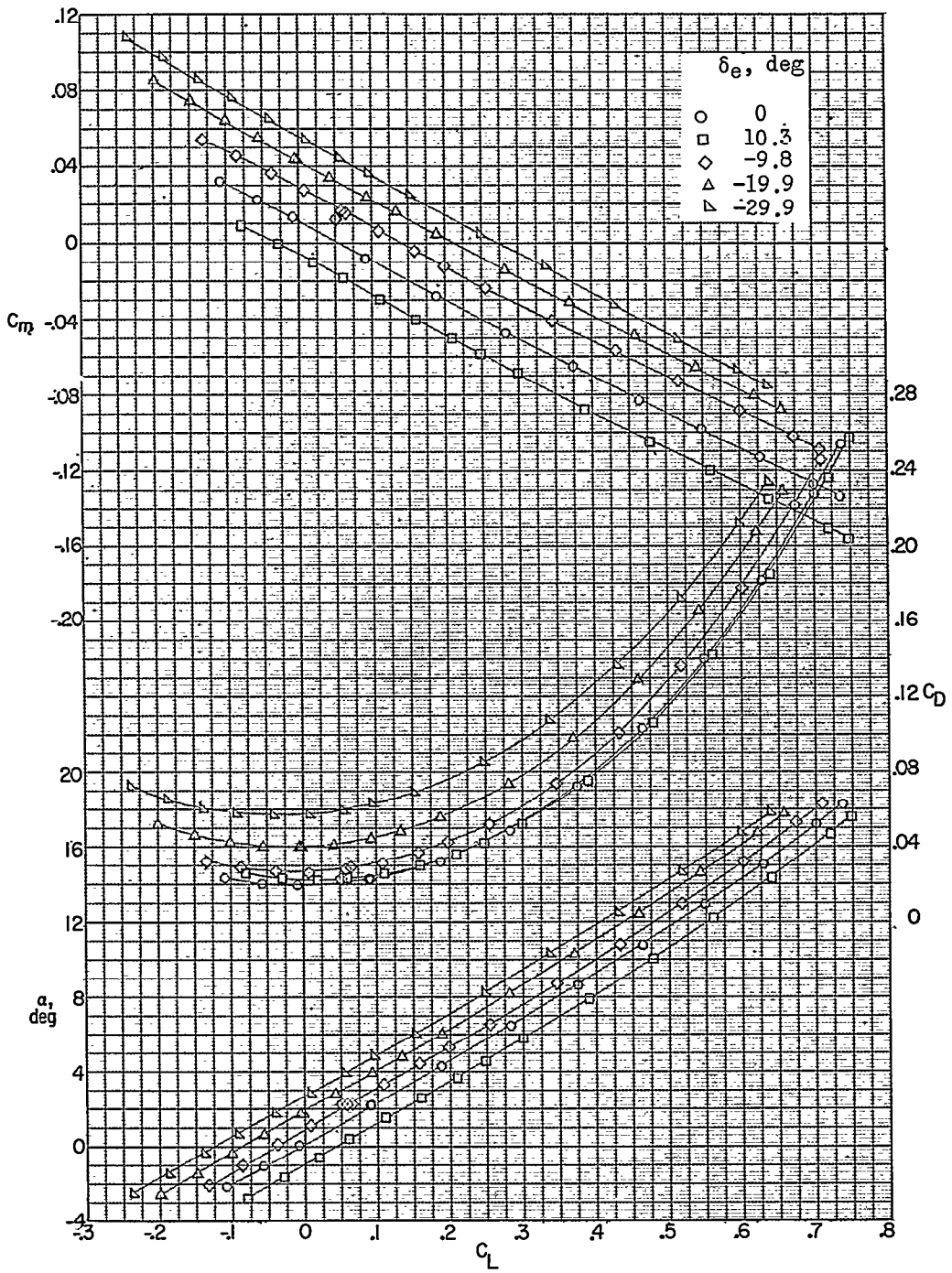

(a) M = 1.60.

Figure 7.- Effect of elevator deflection on the longitudinal aerodynamic characteristics of the test model; $\delta_r = \delta_a = 0^o$.

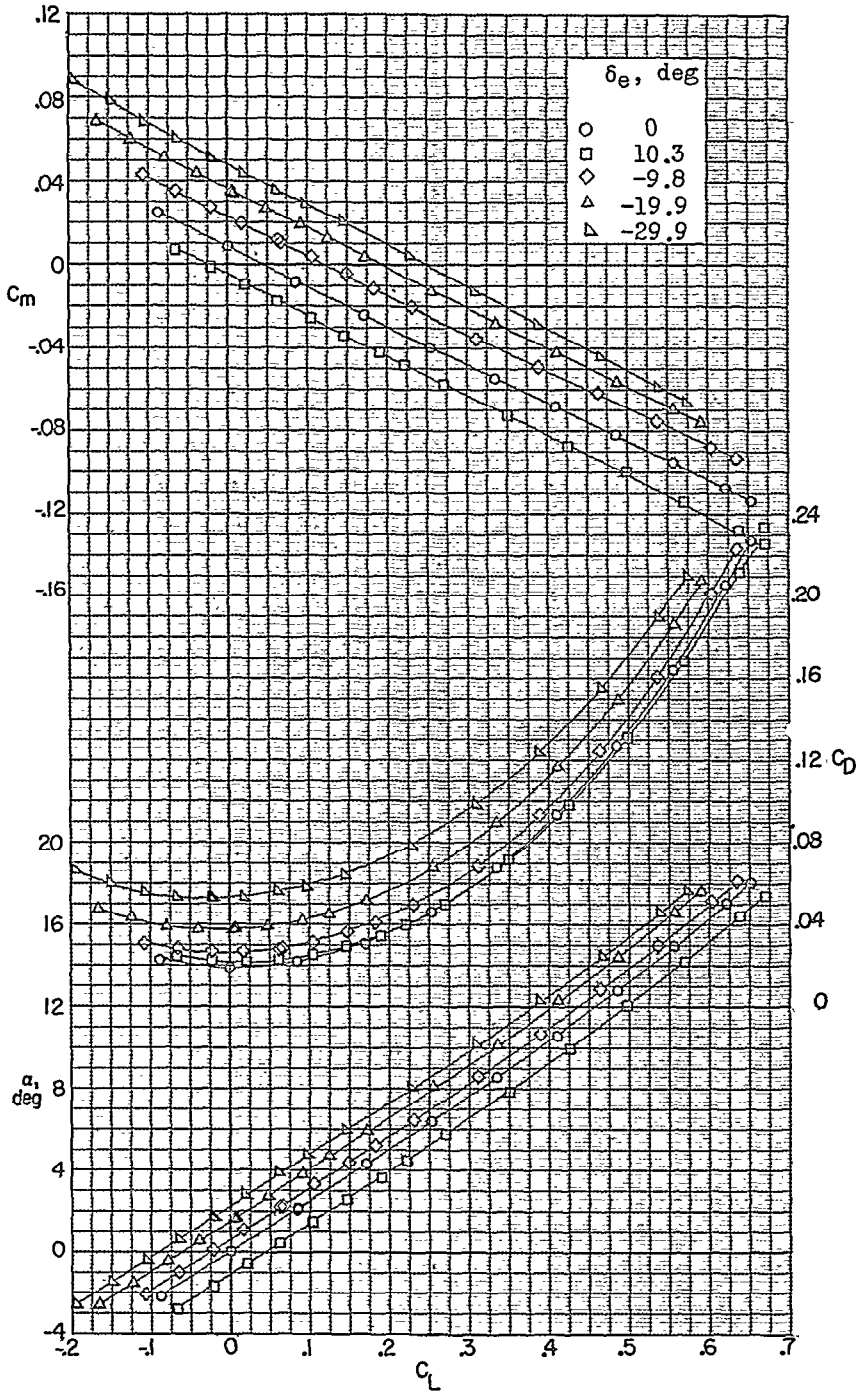

(b) M = 1.80.

Figure 7.- Continued.

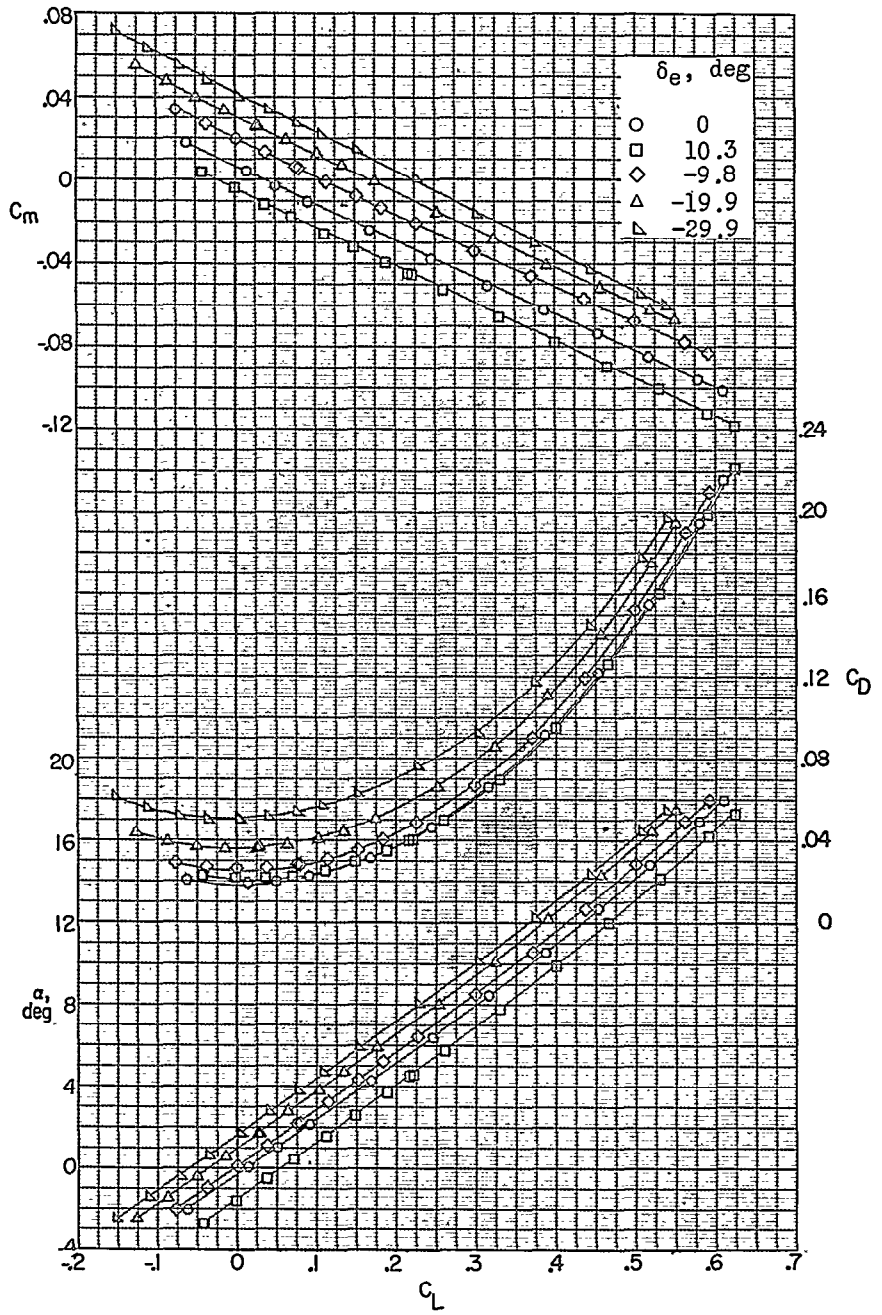

(c) M = 2.00.

Figure 7.- Concluded.

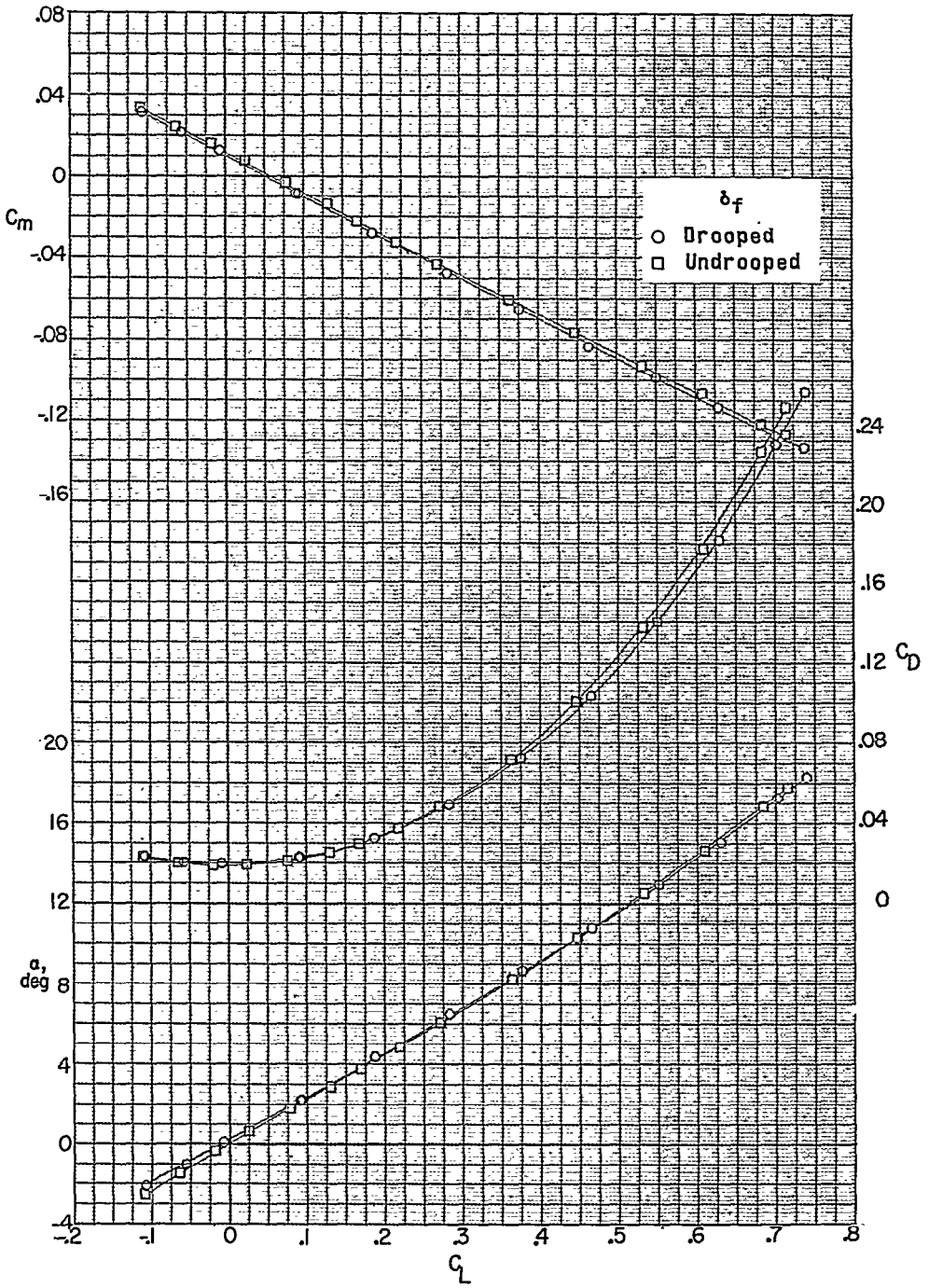

(a) M = 1.60.

Figure 8.- Effect of deflection of outboard wing-leading-edge flap on the longitudinal aerodynamic characteristics of the test model; $\delta_e = \delta_r = \delta_a = 0^o$.

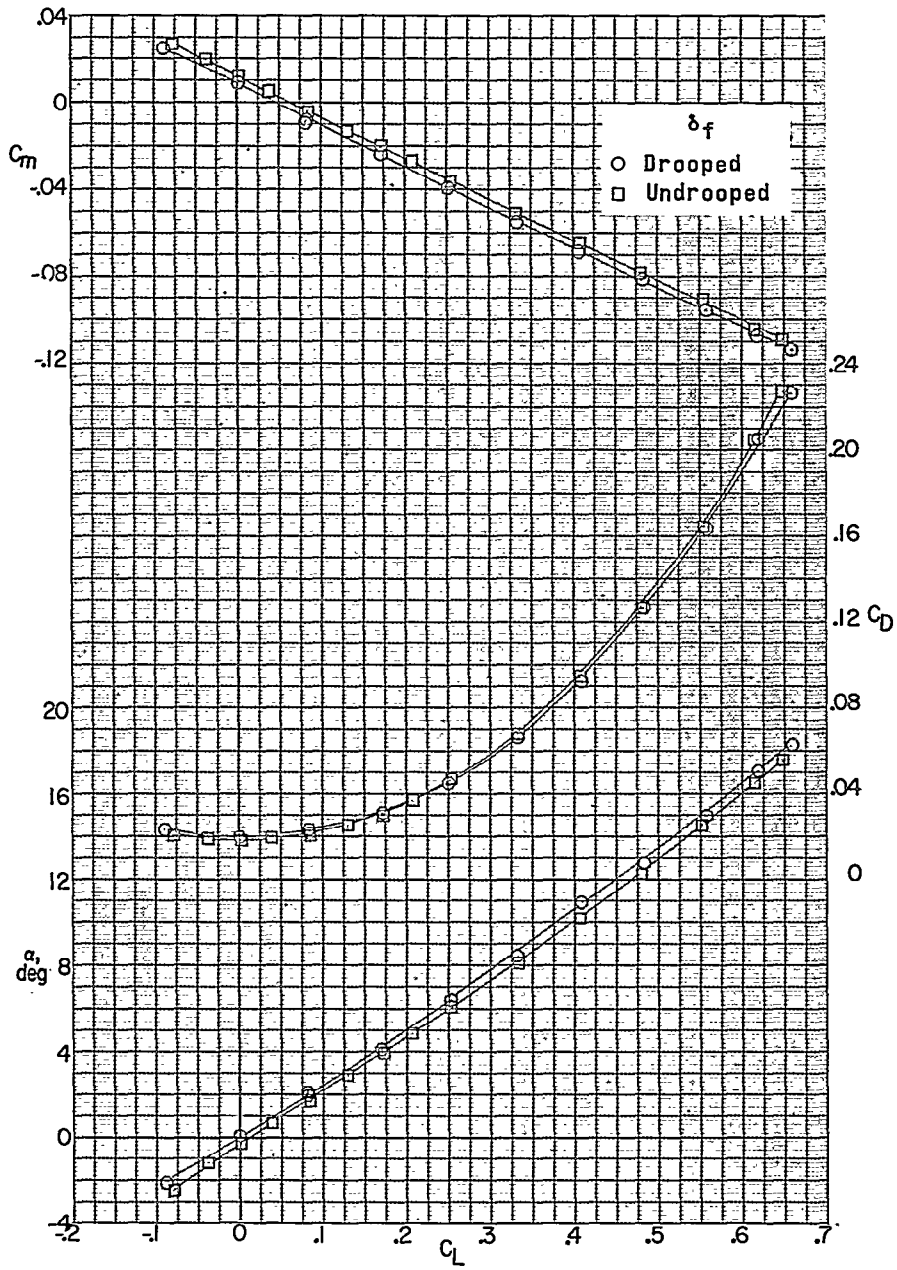

(b) M = 1.80.

Figure 8.- Continued.

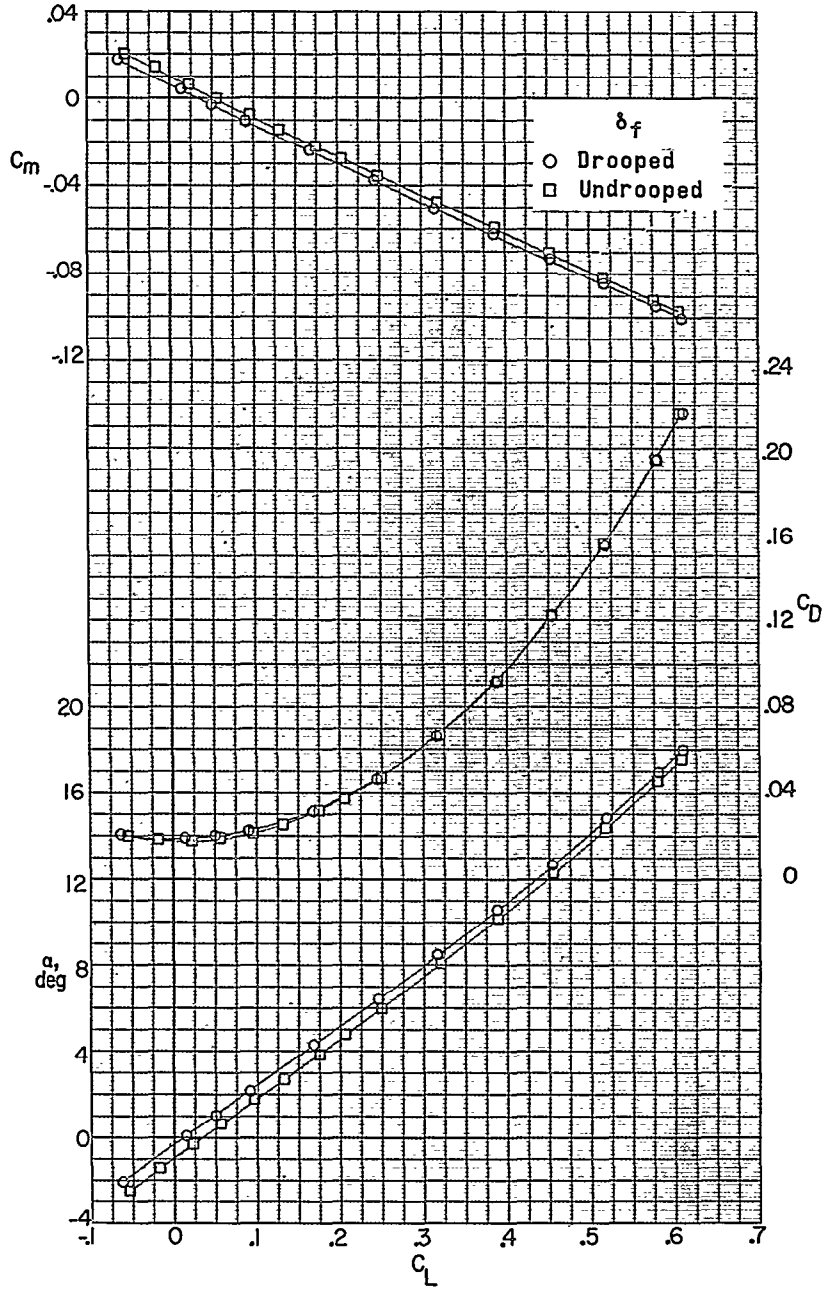

(c) M = 2.00.

Figure 8.- Concluded.

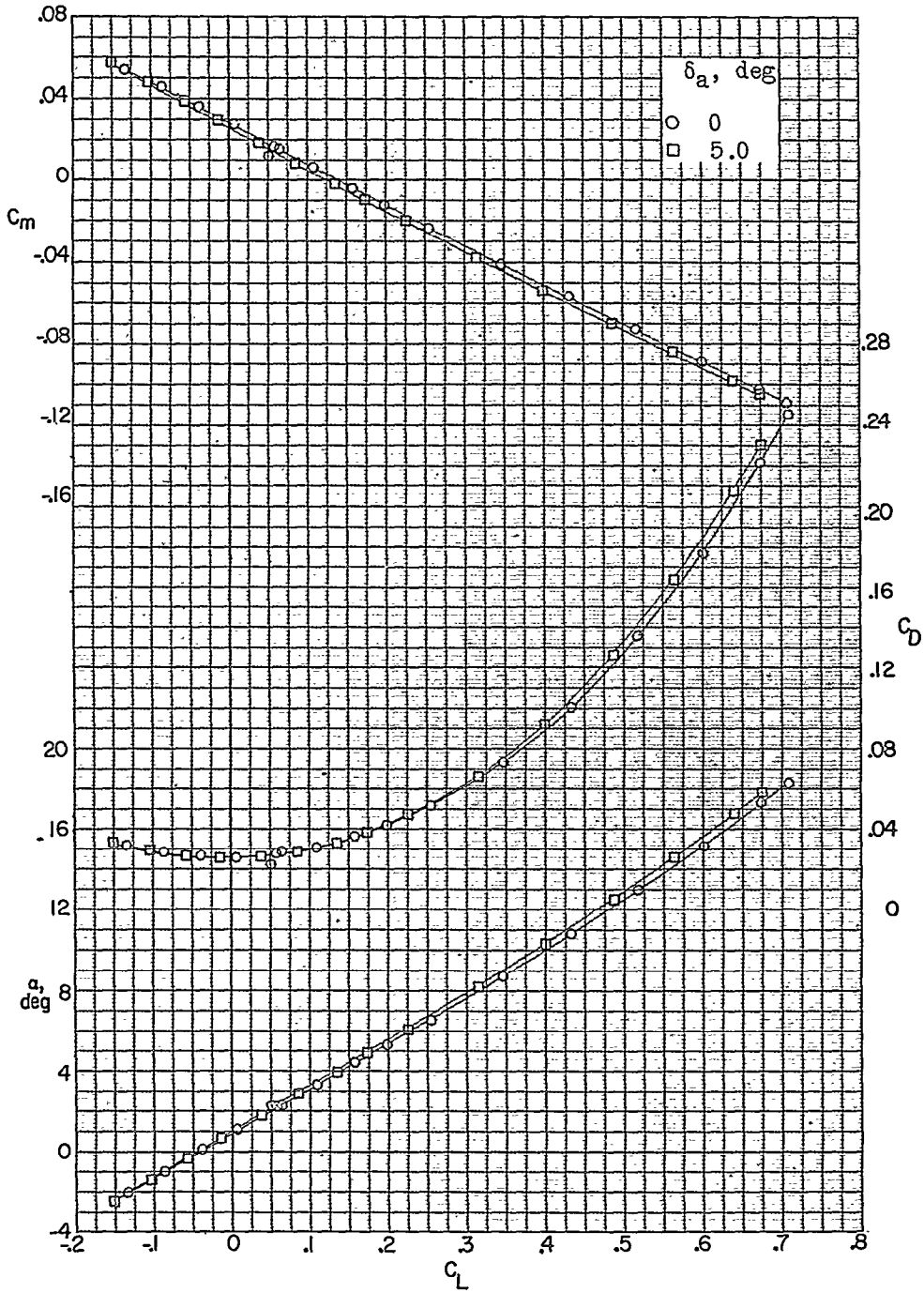

(a) M = 1.60.

Figure 9.- Effect of aileron deflection on the longitudinal aerodynamic characteristics of the test model; $\delta_e = -9.8^\circ$ and $\delta_r = 0^\circ$.

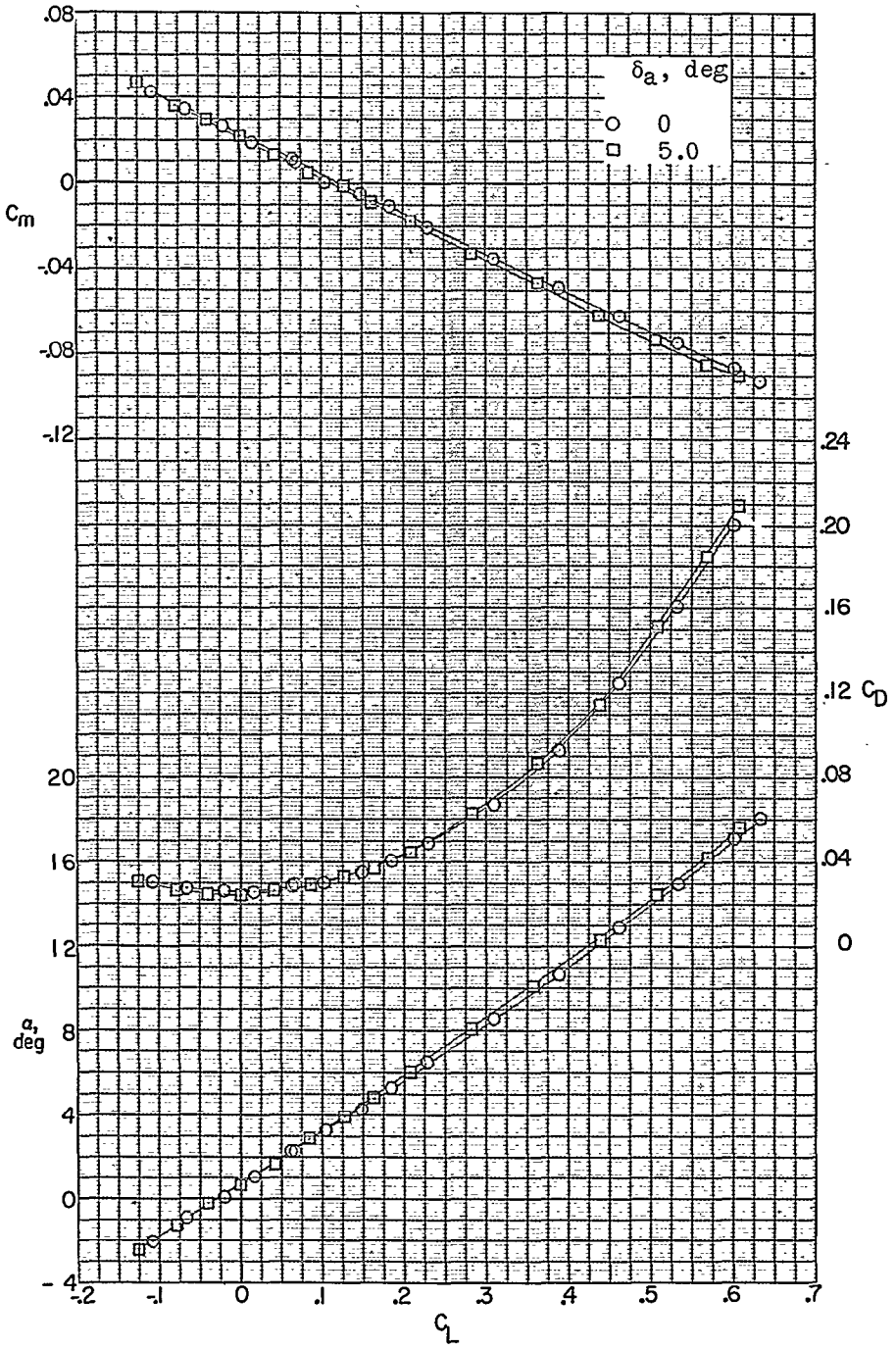

(b) M = 1.80.

Figure 9.- Continued.

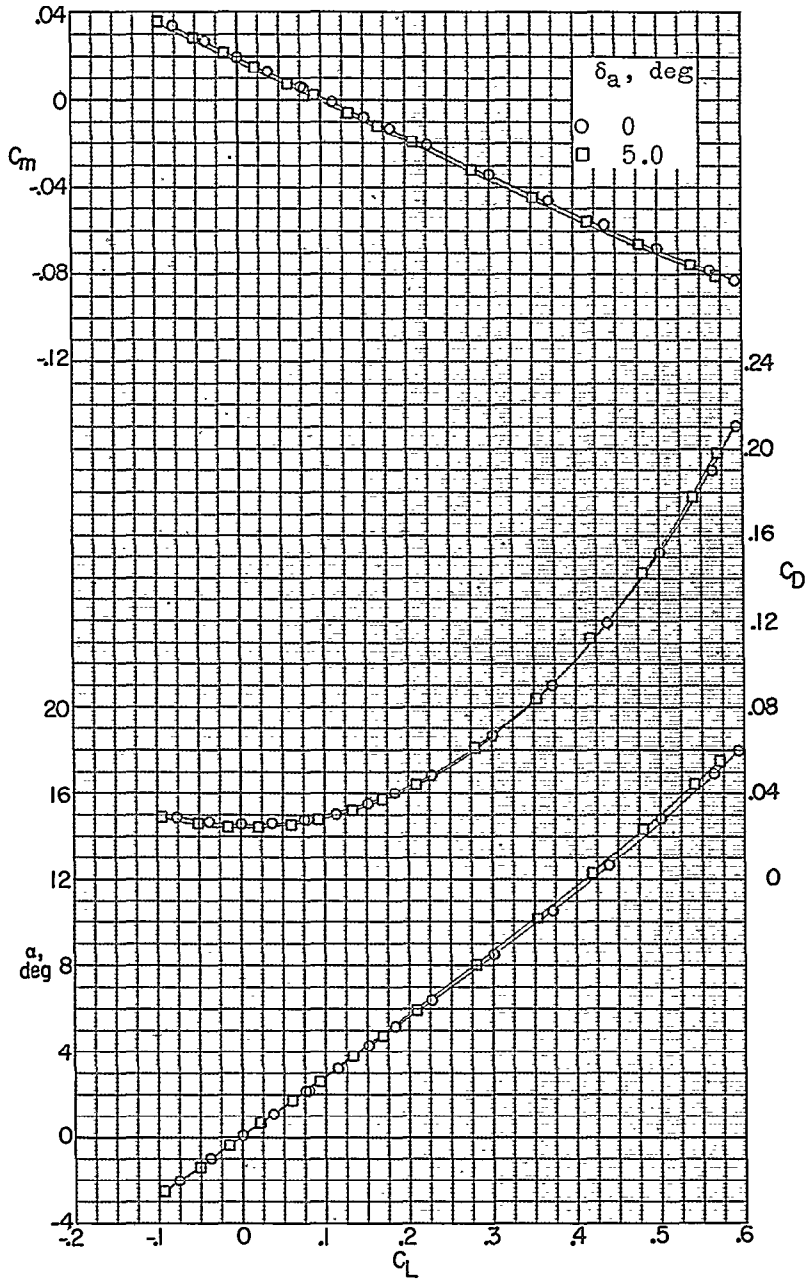

(c) M = 2.00.

Figure 9.- Concluded.

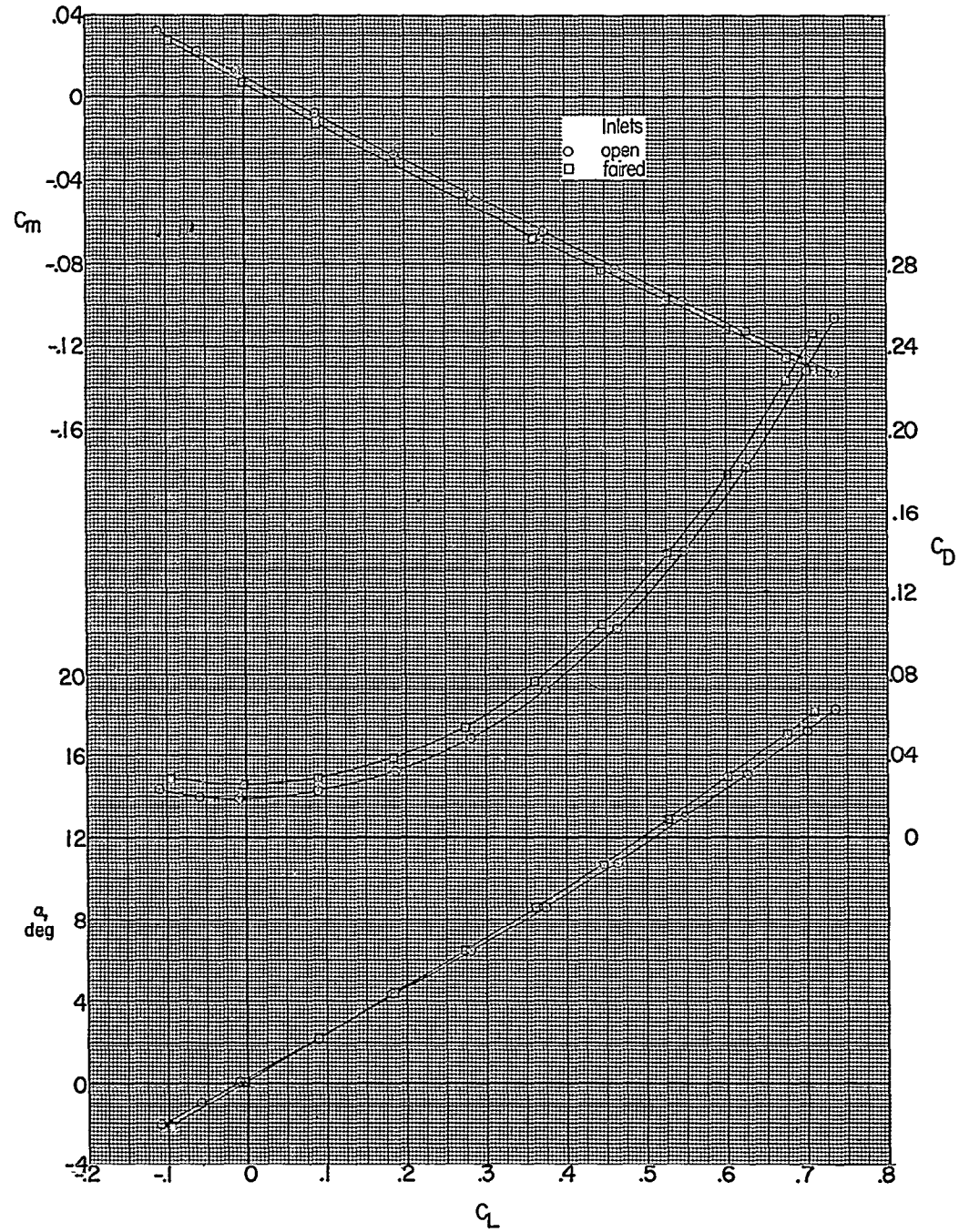

(a) M = 1.60.

Figure 10.- Effect of inlet fairing on longitudinal aerodynamic characteristics of test model; $\delta_e = \delta_r = \delta_a = 0^o$.

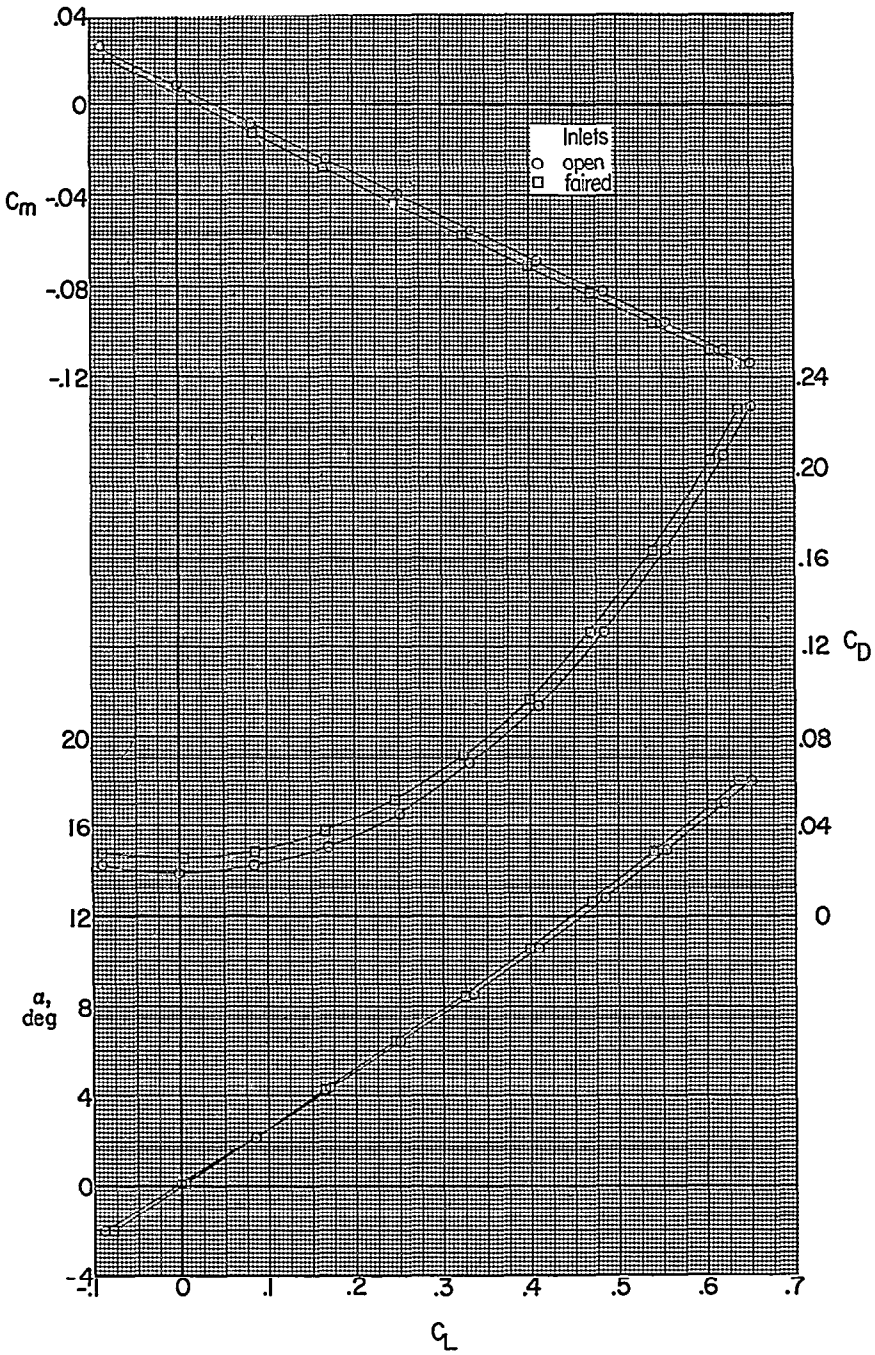

(b) M = 1.80.

Figure 10.- Continued.

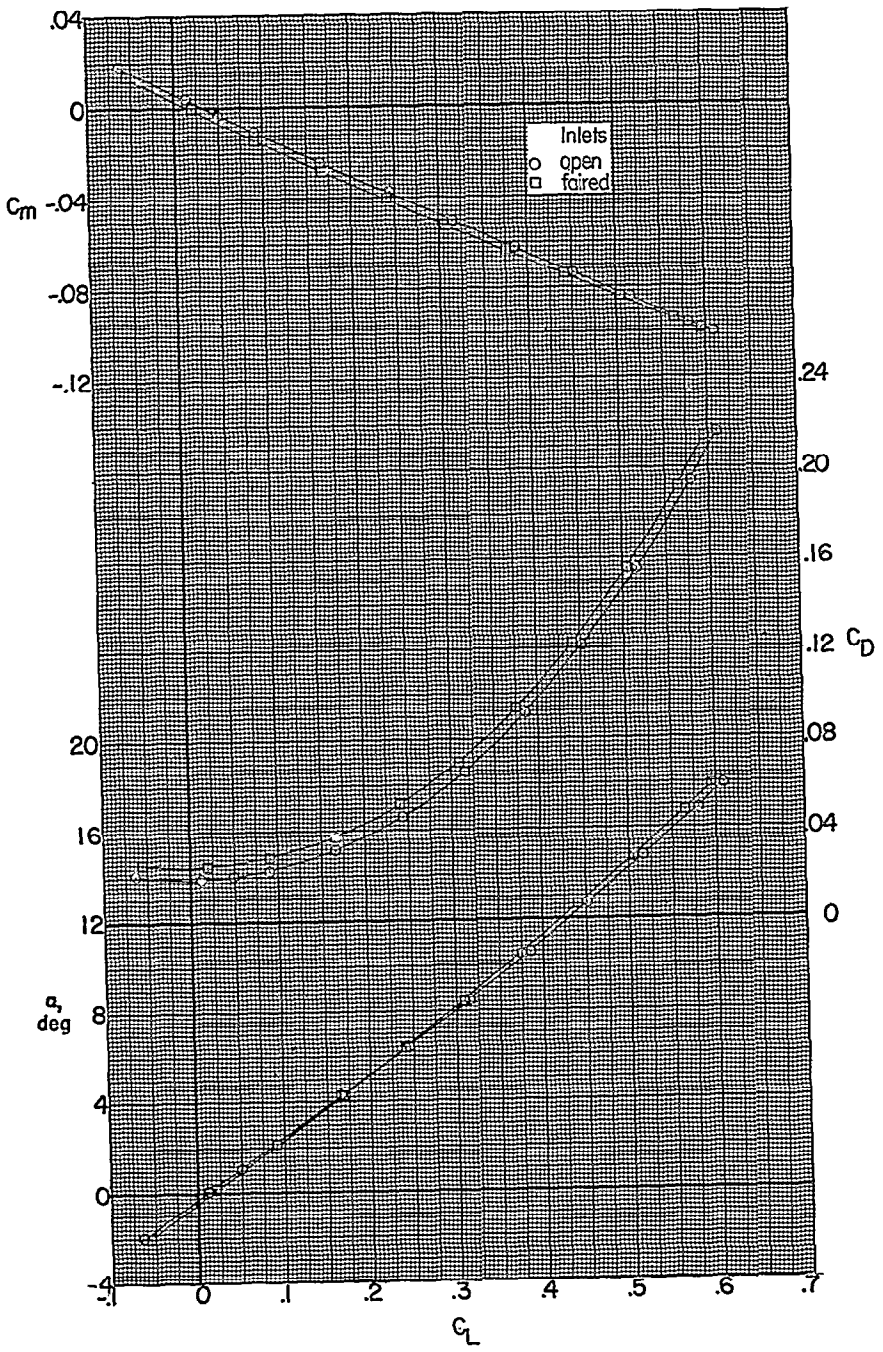

(c) M = 2.00.

Figure 10.- Concluded.

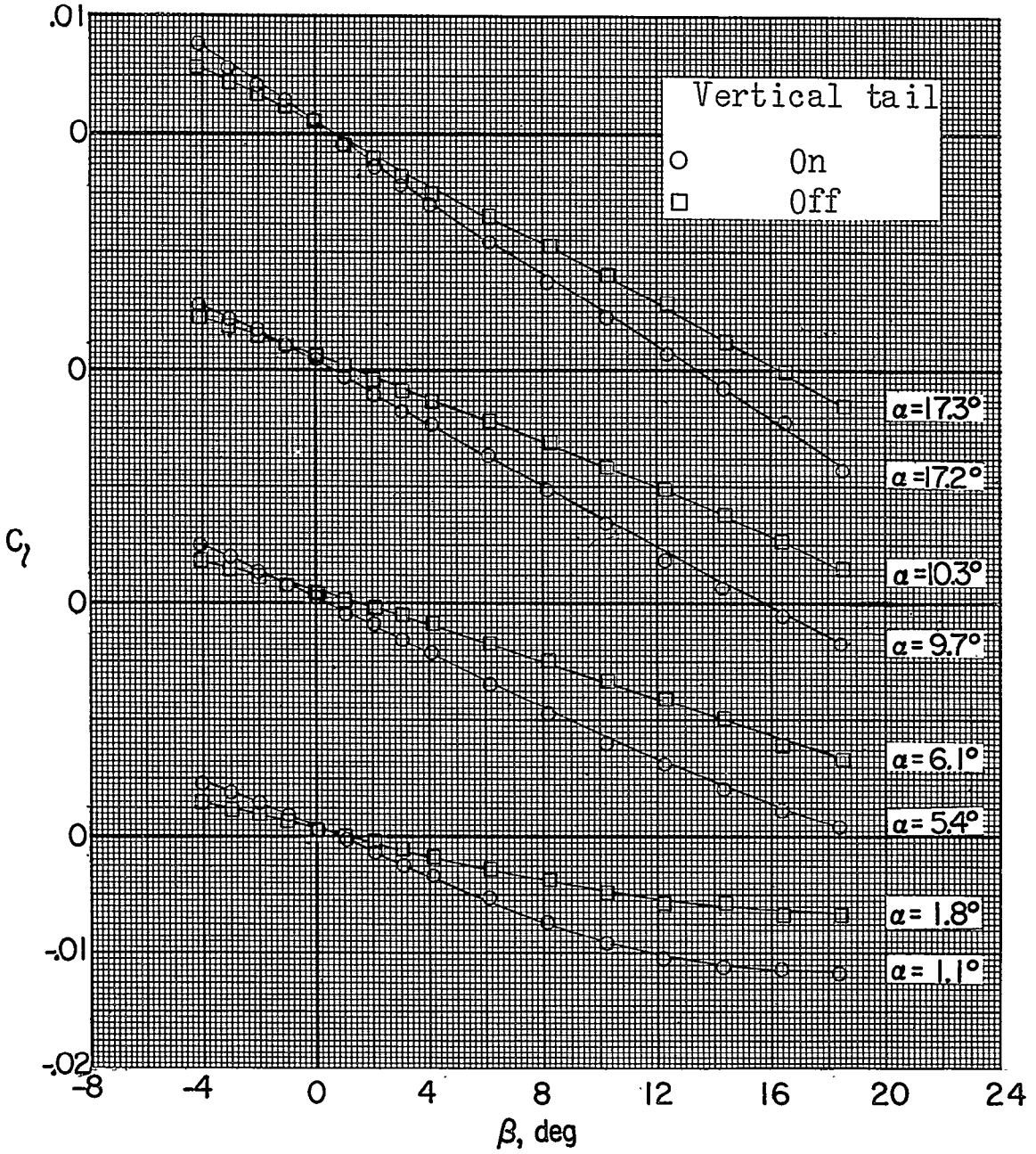

(a) M = 1.60.

Figure 11.- Variation of lateral stability characteristics of test model with angle of sideslip; $\delta_e = \delta_a = 0^\circ$.

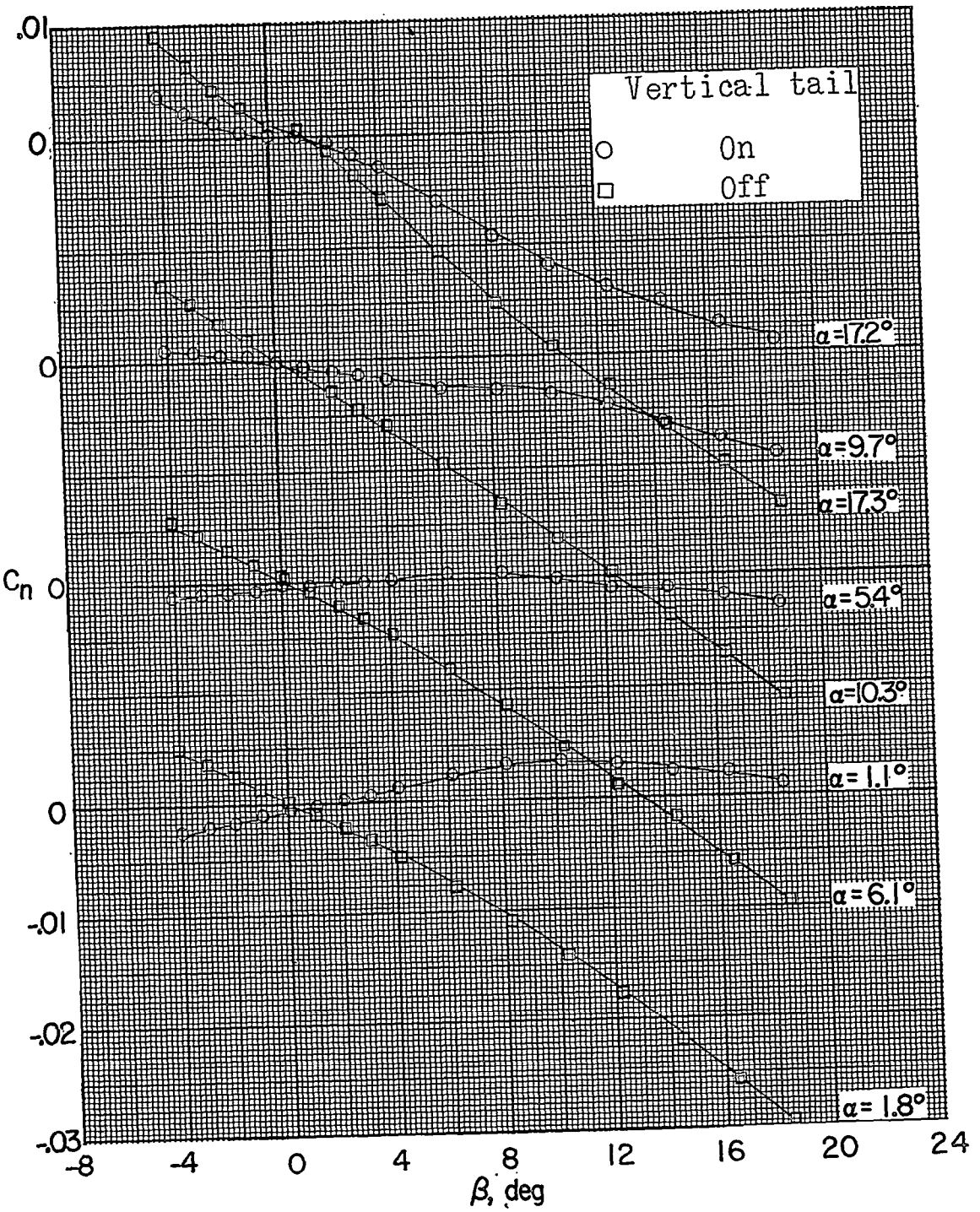

(a) Continued.

Figure 11.- Continued.

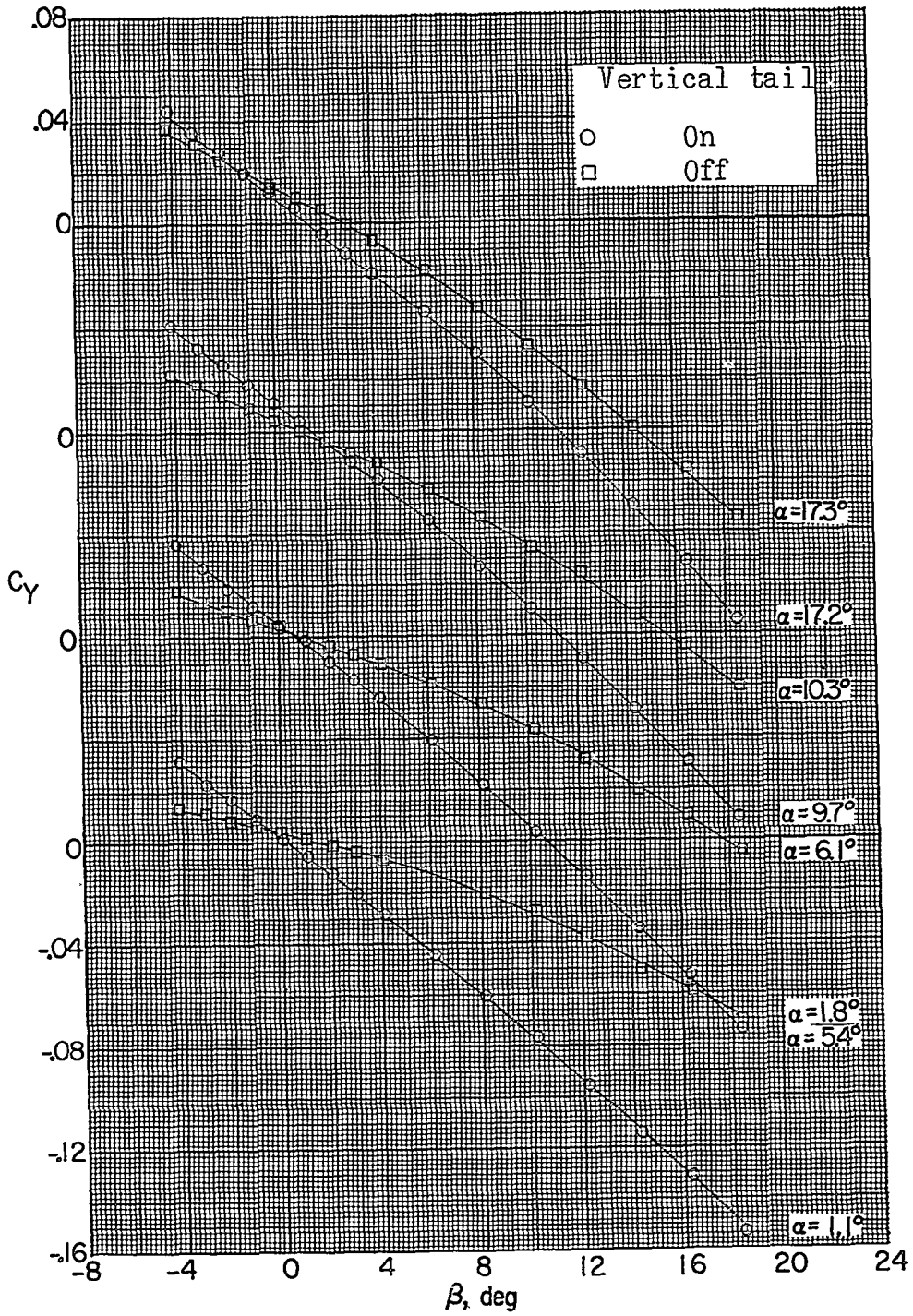

(a) Concluded.

Figure 11.- Continued.

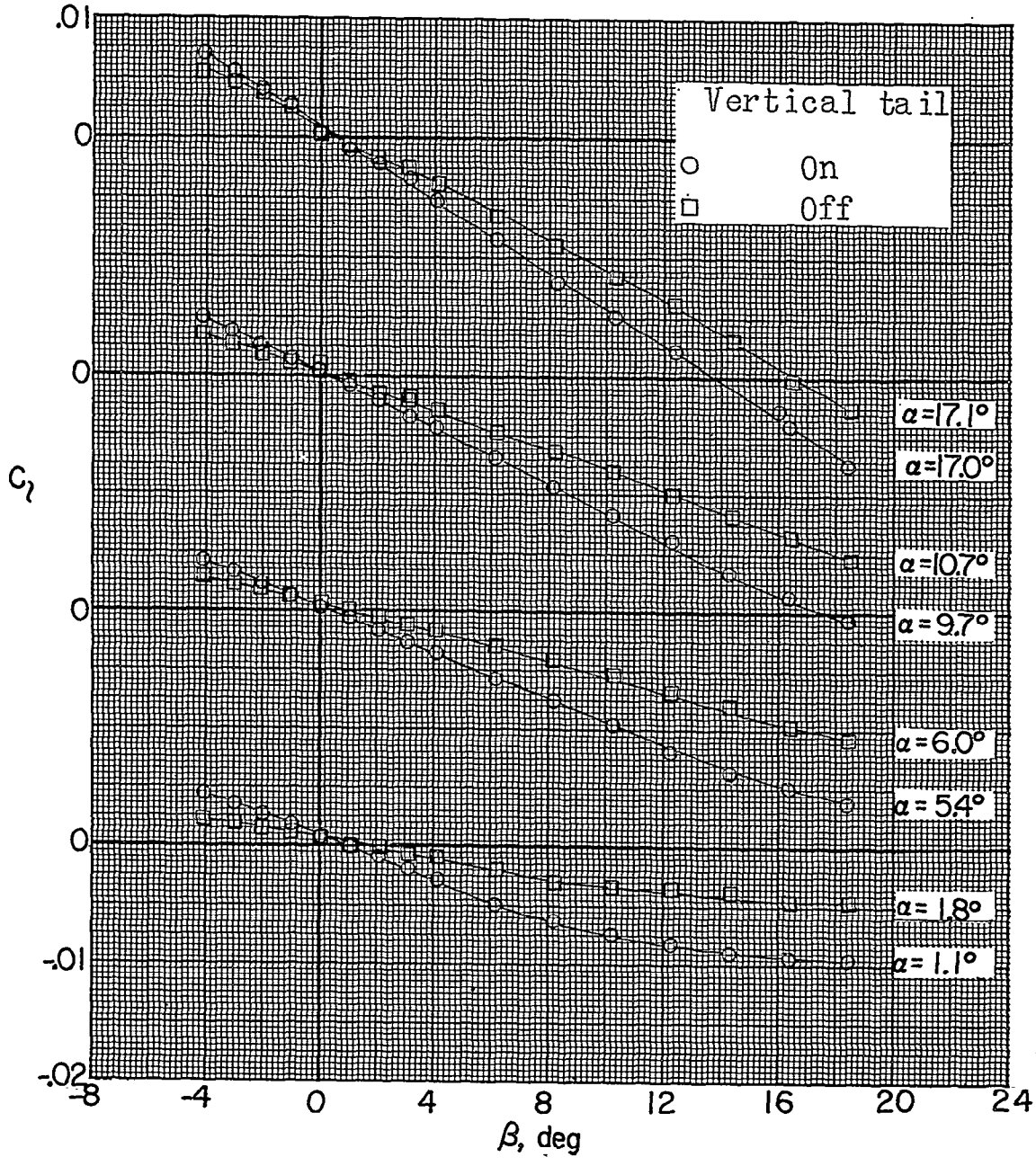

(b) M = 1.80.

Figure 11.- Continued.

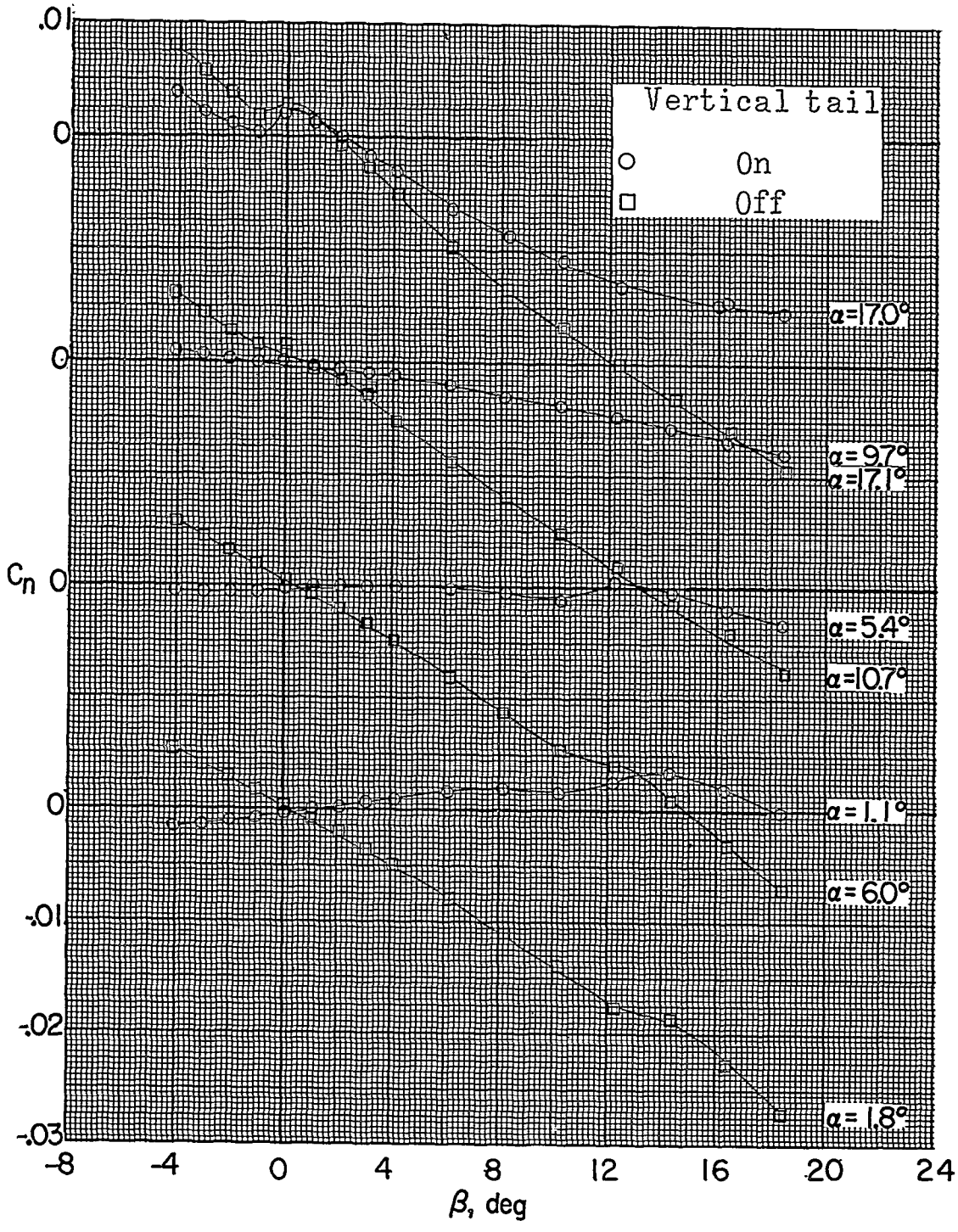

(b) Continued.

Figure 11.- Continued.

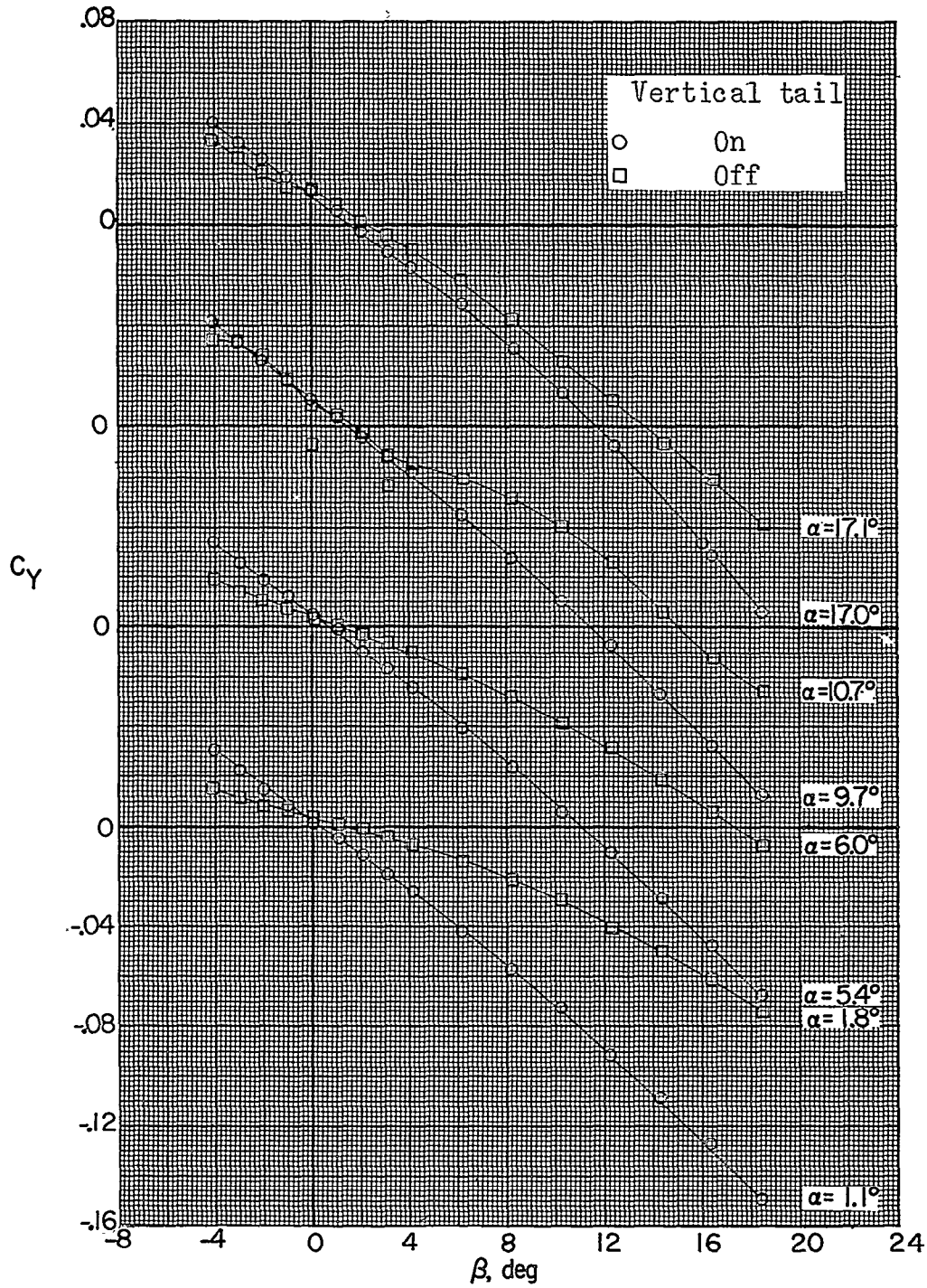

(b) Concluded.

Figure 11.- Continued.

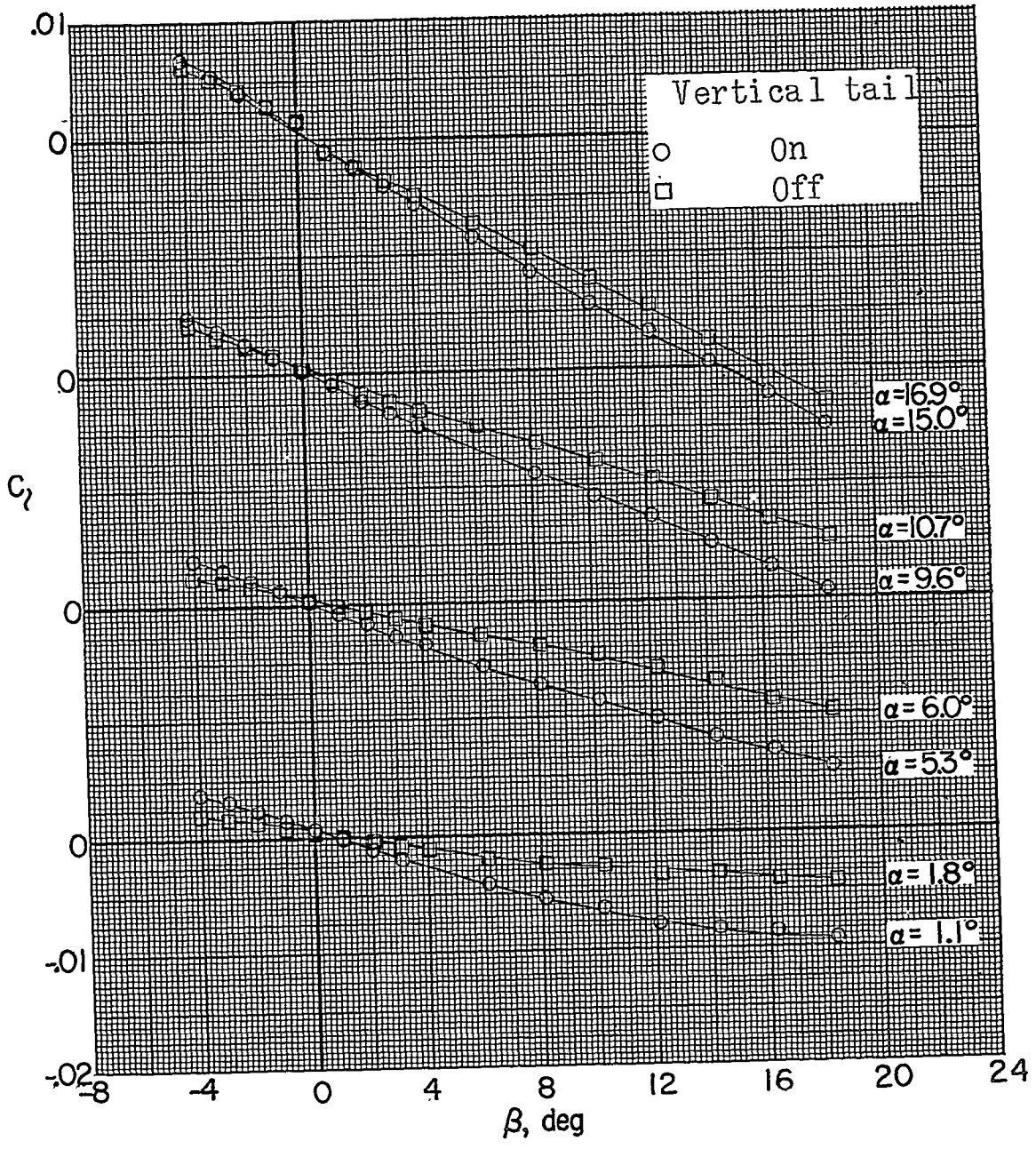

(c) M = 2.00.

Figure 11.- Continued.

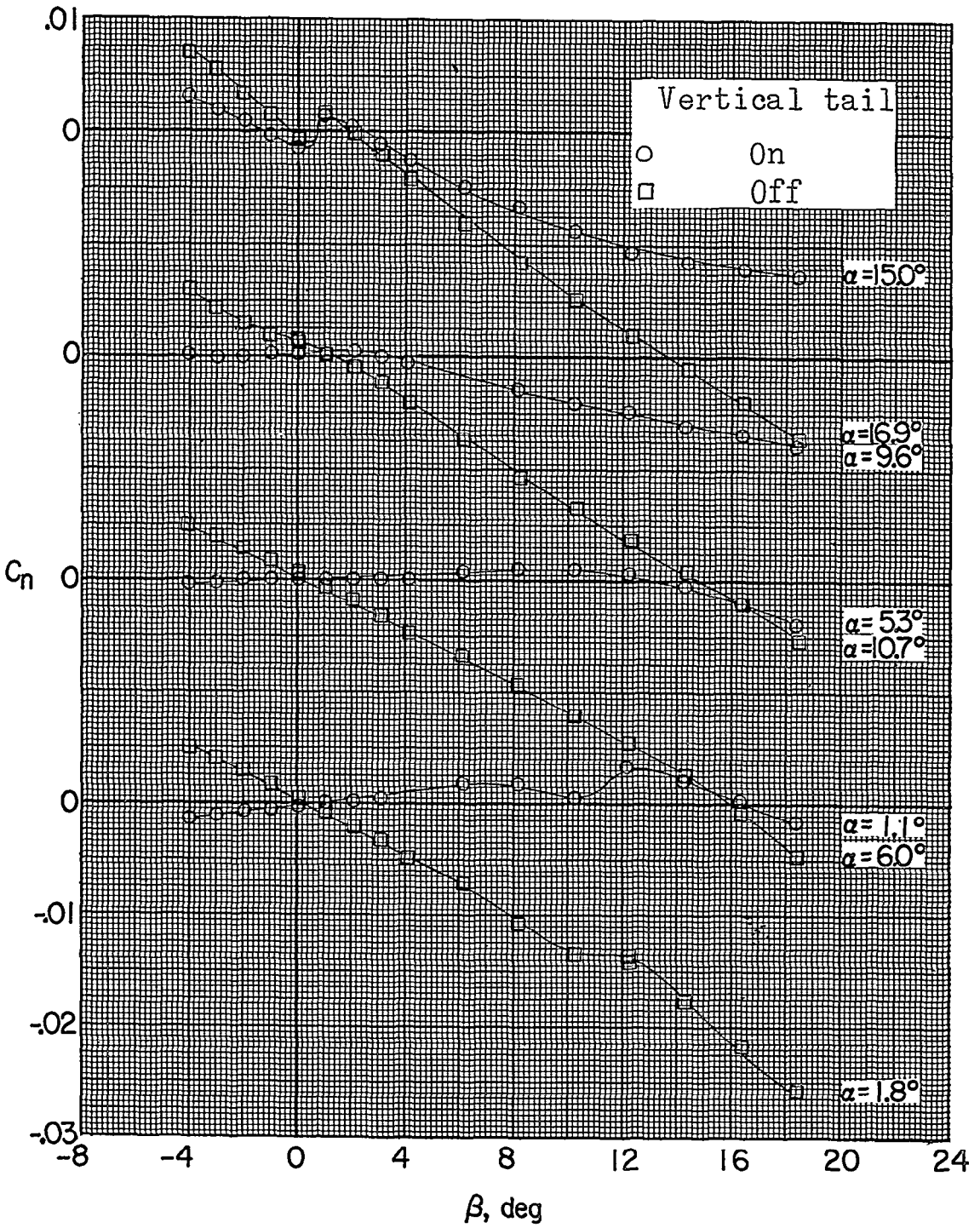

(c) Continued.

Figure 11.- Continued.

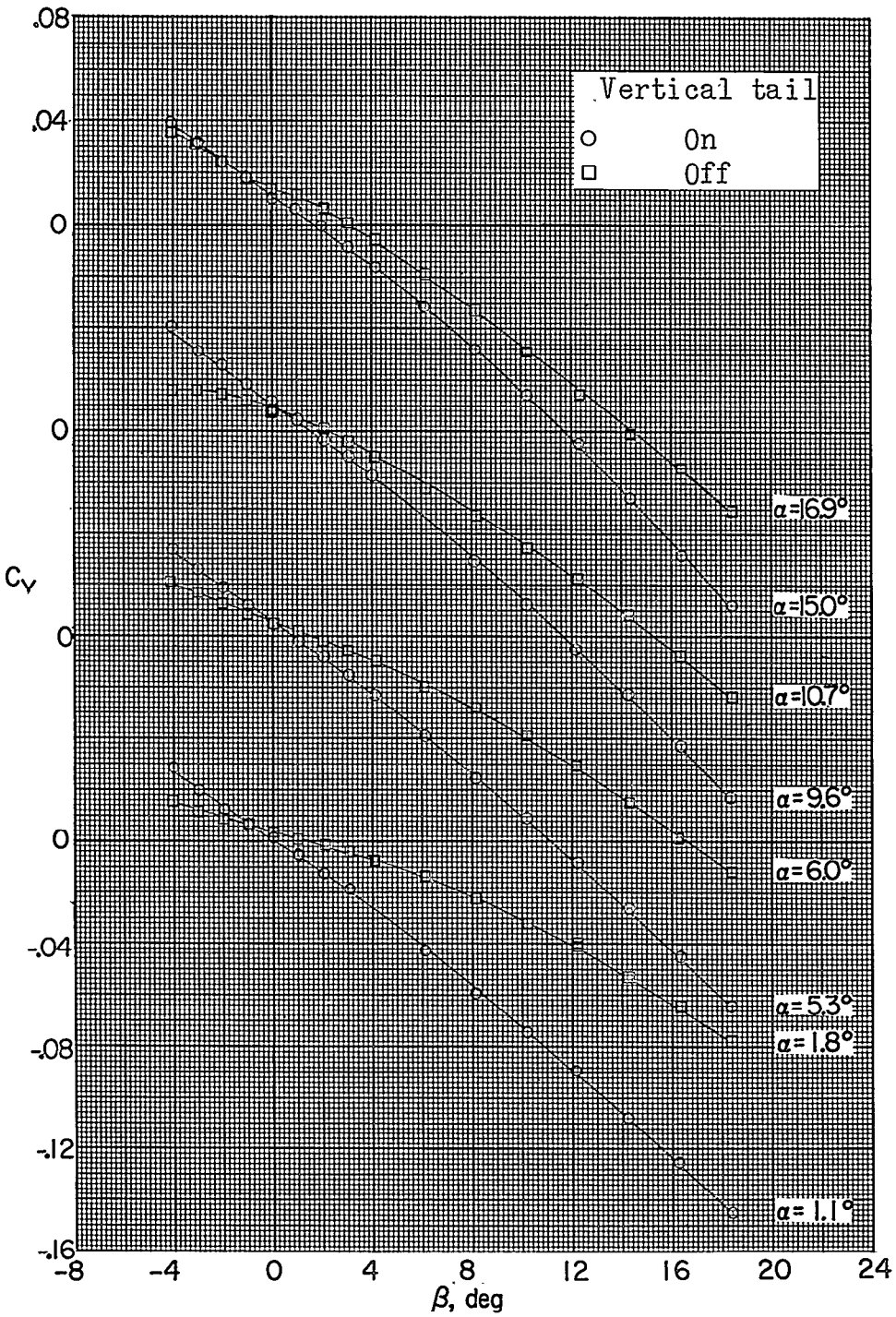

(c) Concluded.

Figure 11.- Concluded.

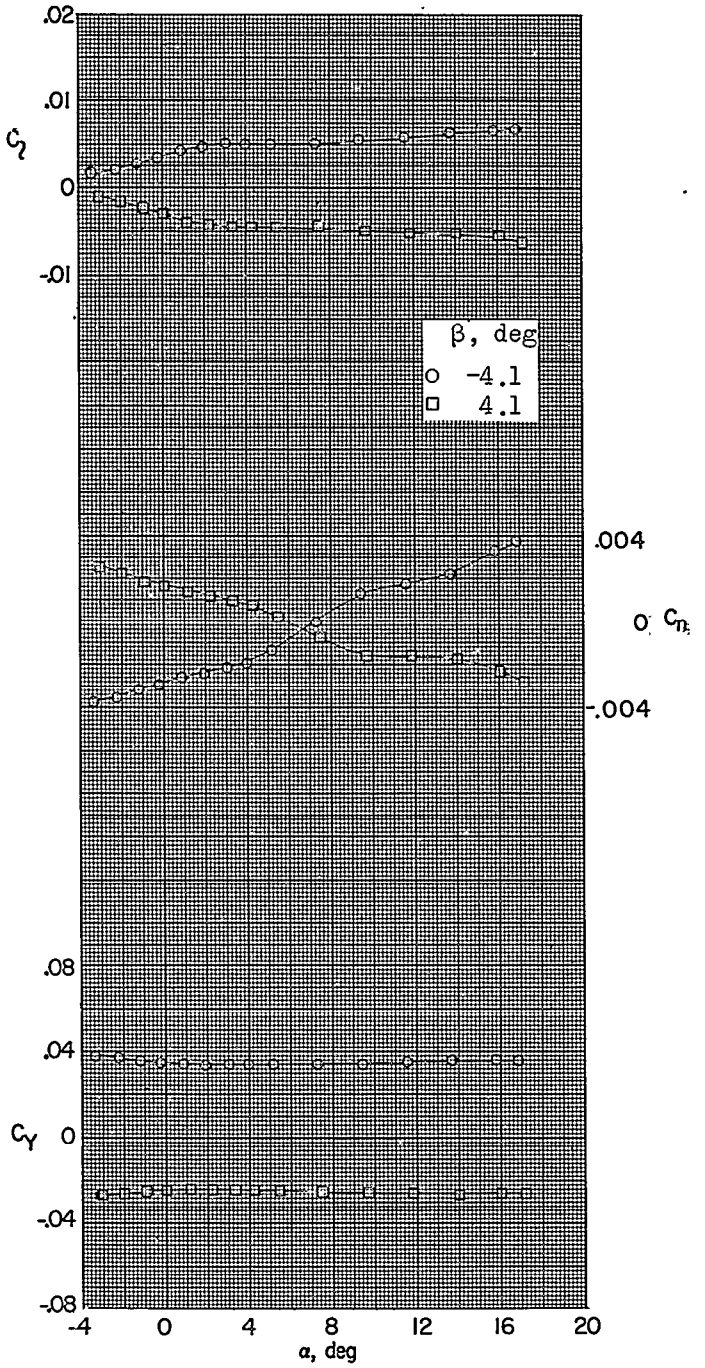

(a) M = 1.60.

Figure 12.- Variation of lateral stability characteristics of test model with angle of attack; $\delta_e = \delta_r = \delta_a = 0^o$.

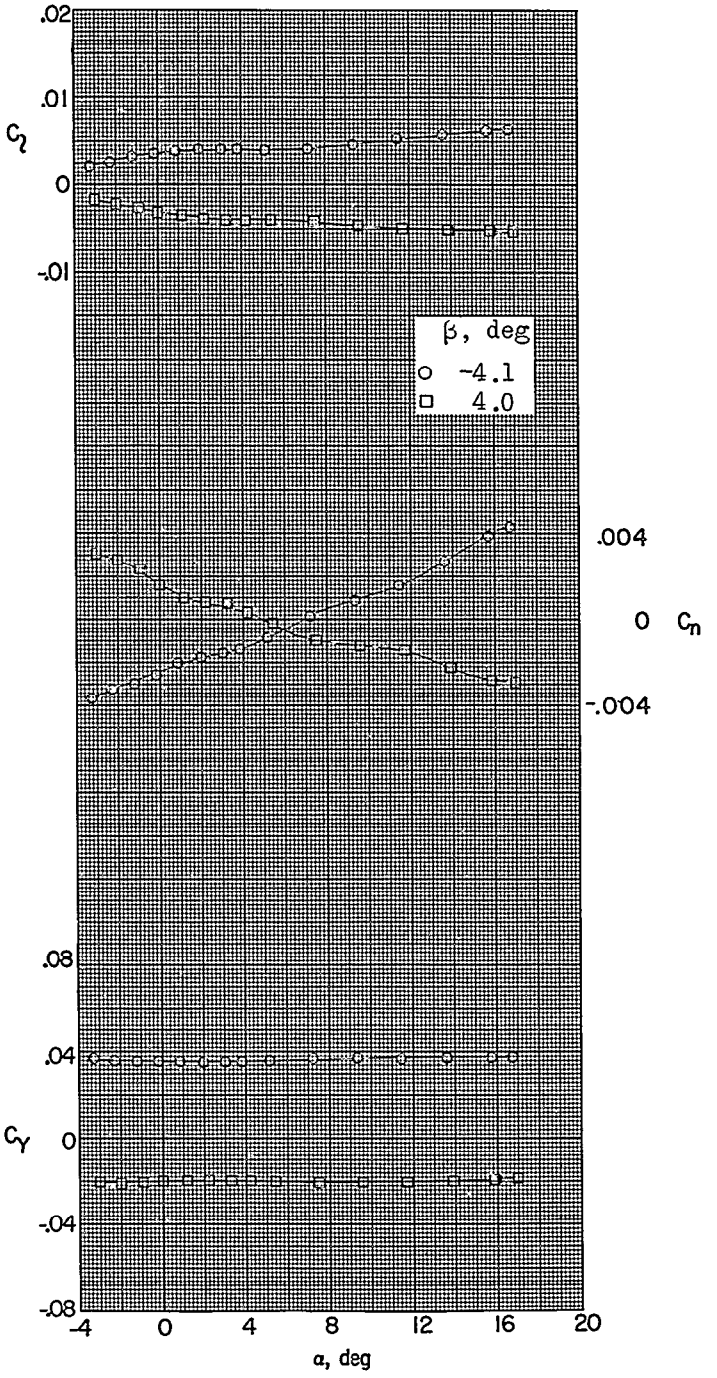

(b) M = 1.80.

Figure 12.- Continued.

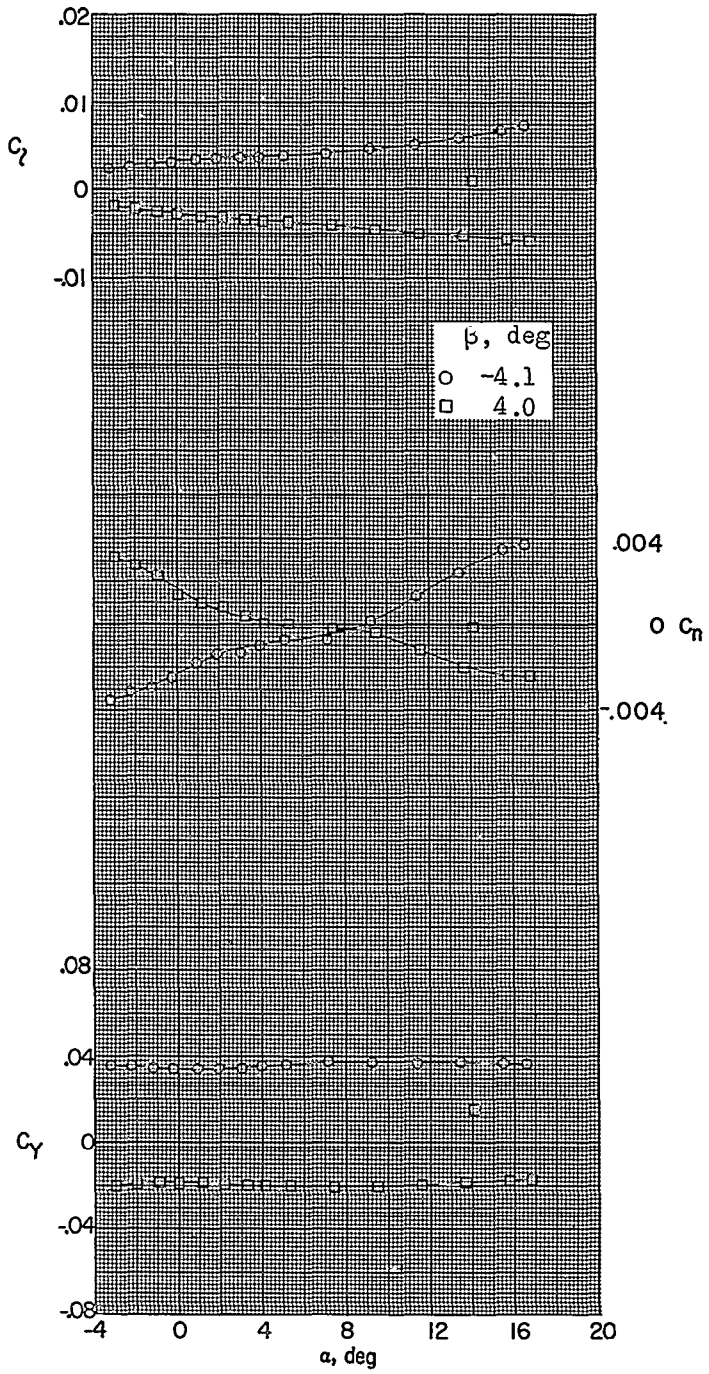

(c) M = 2.00.

Figure 12.- Concluded.

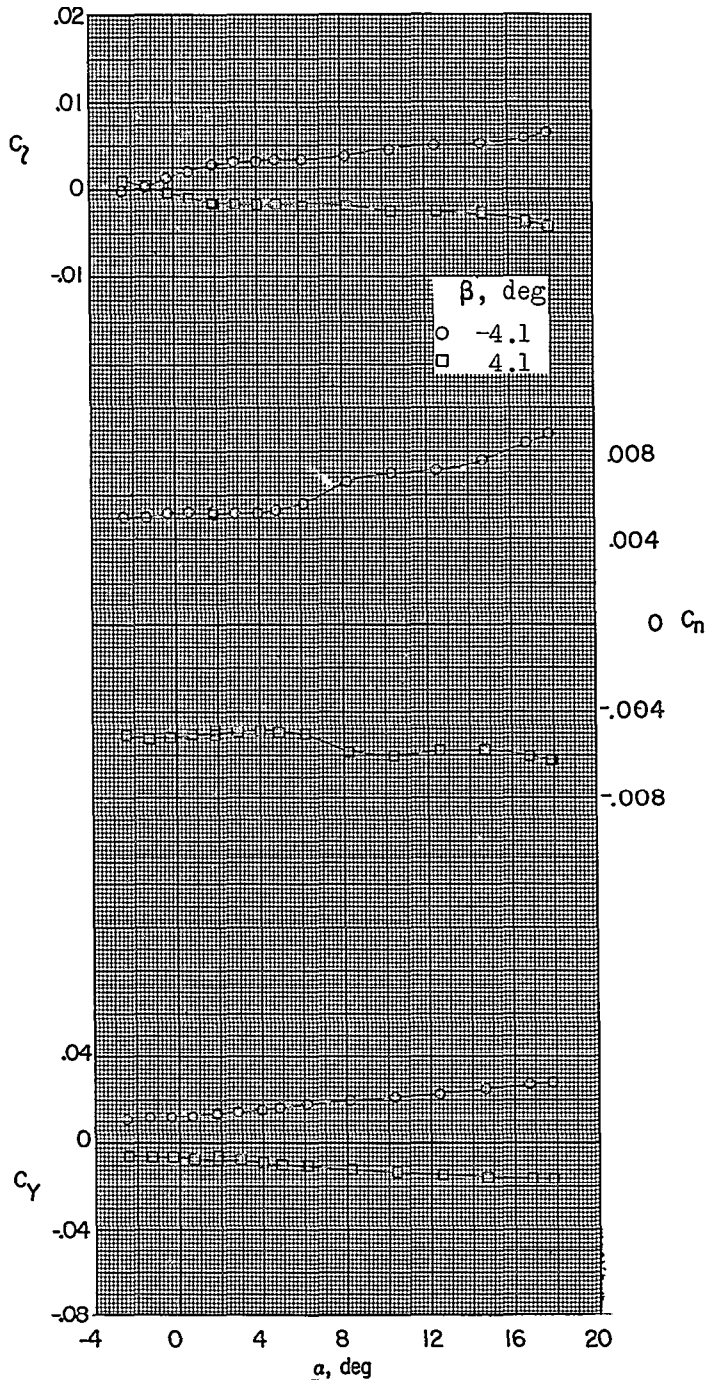

(a) M = 1.60.

Figure 13.- Variation of lateral stability characteristics of test model, vertical tail off, with angle of attack; $\delta_e = \delta_a = 0^o$.

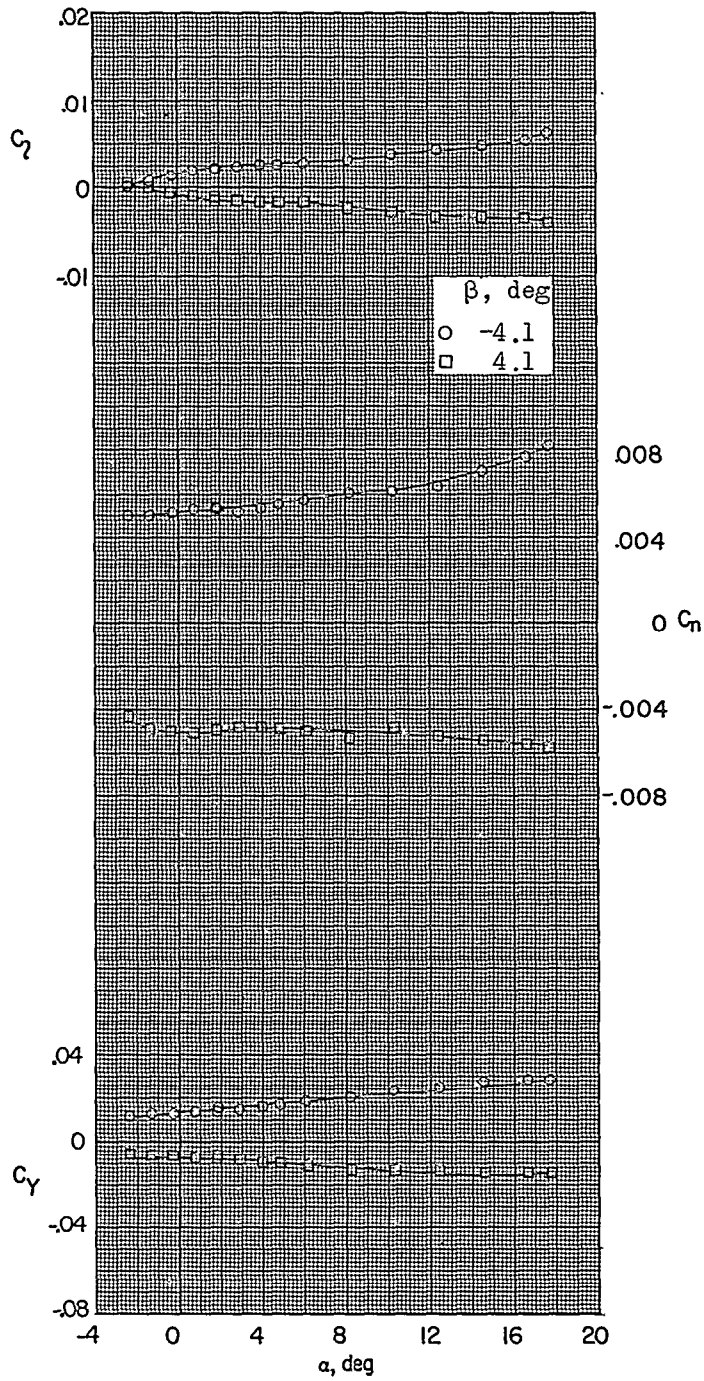

(b) M = 1.80.

Figure 13.- Continued.

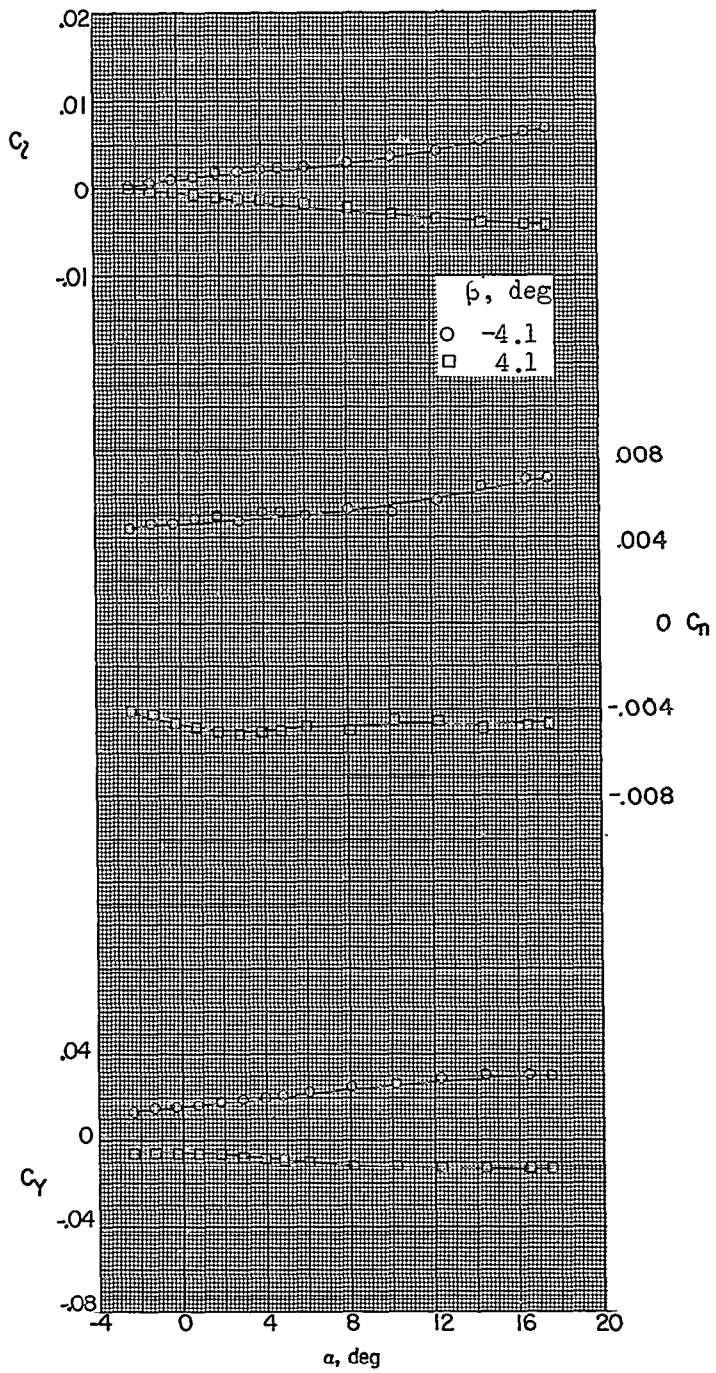

(c) M = 2.00.

Figure 13.- Concluded.

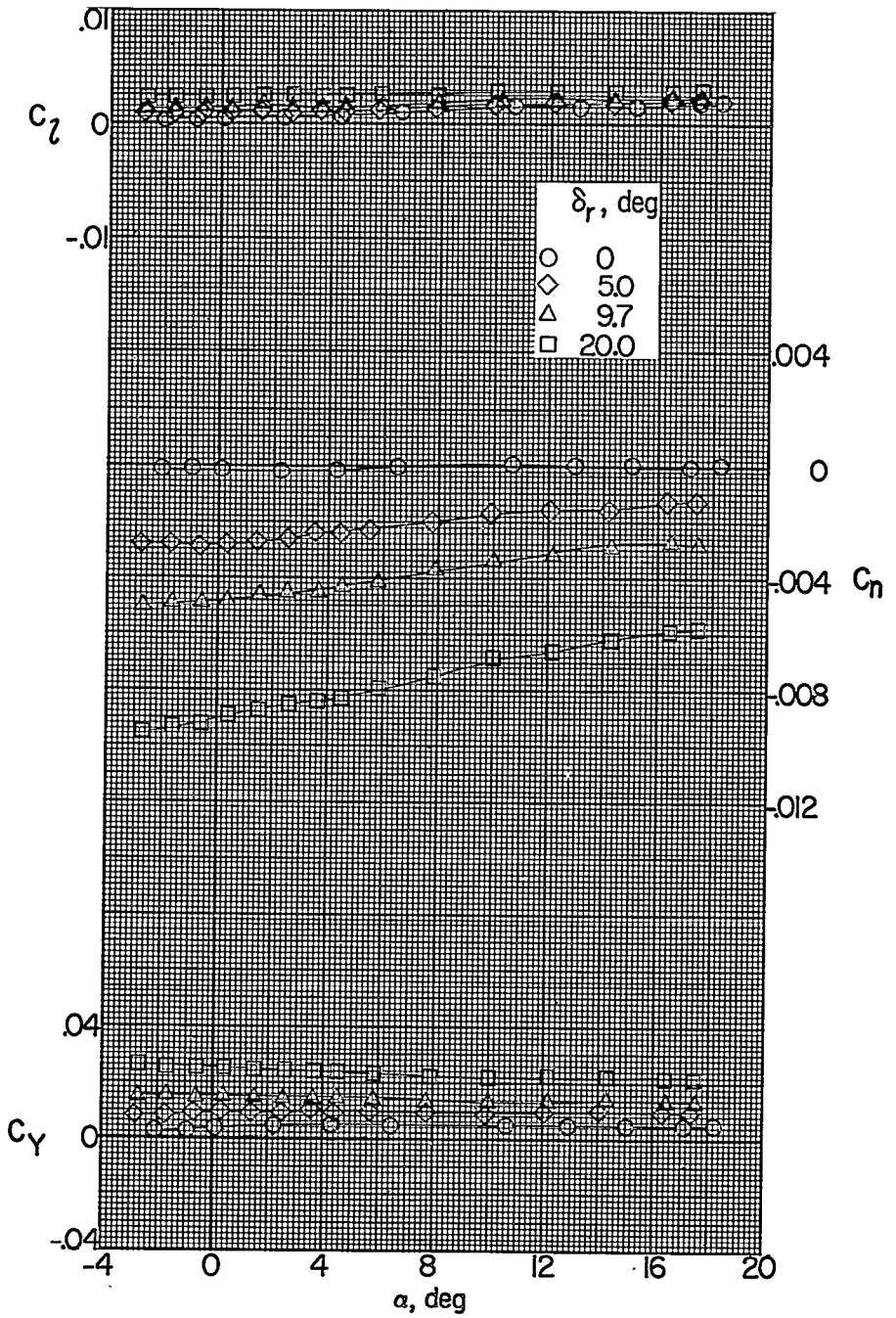

(a) M = 1.60.

Figure 14.- Effect of rudder deflection on lateral aerodynamic characteristics of test model; $\delta_e = \delta_a = 0^o$.

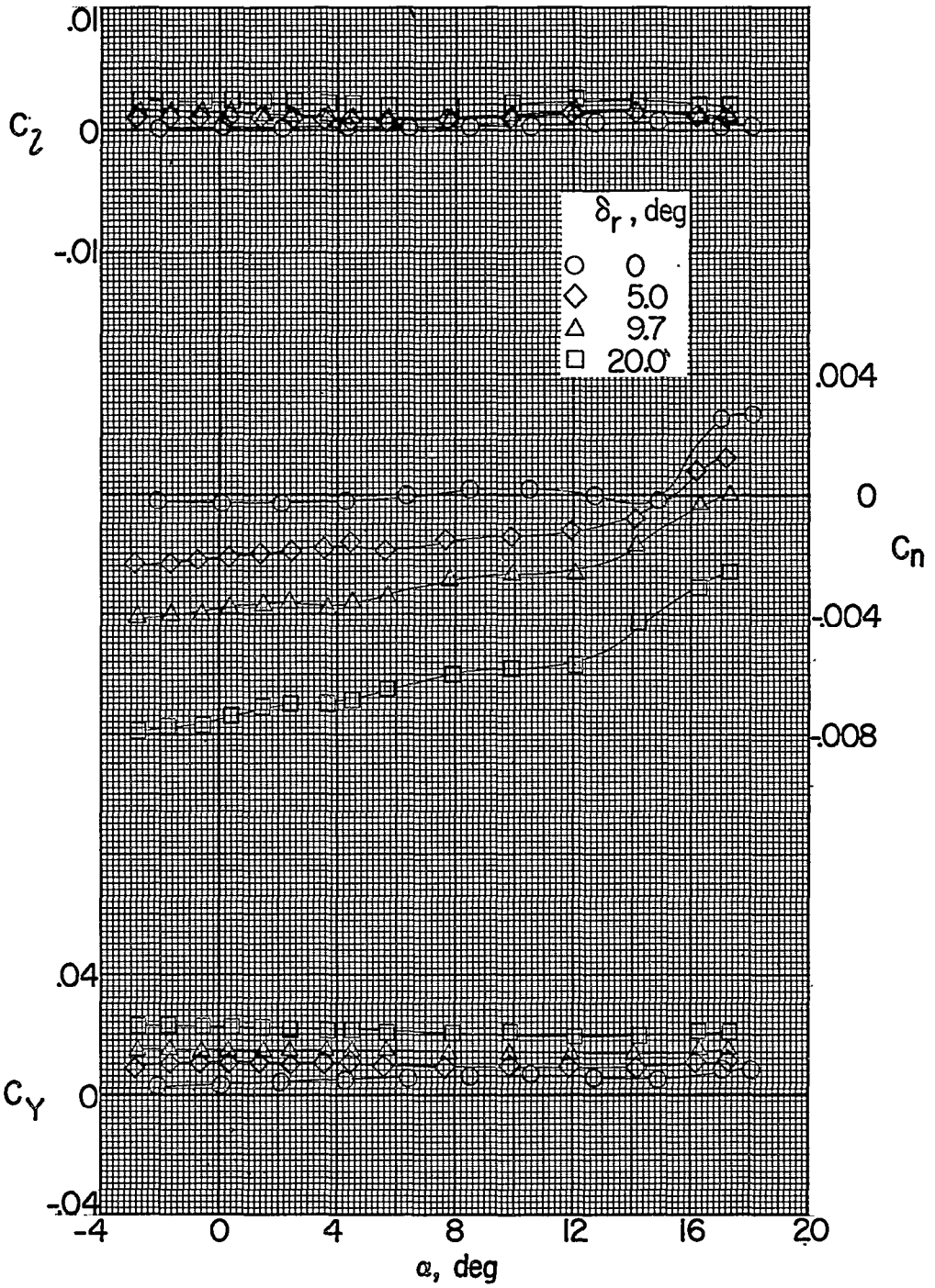

(b) M = 1.80.

Figure 14.- Continued.

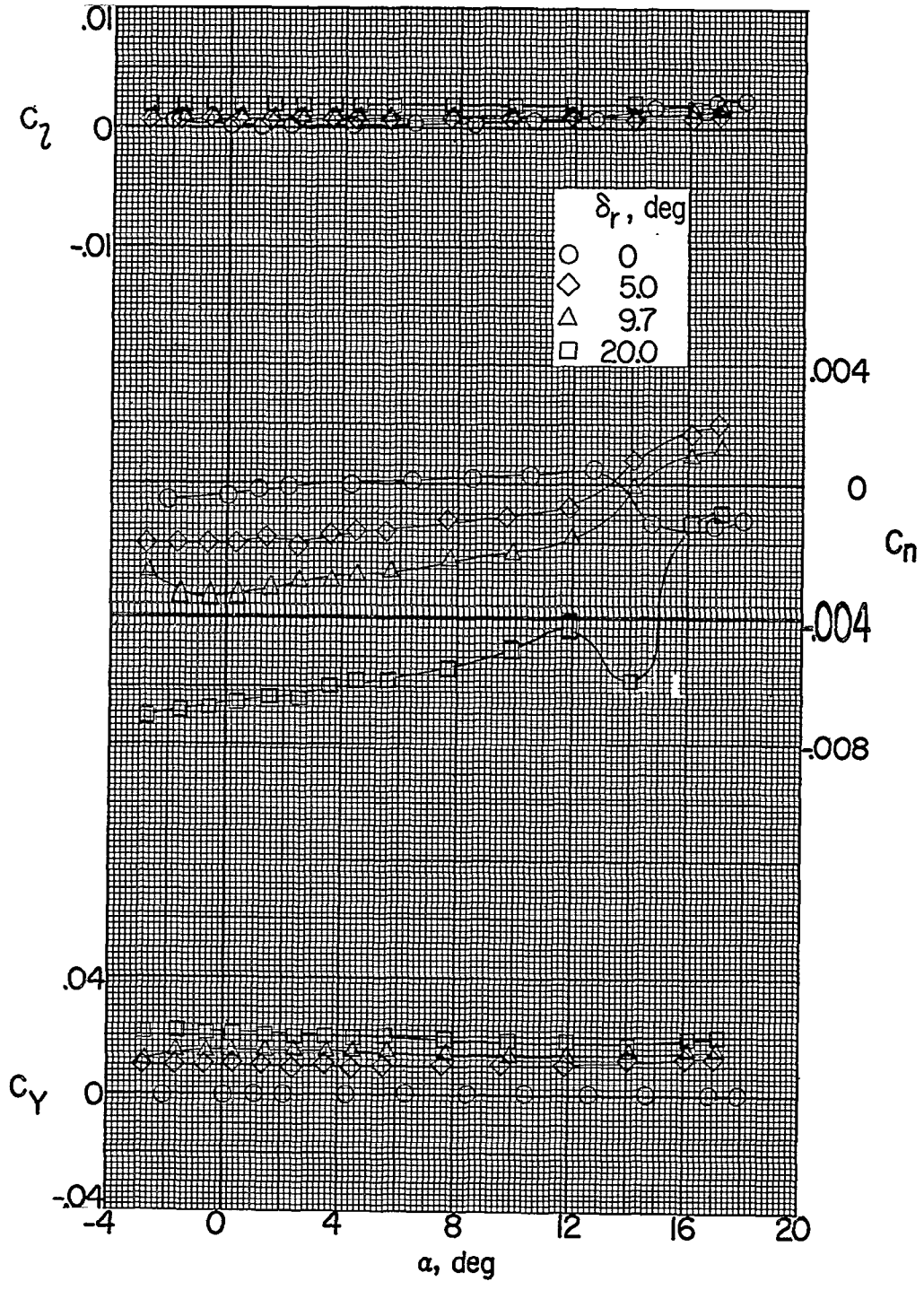

(c) M = 2.00.

Figure 14.- Concluded.

~~CONFIDENTIAL~~

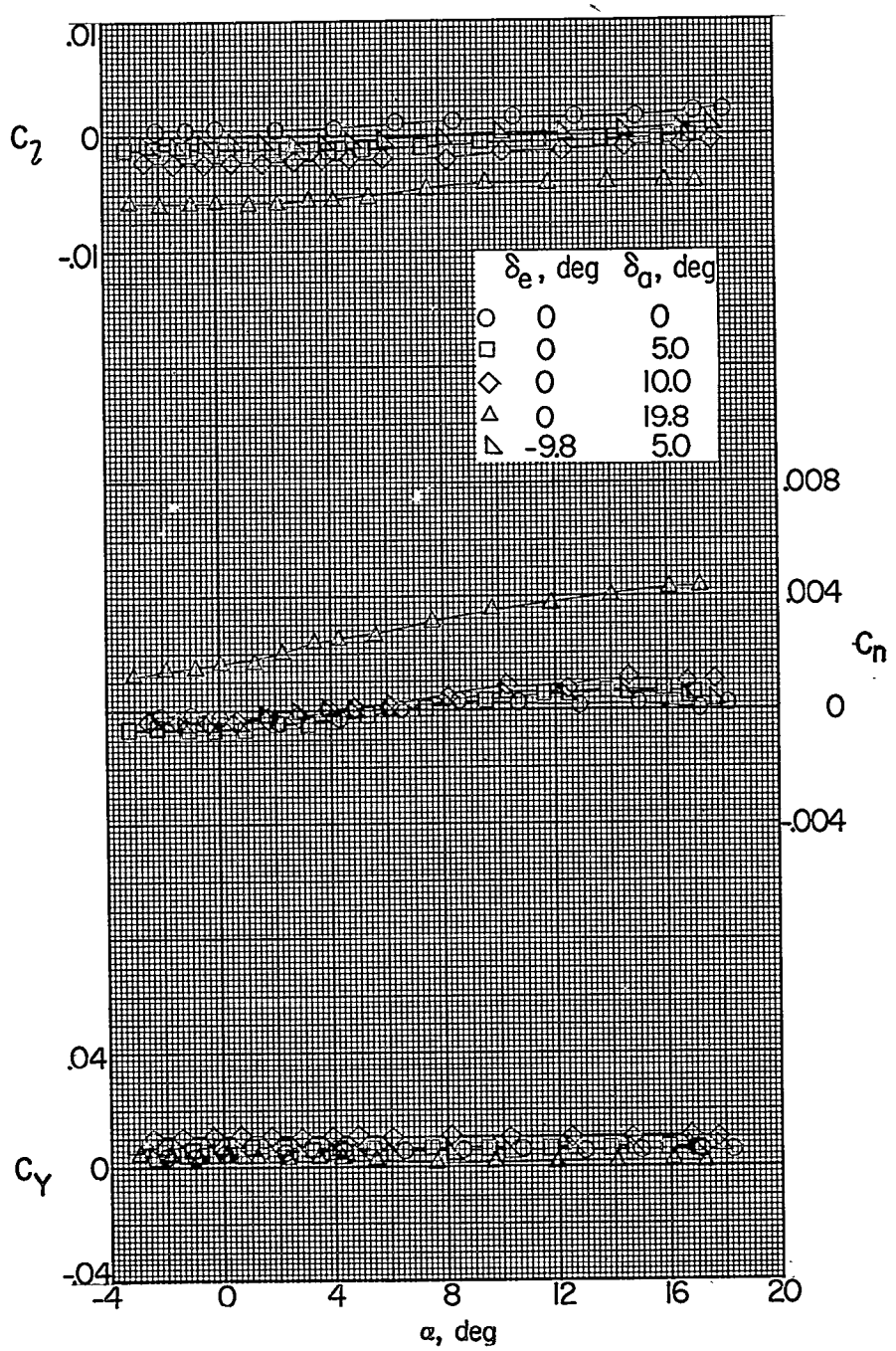

(a) M = 1.60.

Figure 15.- Effect of aileron and elevator deflection on lateral aerodynamic characteristics of test model; $\delta_r = 0^o$.

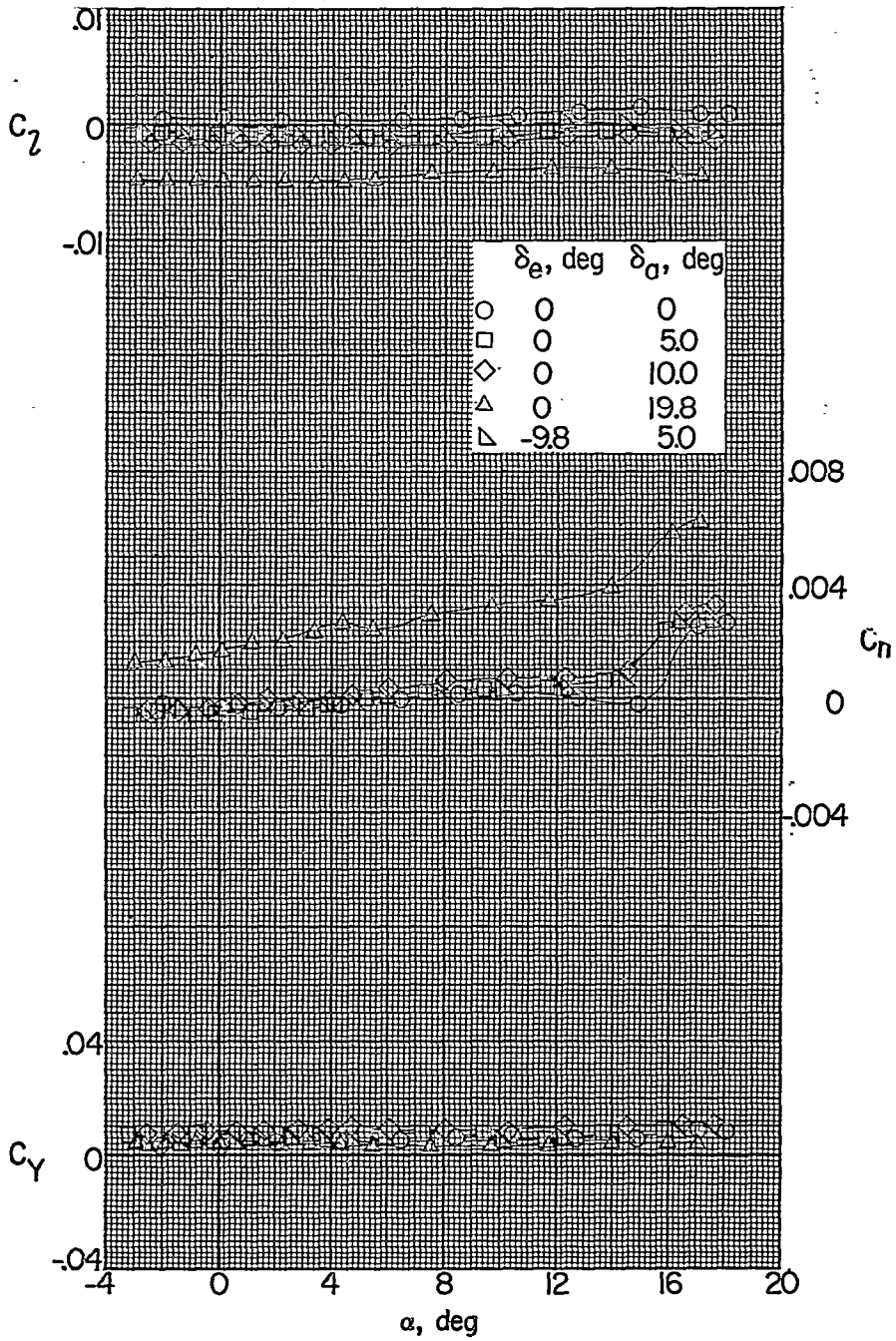

(b) M = 1.80.

Figure 15.- Continued.

[redacted]

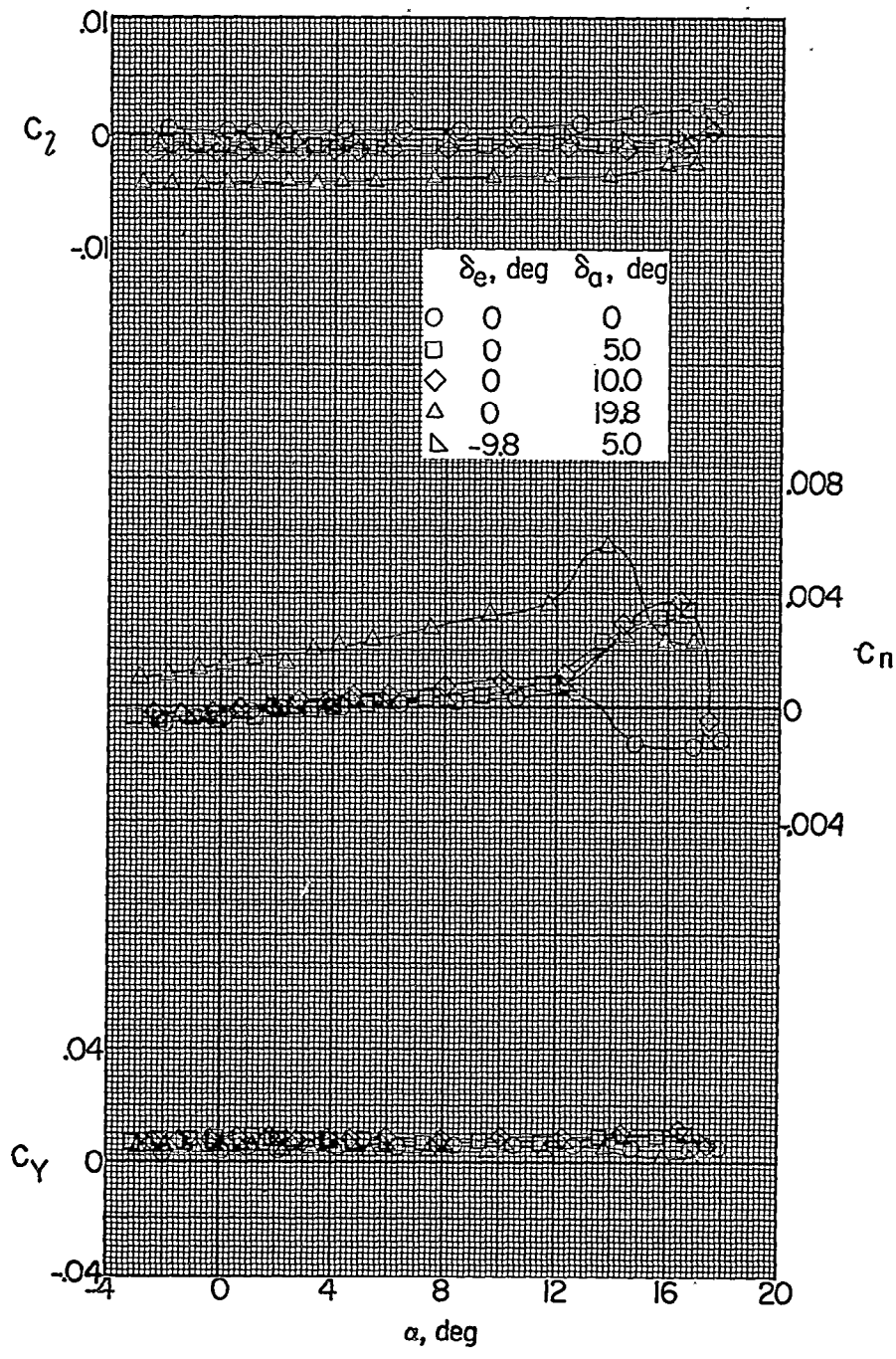

(c) M = 2.00.

Figure 15.- Concluded.

[redacted]

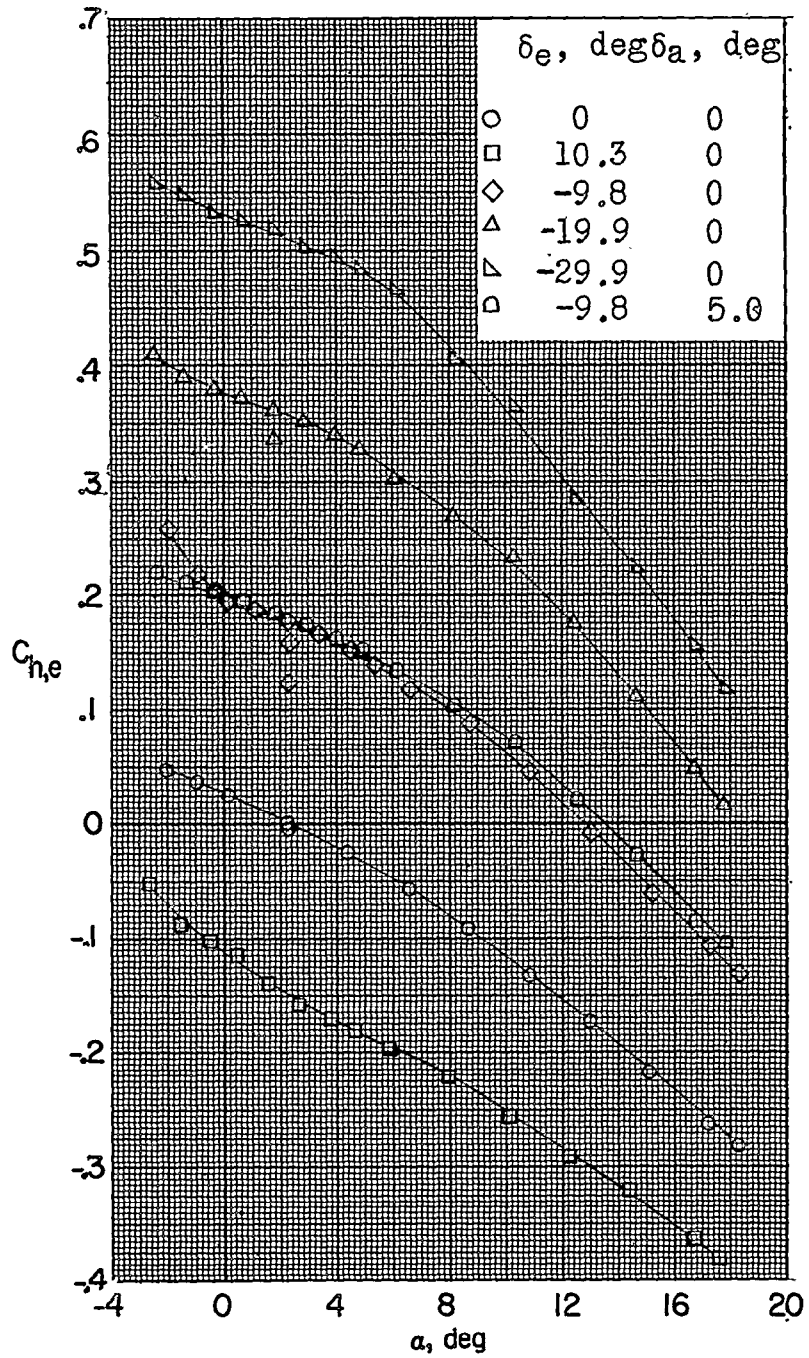

(a) M = 1.60.

Figure 16.- Variation of elevator hinge-moment coefficient with angle of attack.

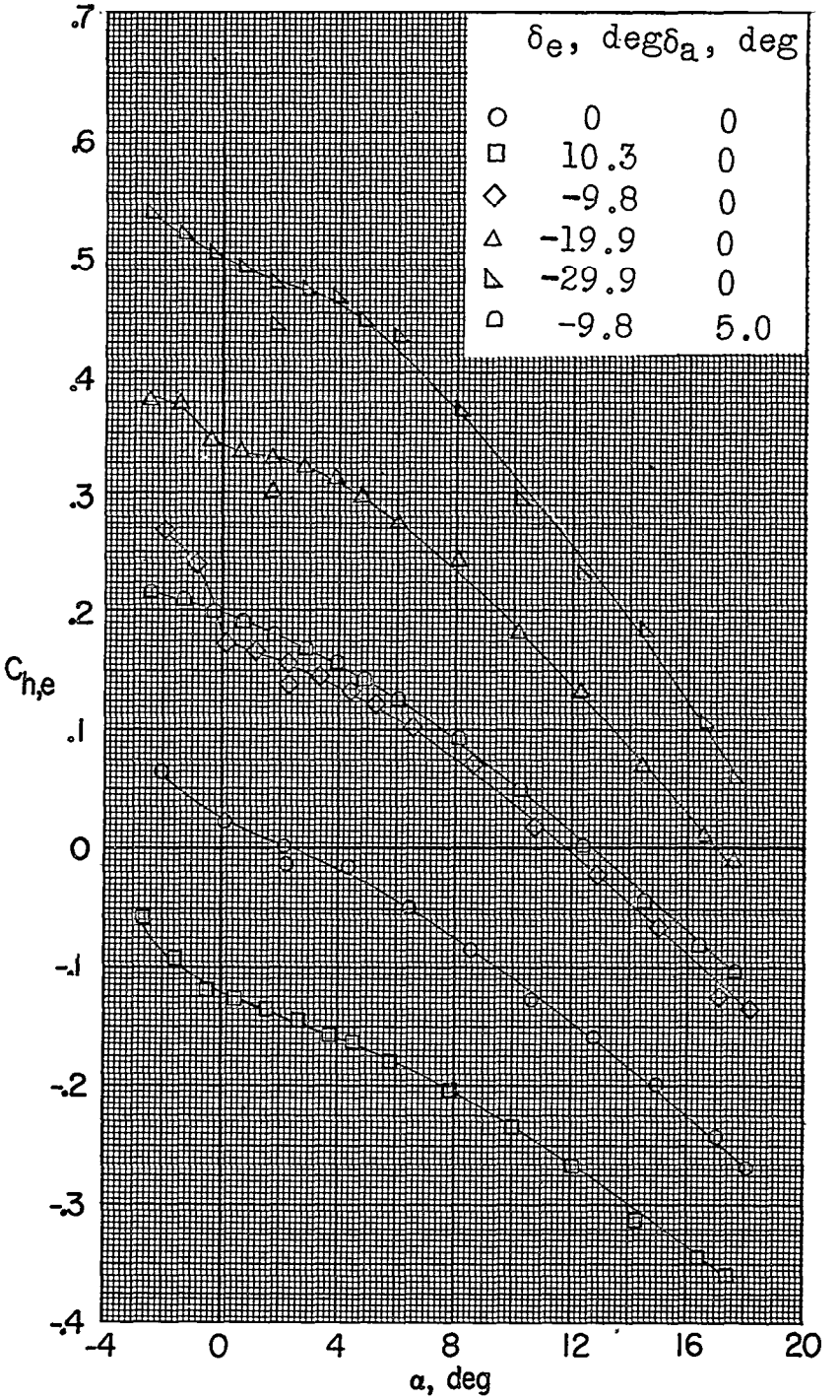

(b) M = 1.80.

Figure 16.- Continued.

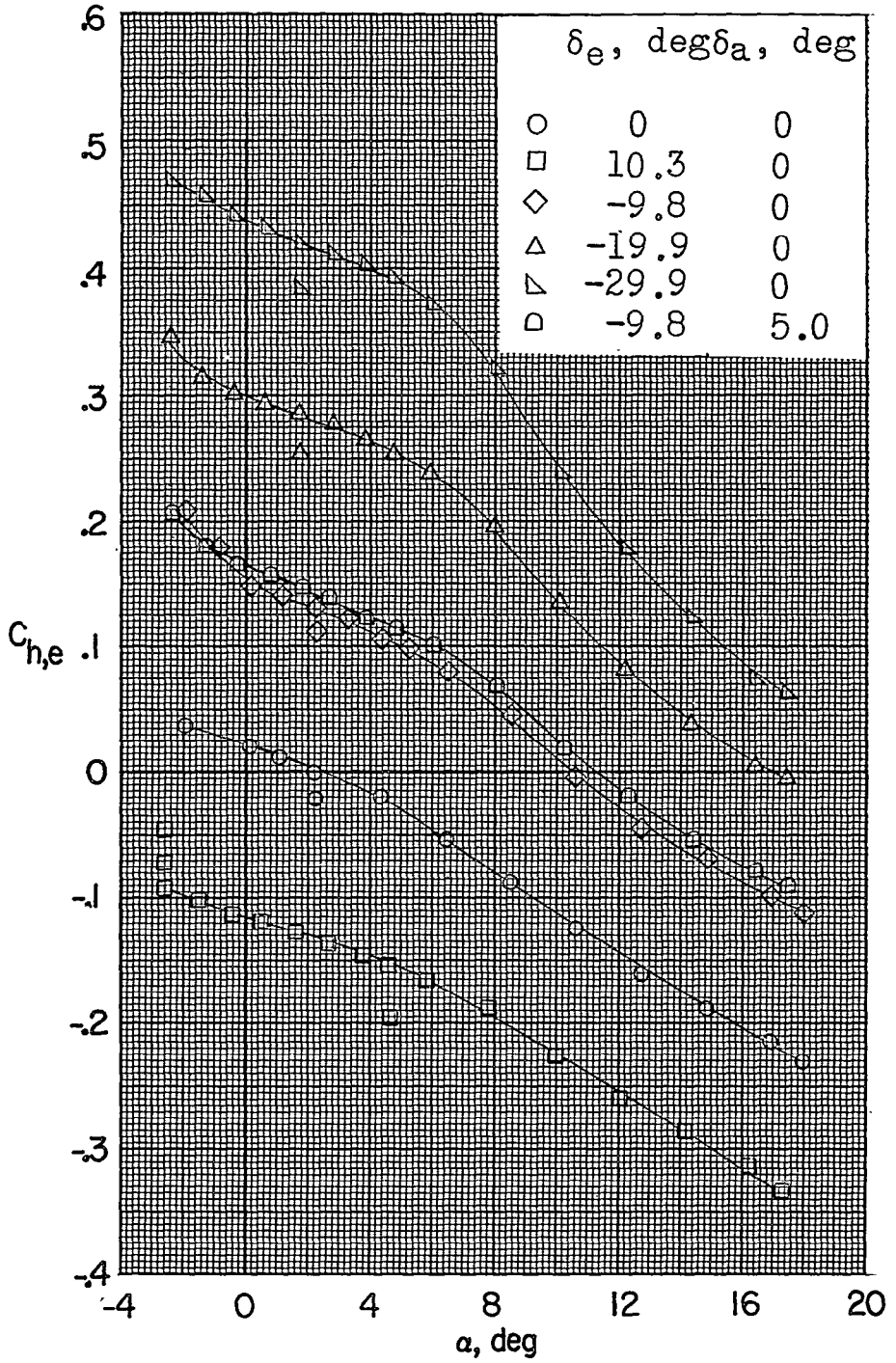

(c) M = 2.00.

Figure 16.- Concluded.

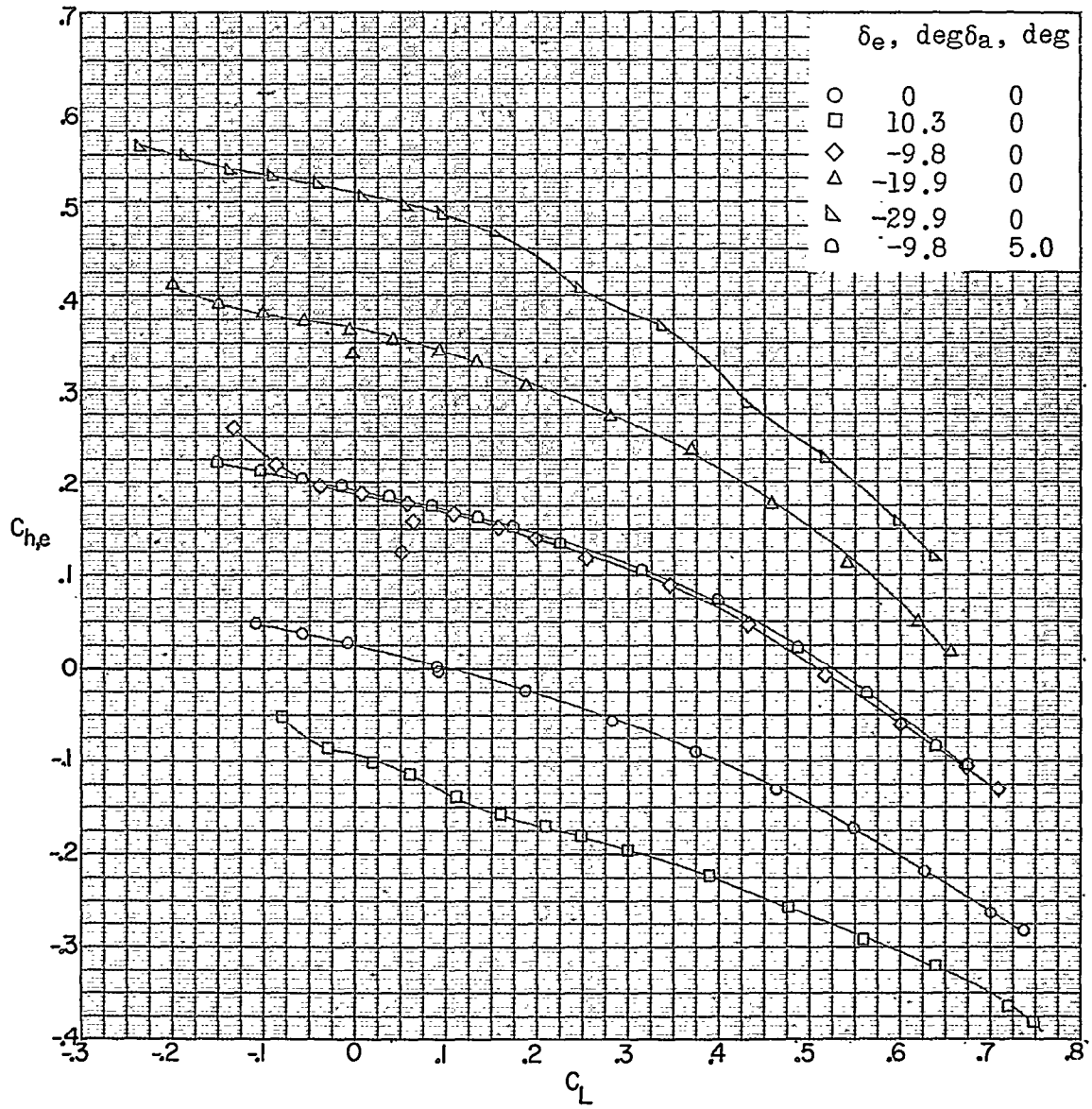

(a) M = 1.60.

Figure 17.- Variation of elevator hinge-moment coefficient with lift coefficient.

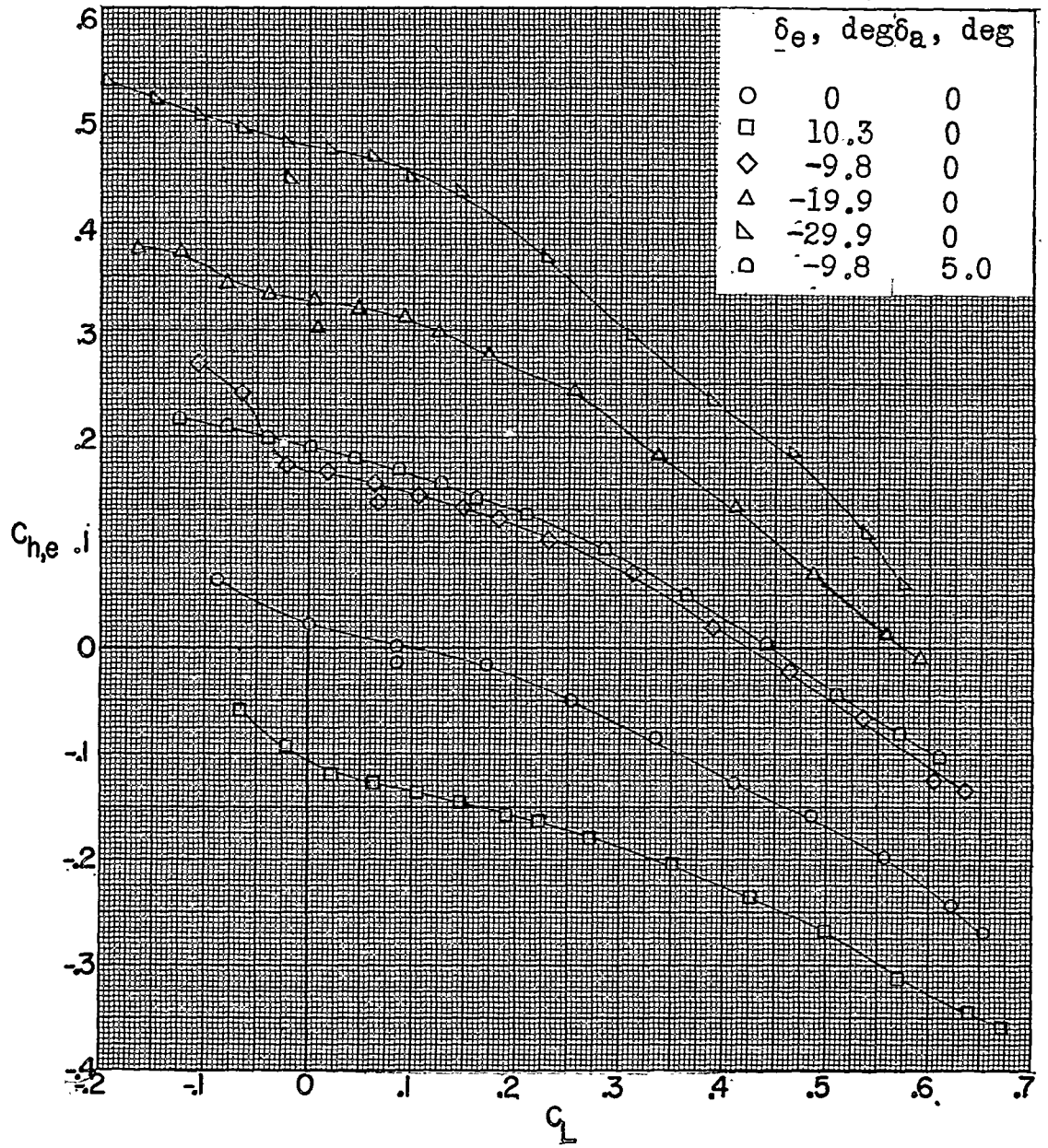

(b) M = 1.80.

Figure 17.- Continued.

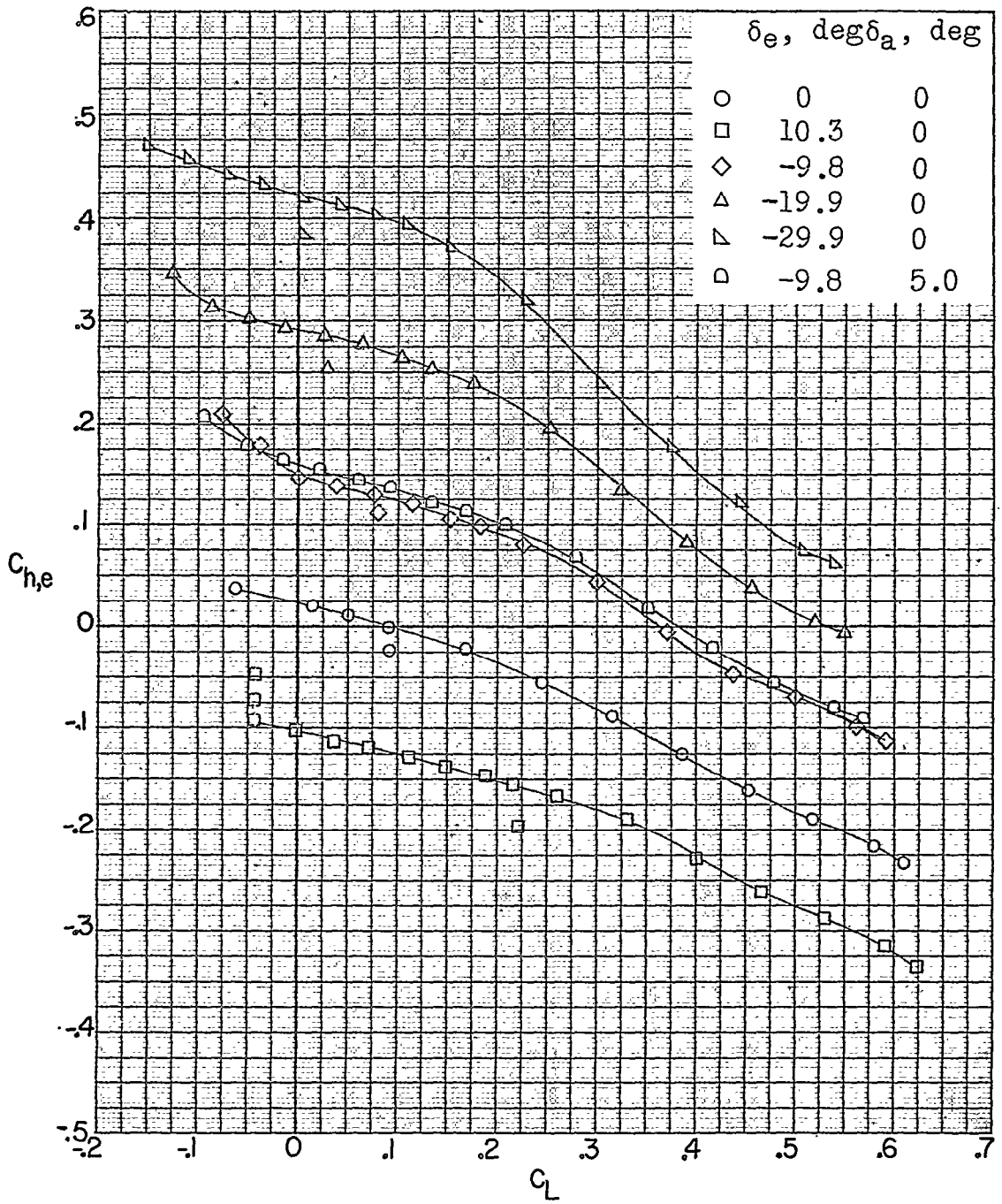

(c) M = 2.00.

Figure 17.- Concluded.

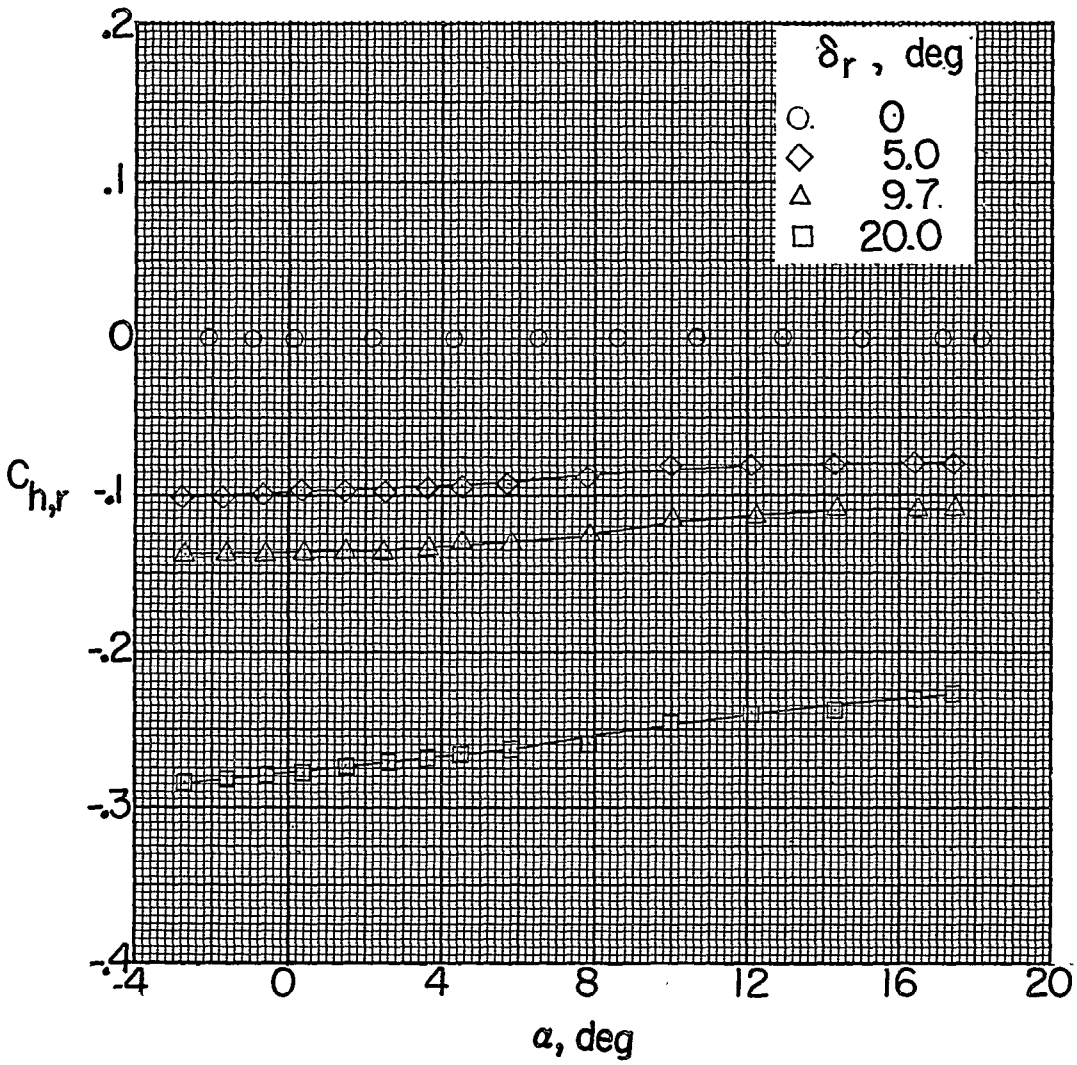

(a) M = 1.60.

Figure 18.- Variation of rudder hinge-moment coefficient with angle of attack.

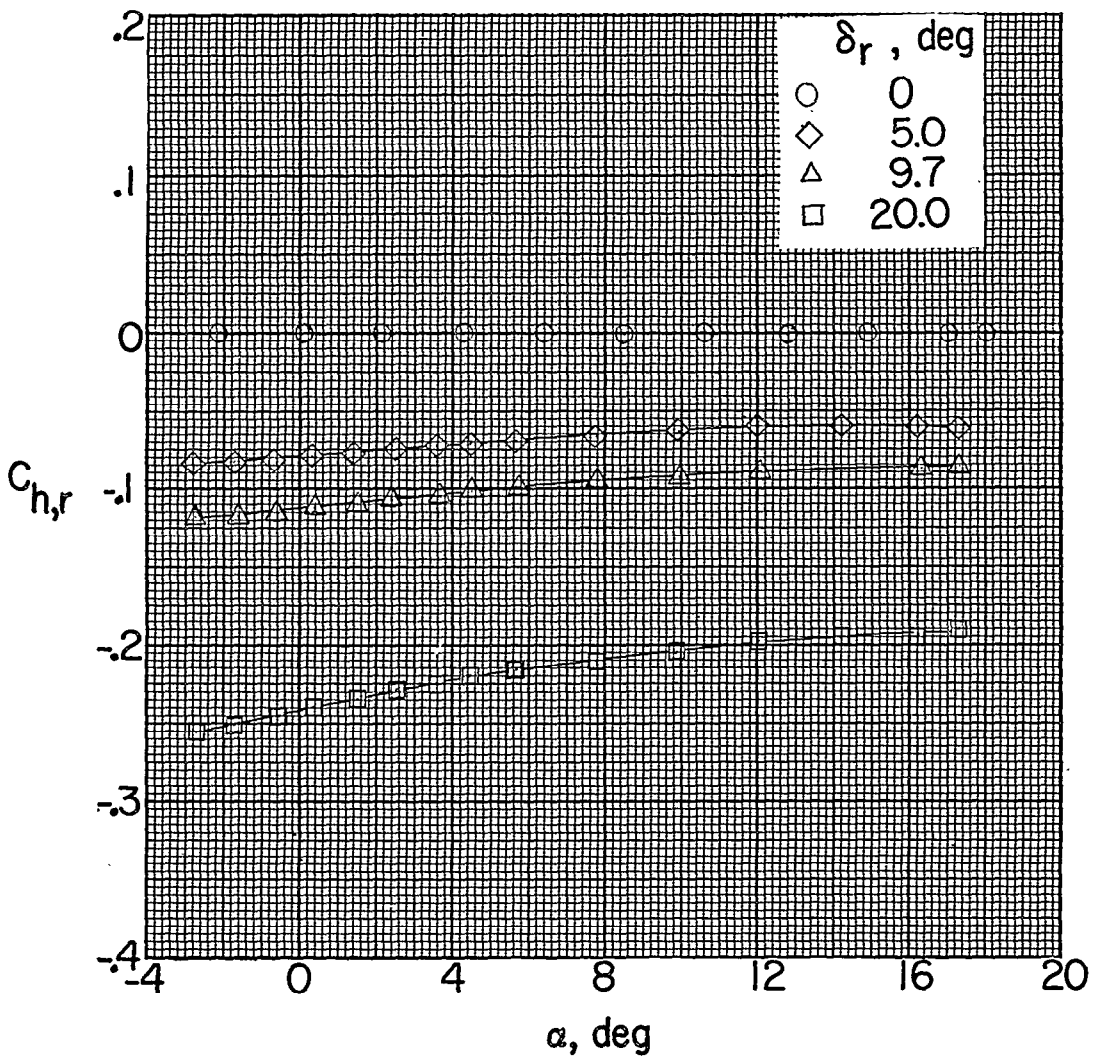

(b) M = 1.80.

Figure 18.- Continued.

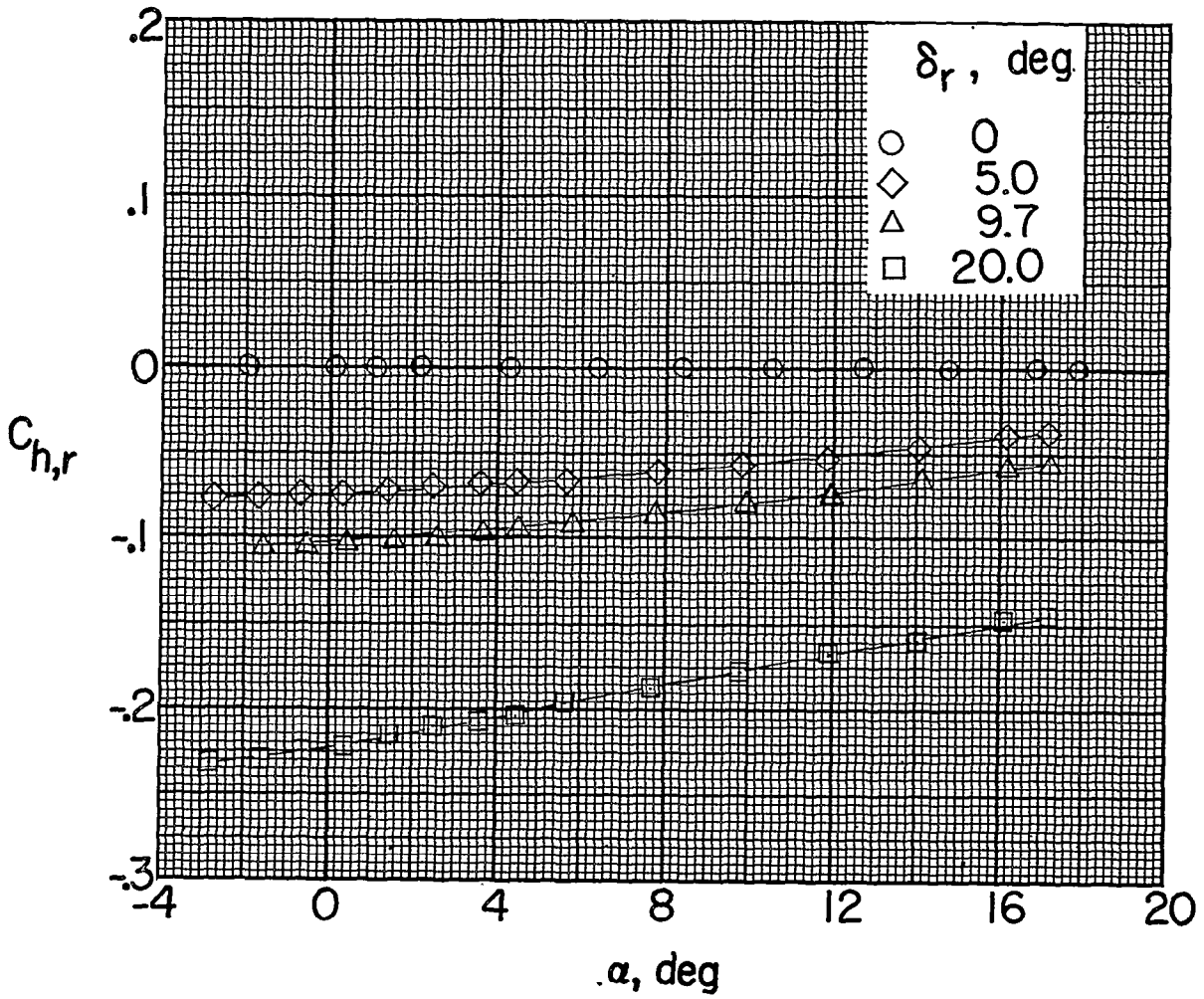

(c) M = 2.00.

Figure 18.- Concluded.

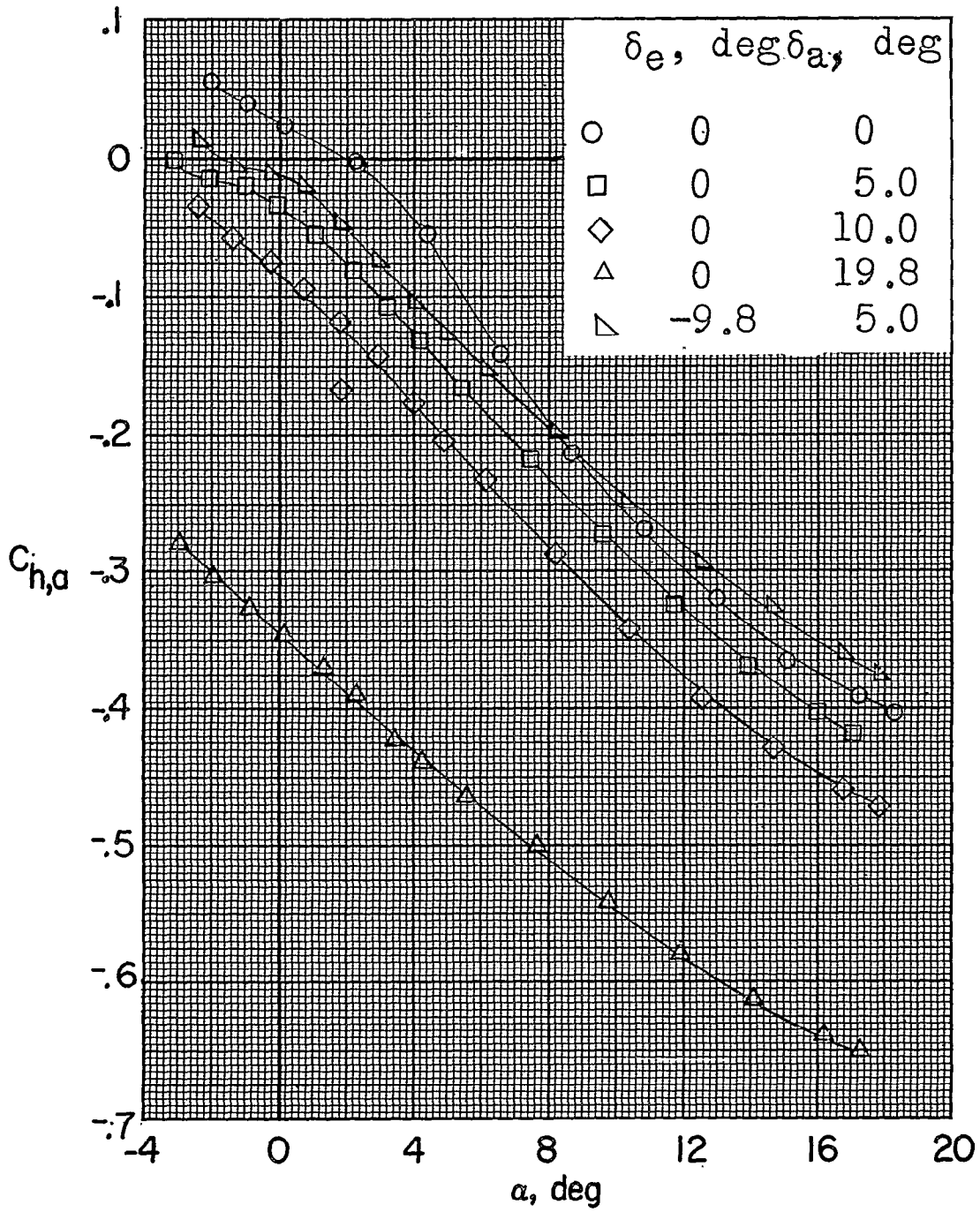

(a) M = 1.60.

Figure 19.- Variation of aileron hinge-moment coefficient with angle of attack.

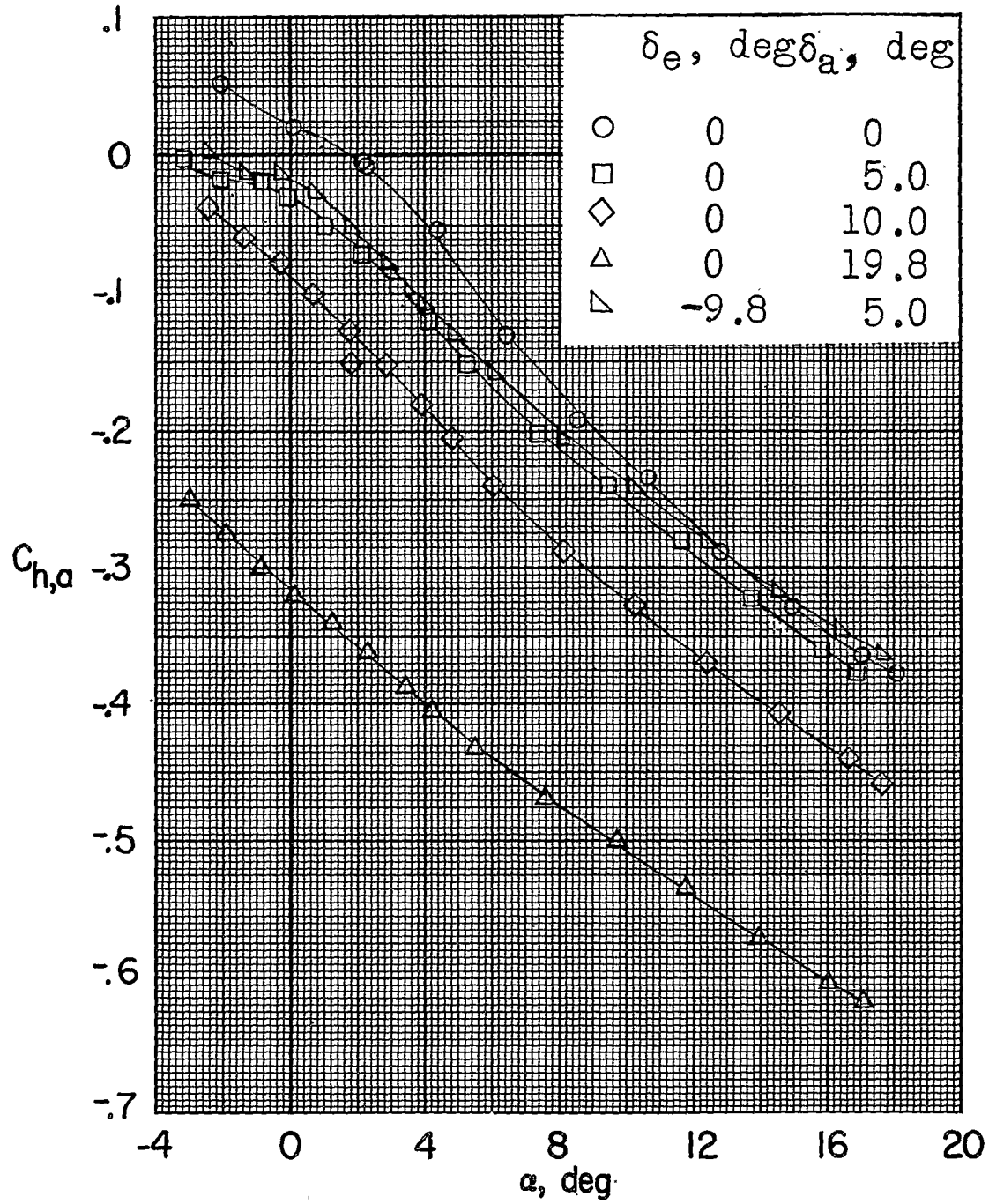

(b) M = 1.80.

Figure 19.- Continued.

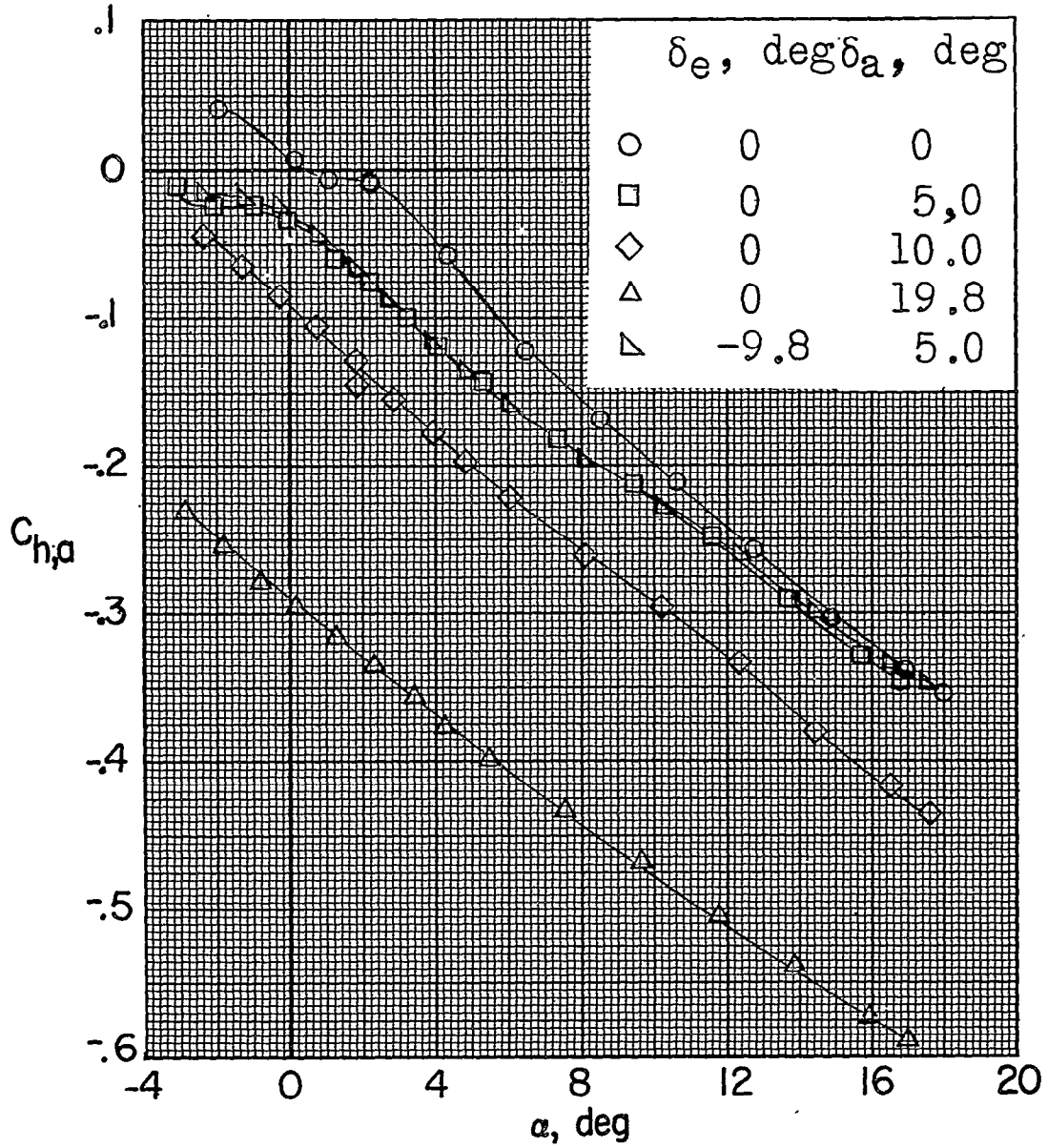

(c) M = 2.00.

Figure 19.- Concluded.

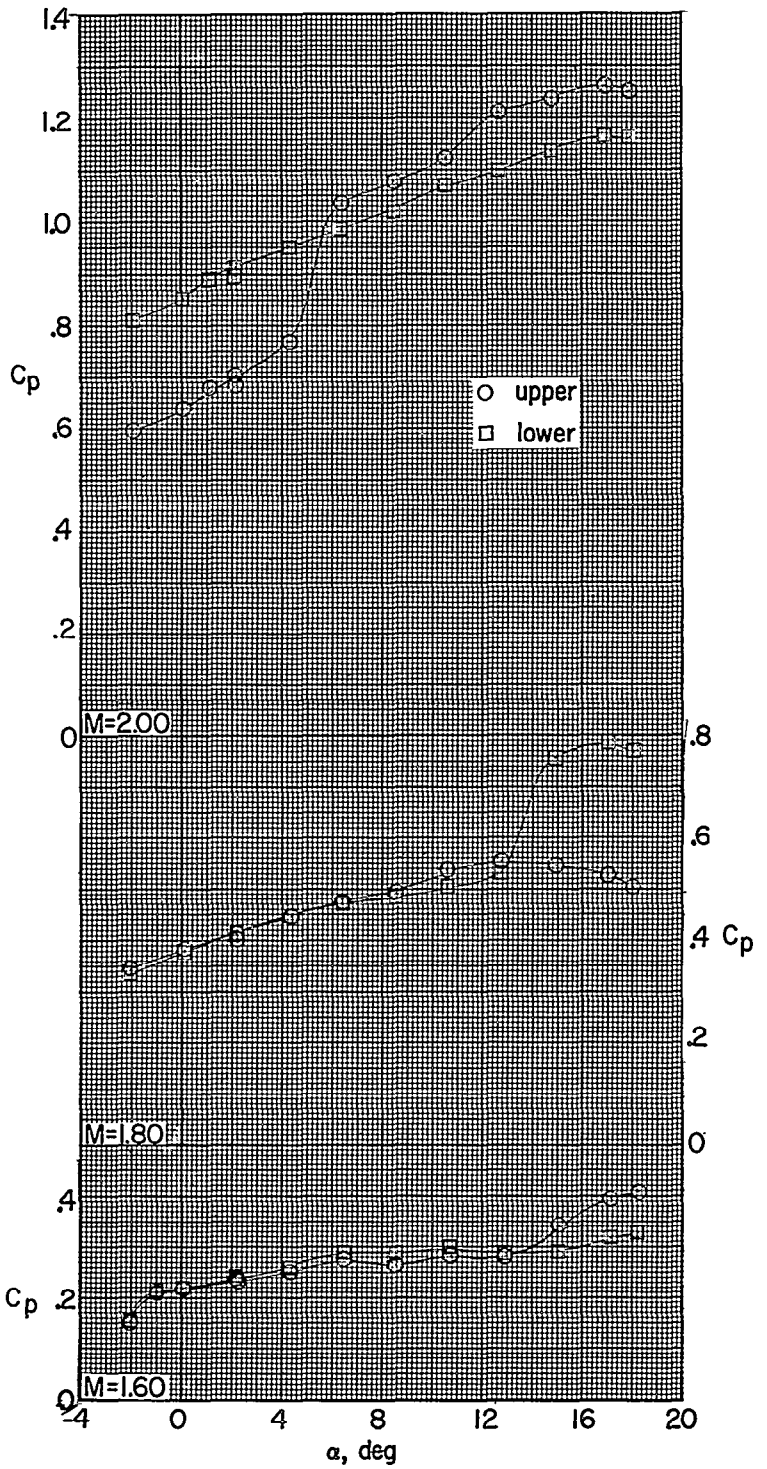

Figure 20.-Variation of pressure coefficient with angle of attack for probes at tip of vertical tail.

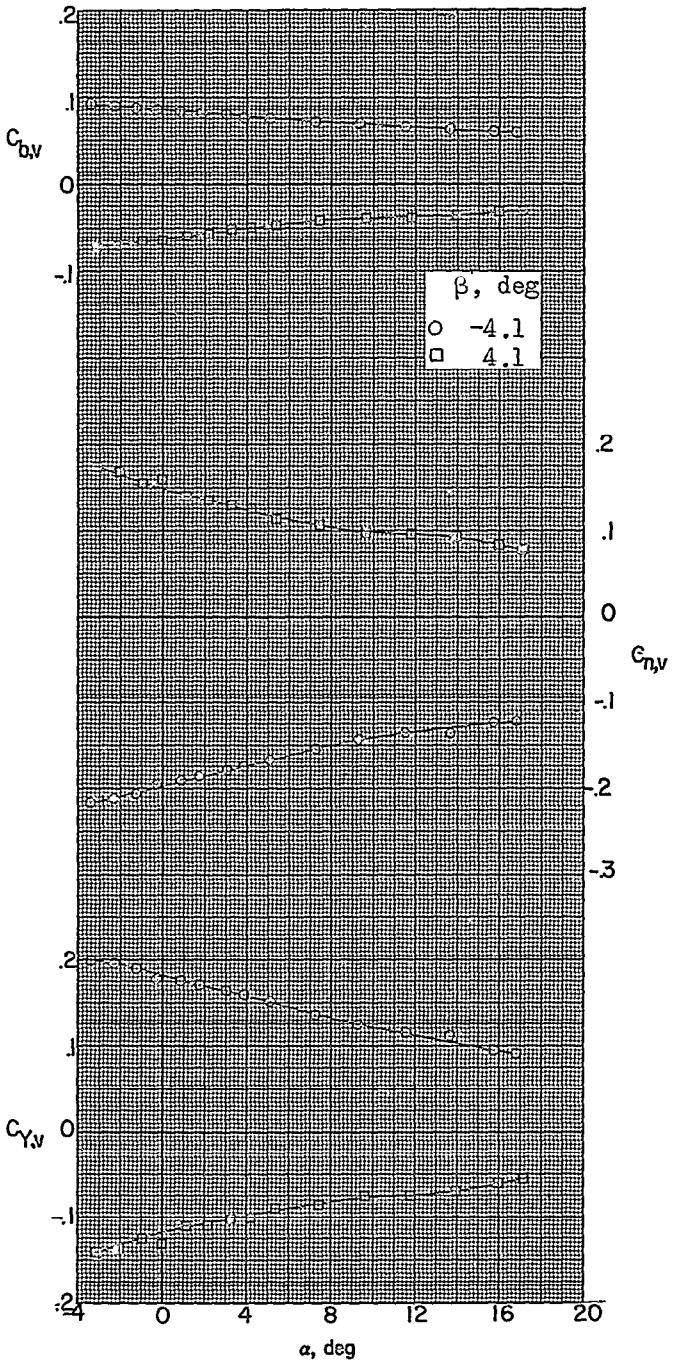

(a) M = 1.60.

Figure 21.- Variation of vertical-tail loads of test model with angle of attack; $\delta_e = \delta_r = \delta_a = 0^o$.

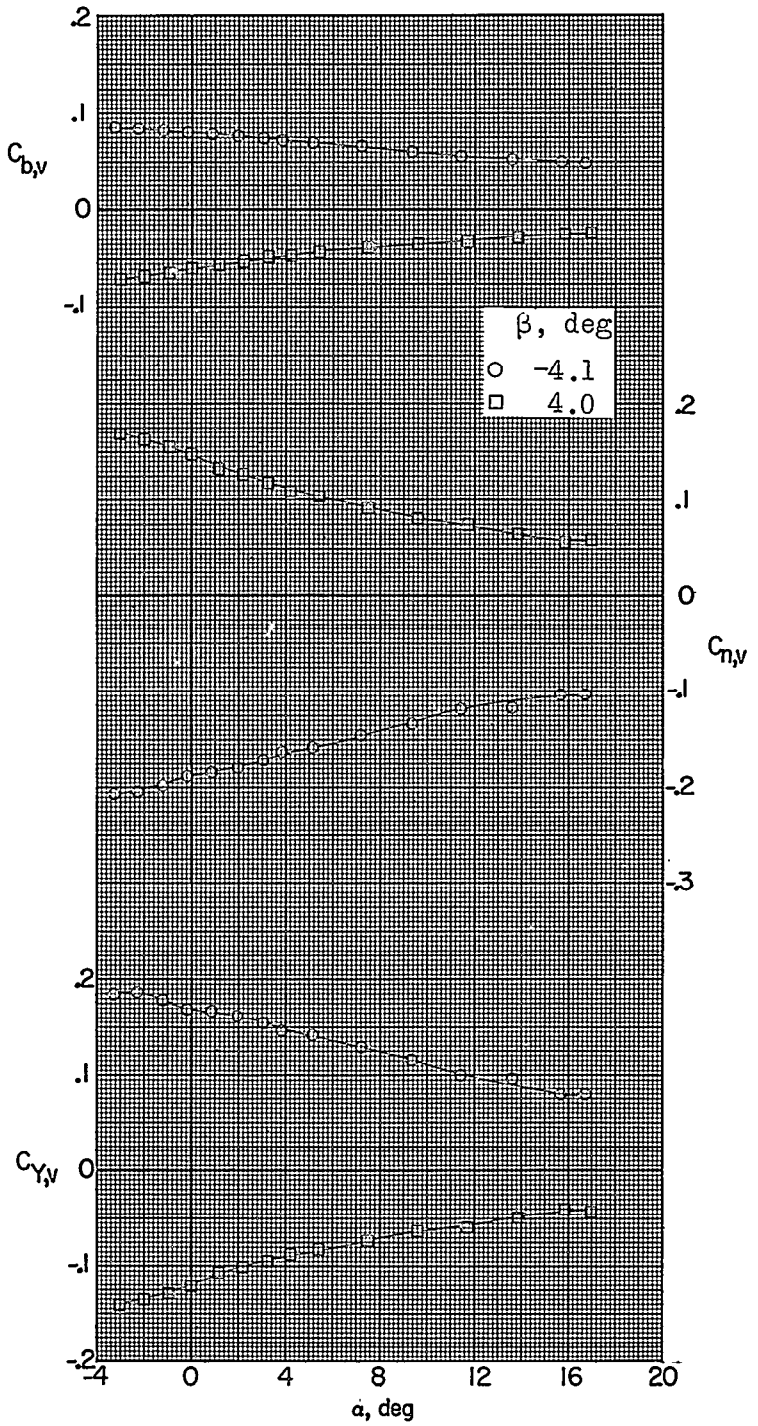

(b) M = 1.80.

Figure 21.- Continued.

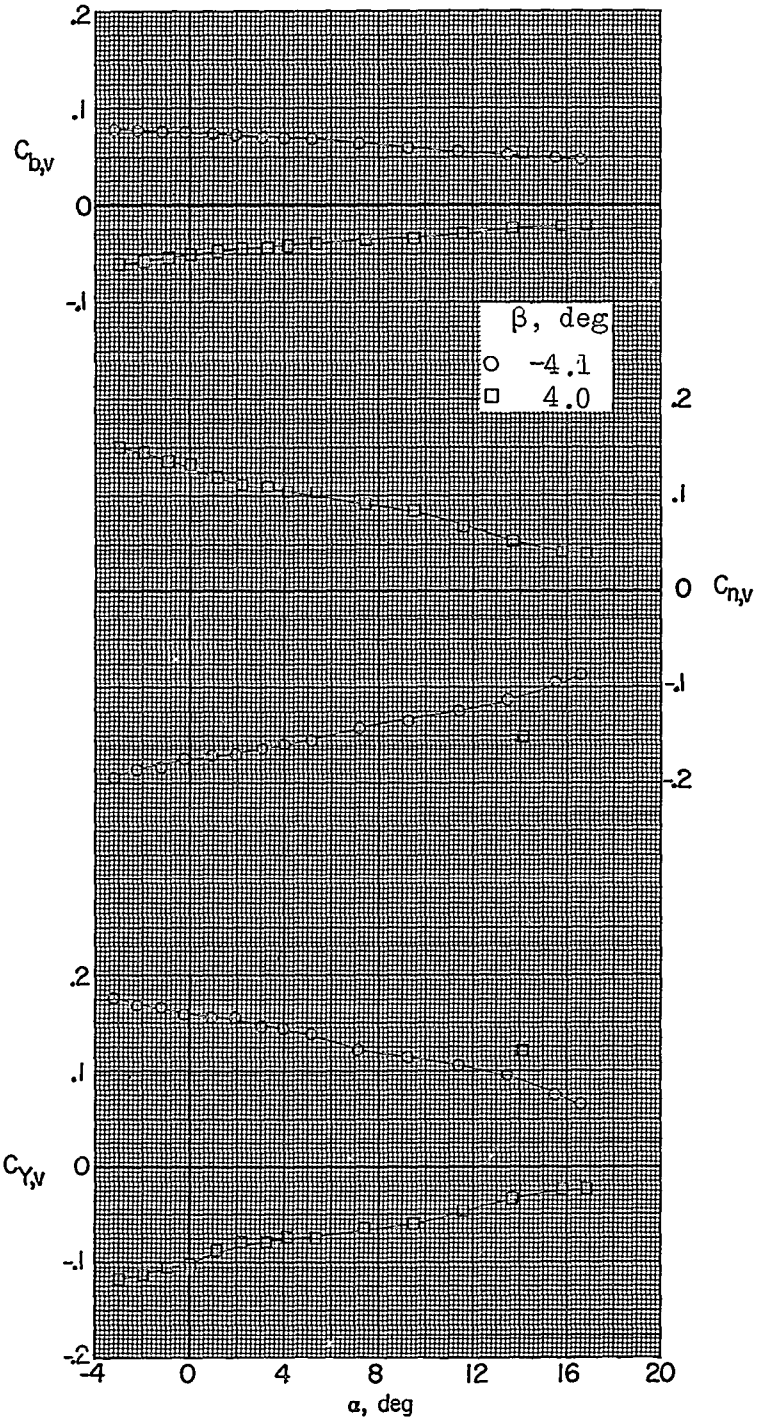

(c) M = 2.00.

Figure 21.- Concluded.

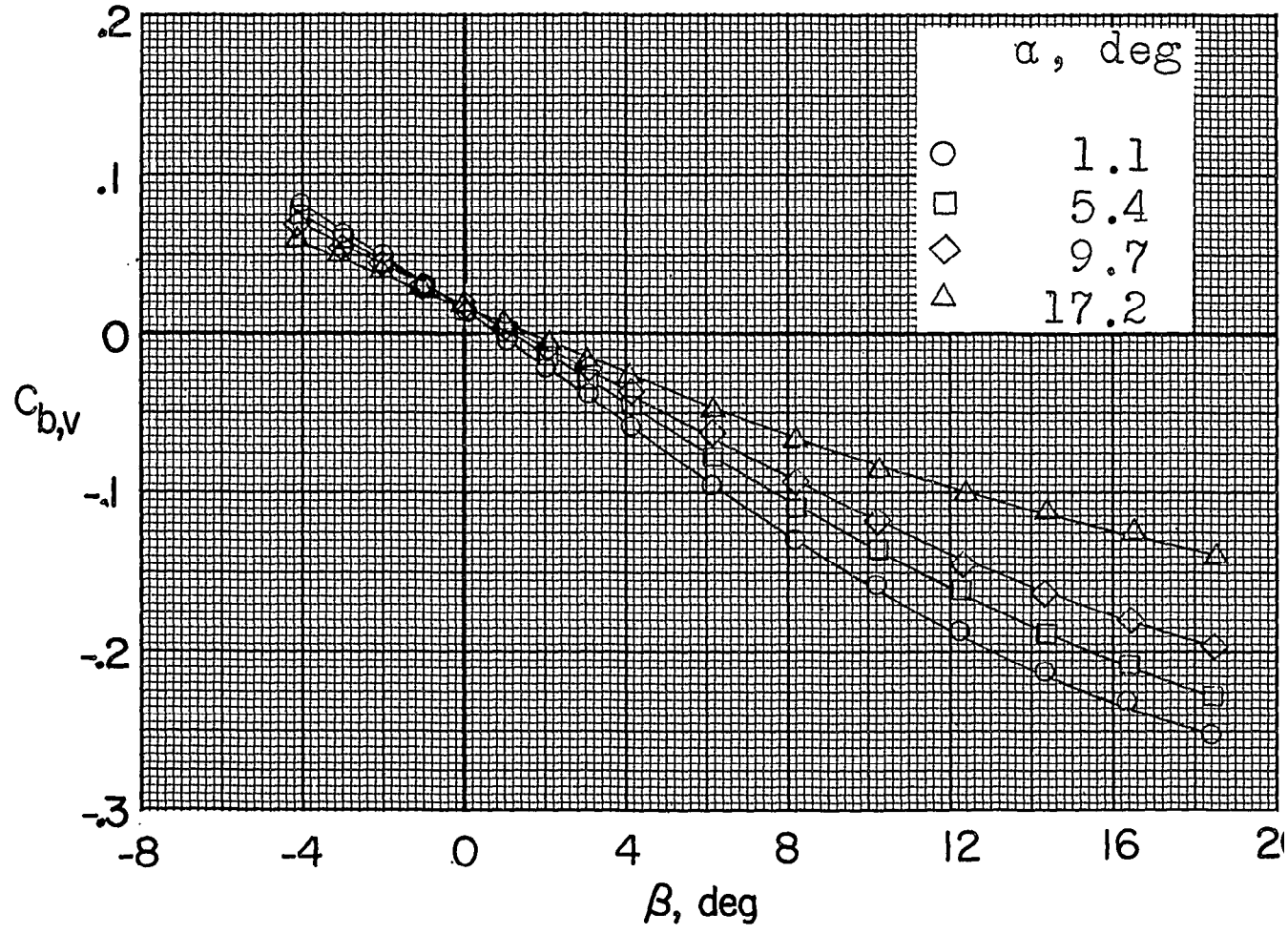

(a) M = 1.60.

Figure 22.- Variation of aerodynamic characteristics of vertical-tail loads with ang sideslip.

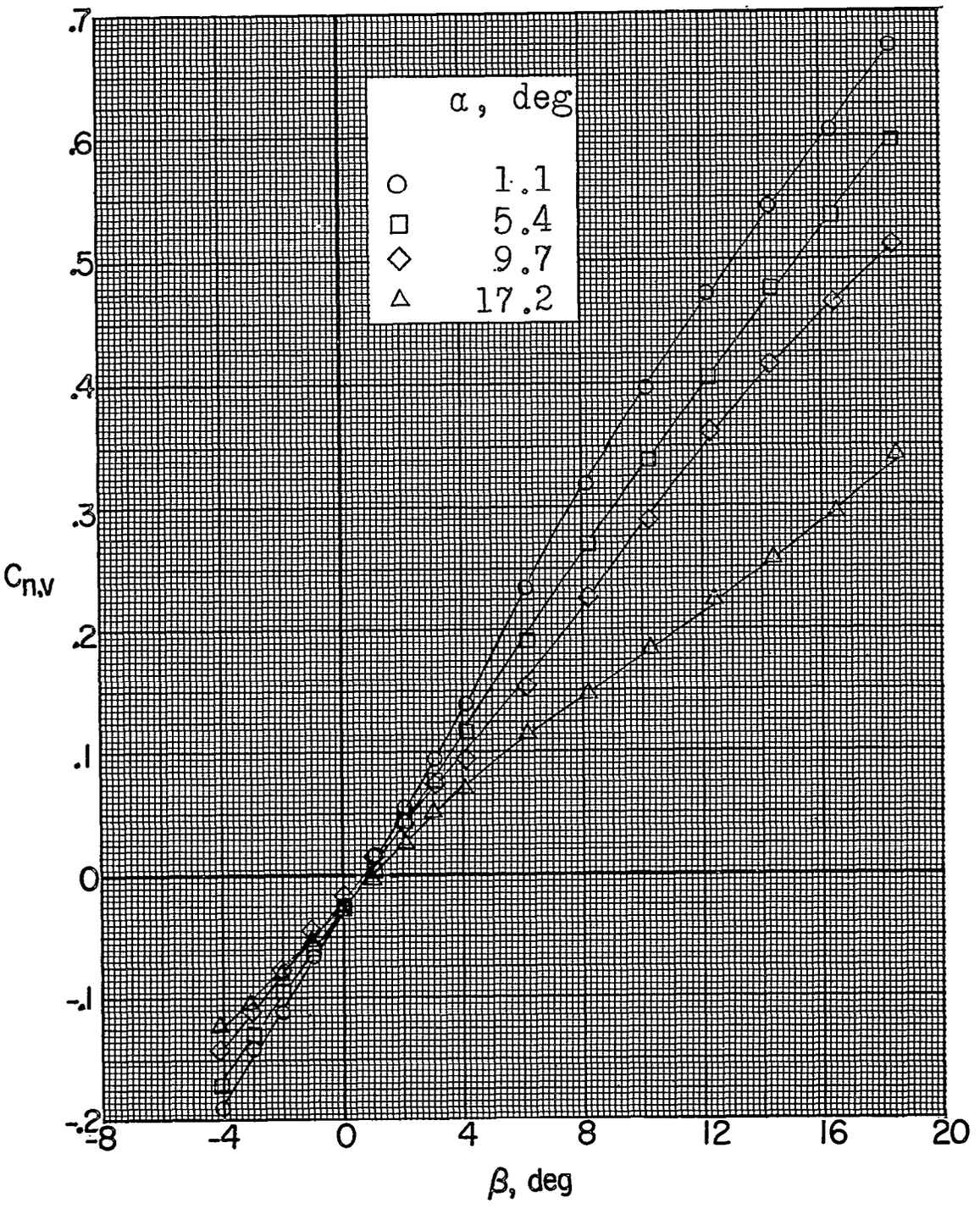

(a) Continued.

Figure 22.- Continued.

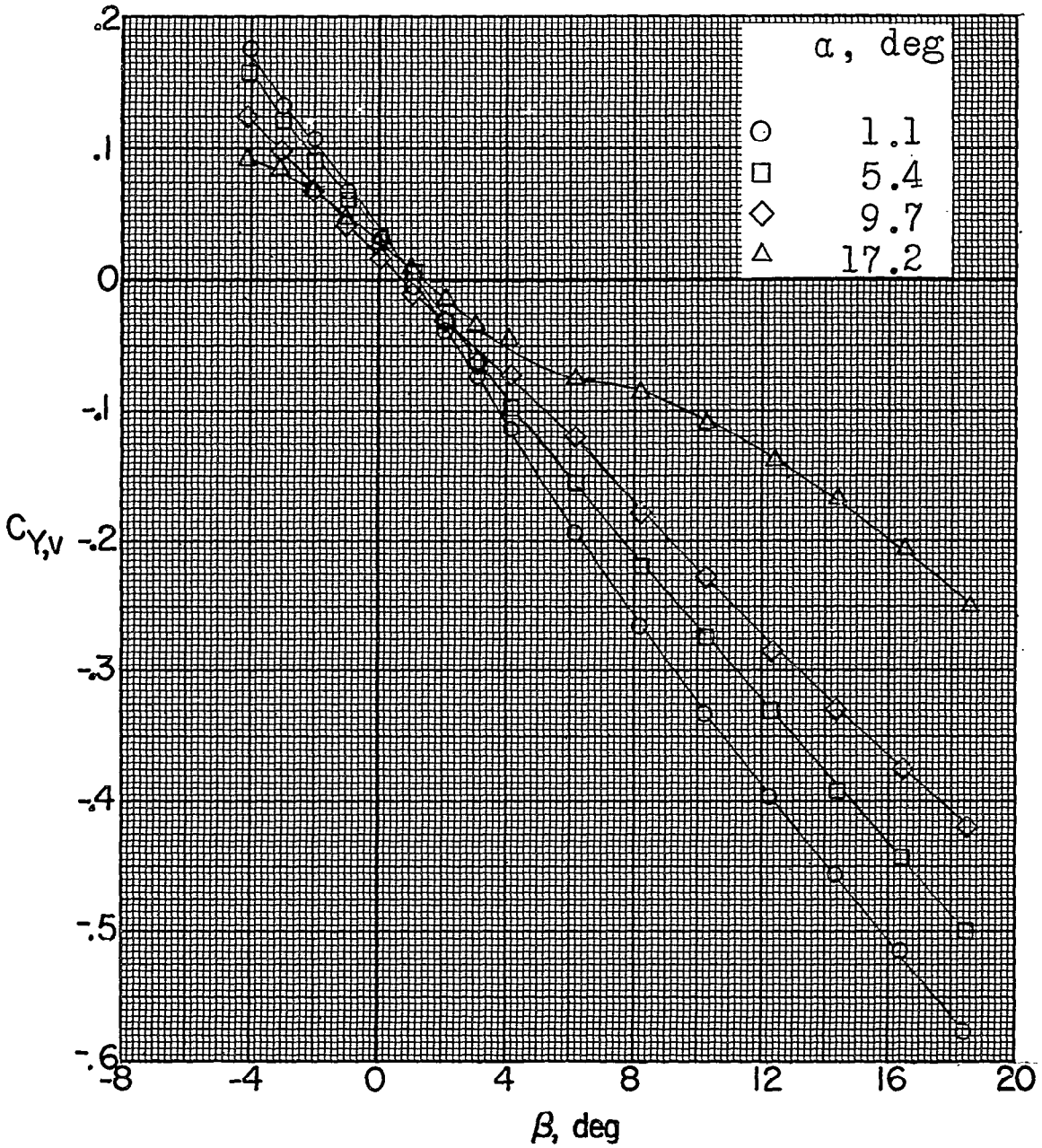

(a) Concluded.

Figure 22.- Continued.

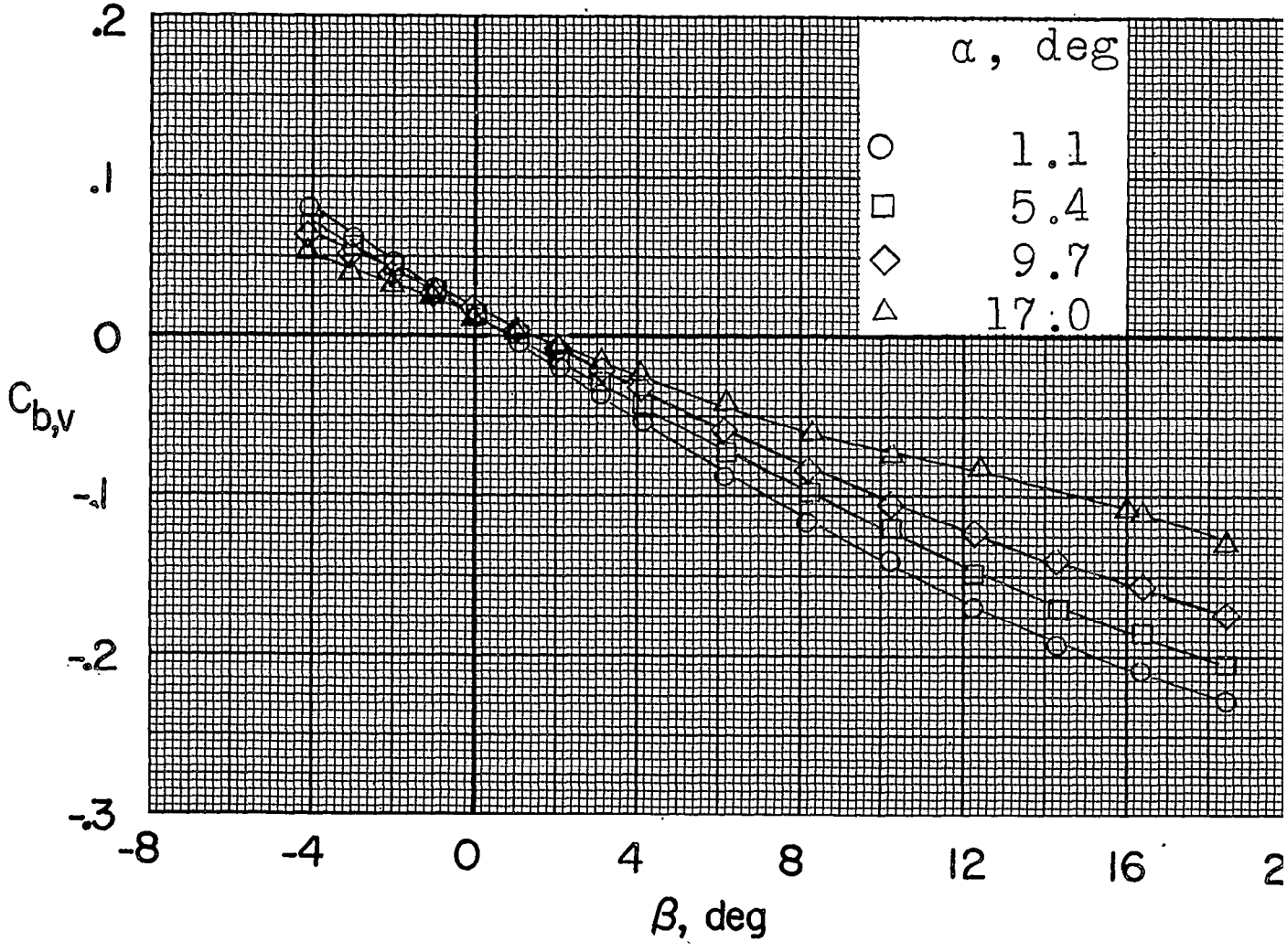

(b) M = 1.80.

Figure 22.- Continued.

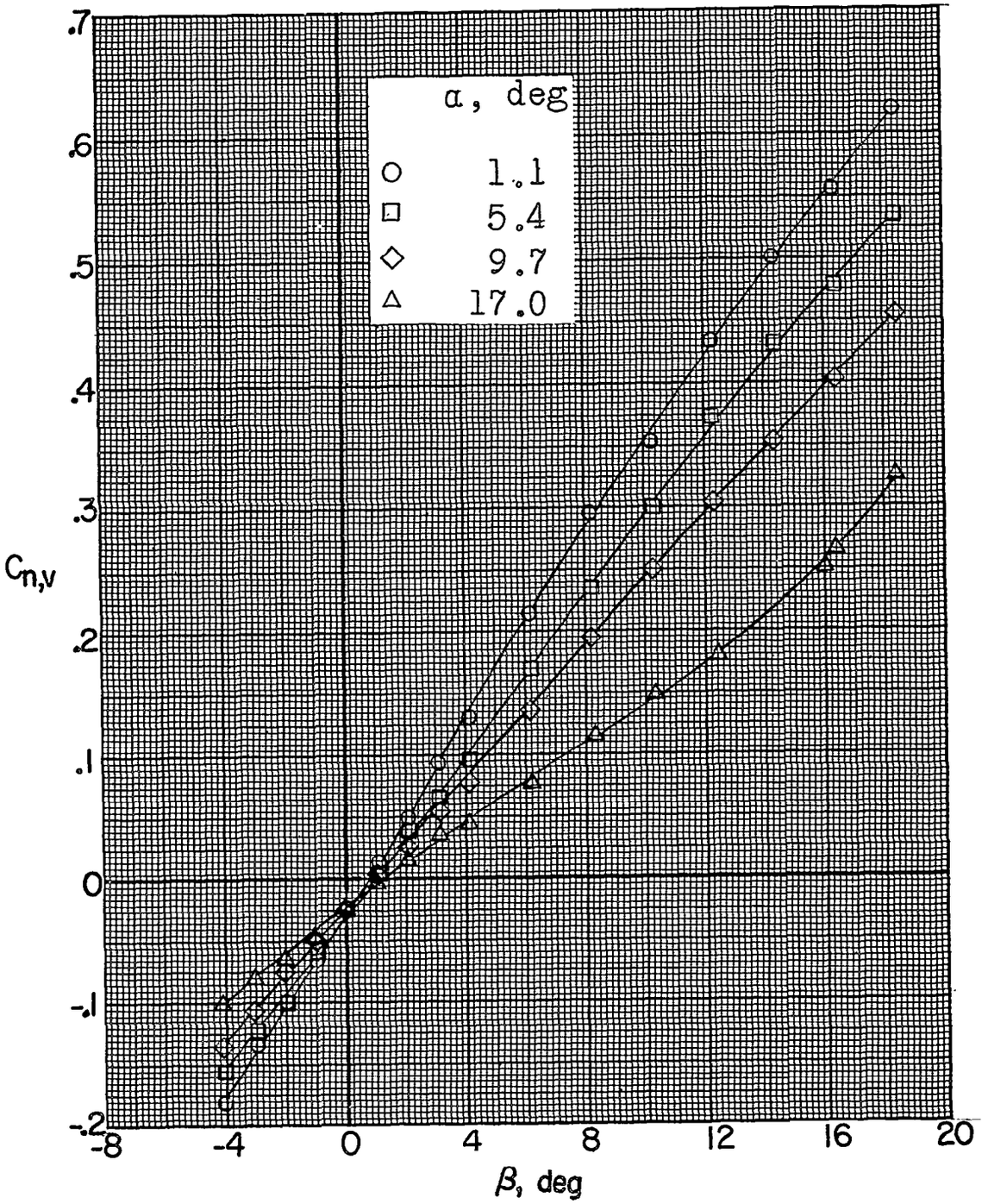

(b) Continued.

Figure 22.- Continued.

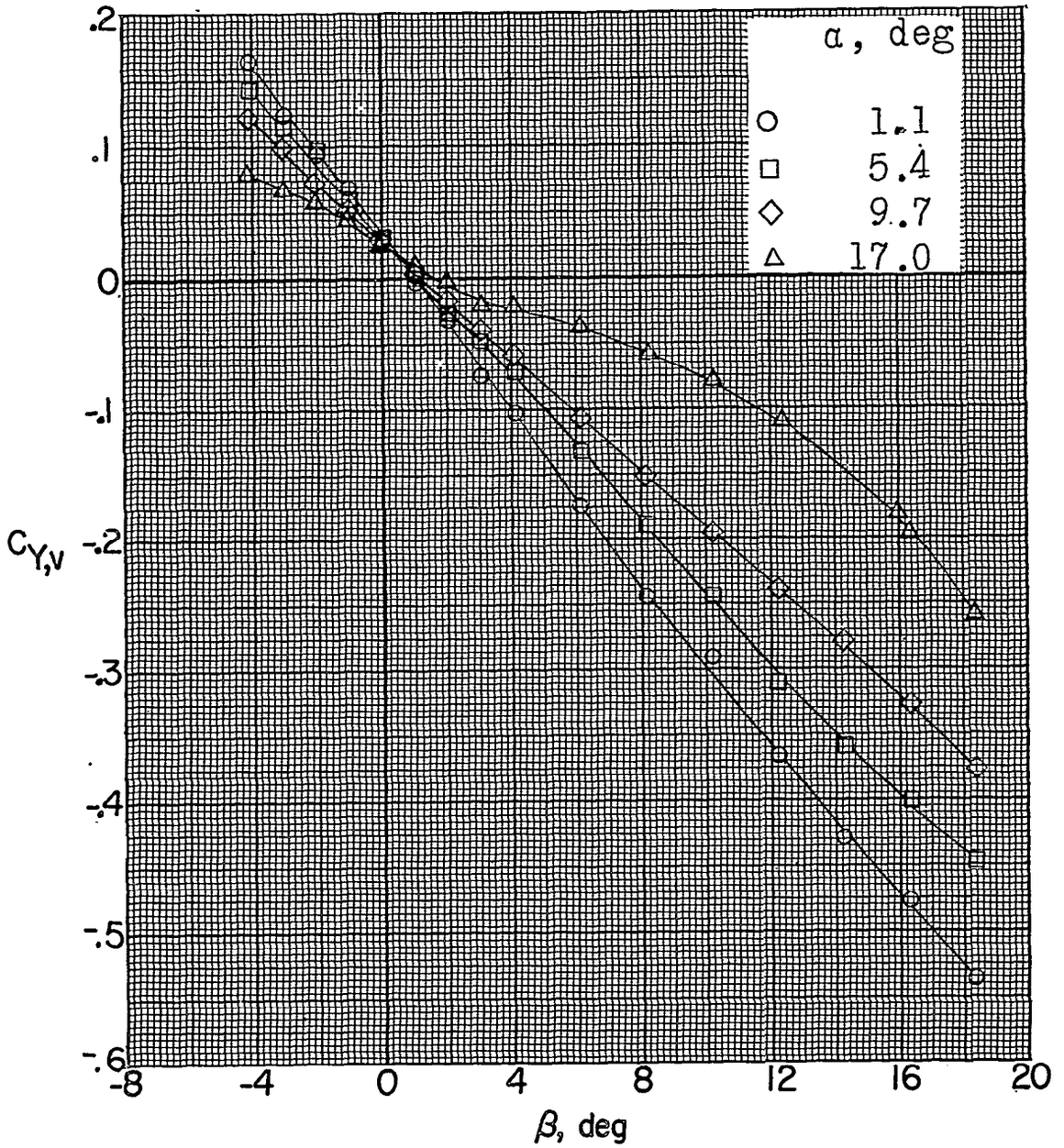

(b) Concluded.

Figure 22.- Continued.

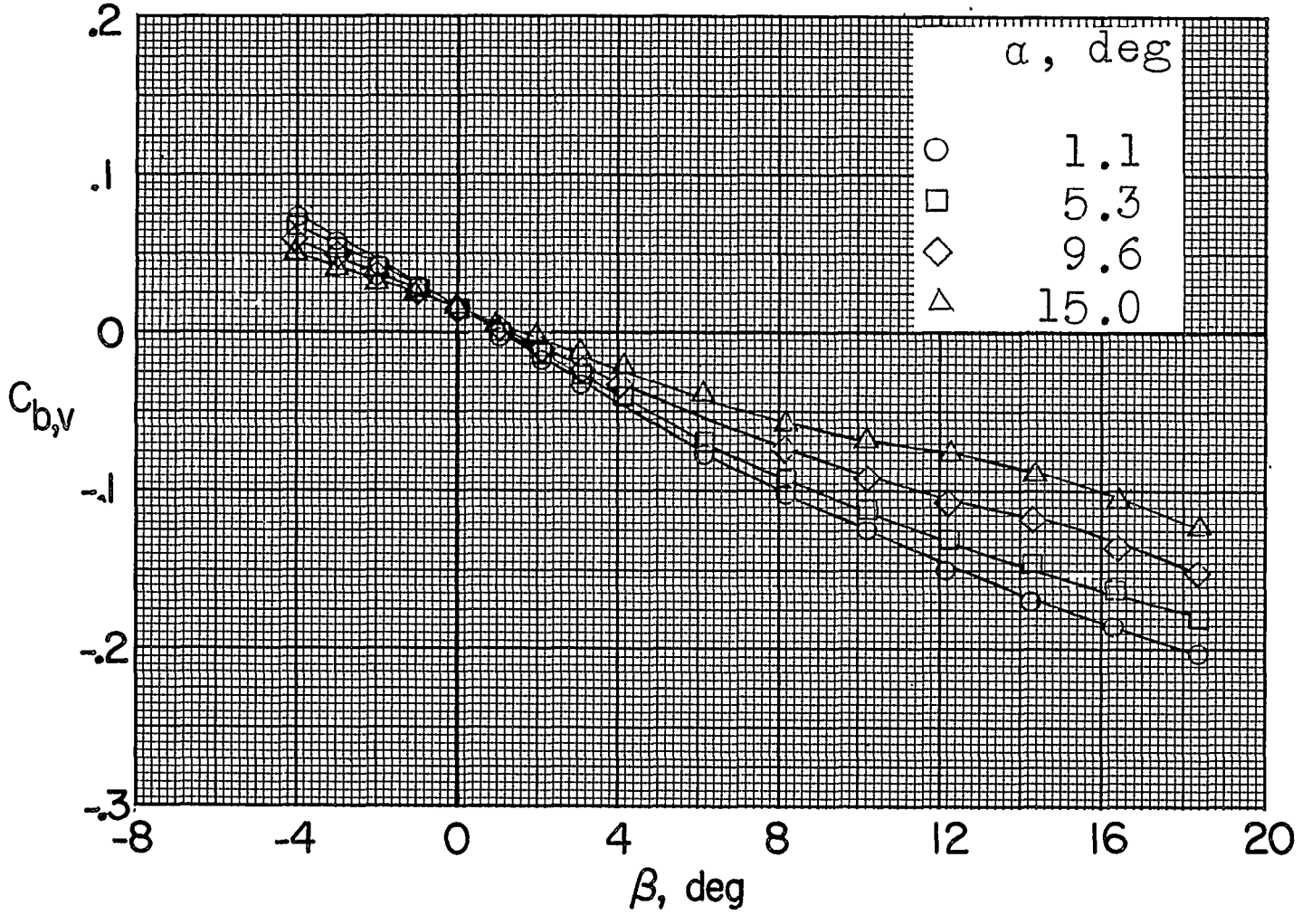

(c) M = 2.00.

Figure 22.- Continued.

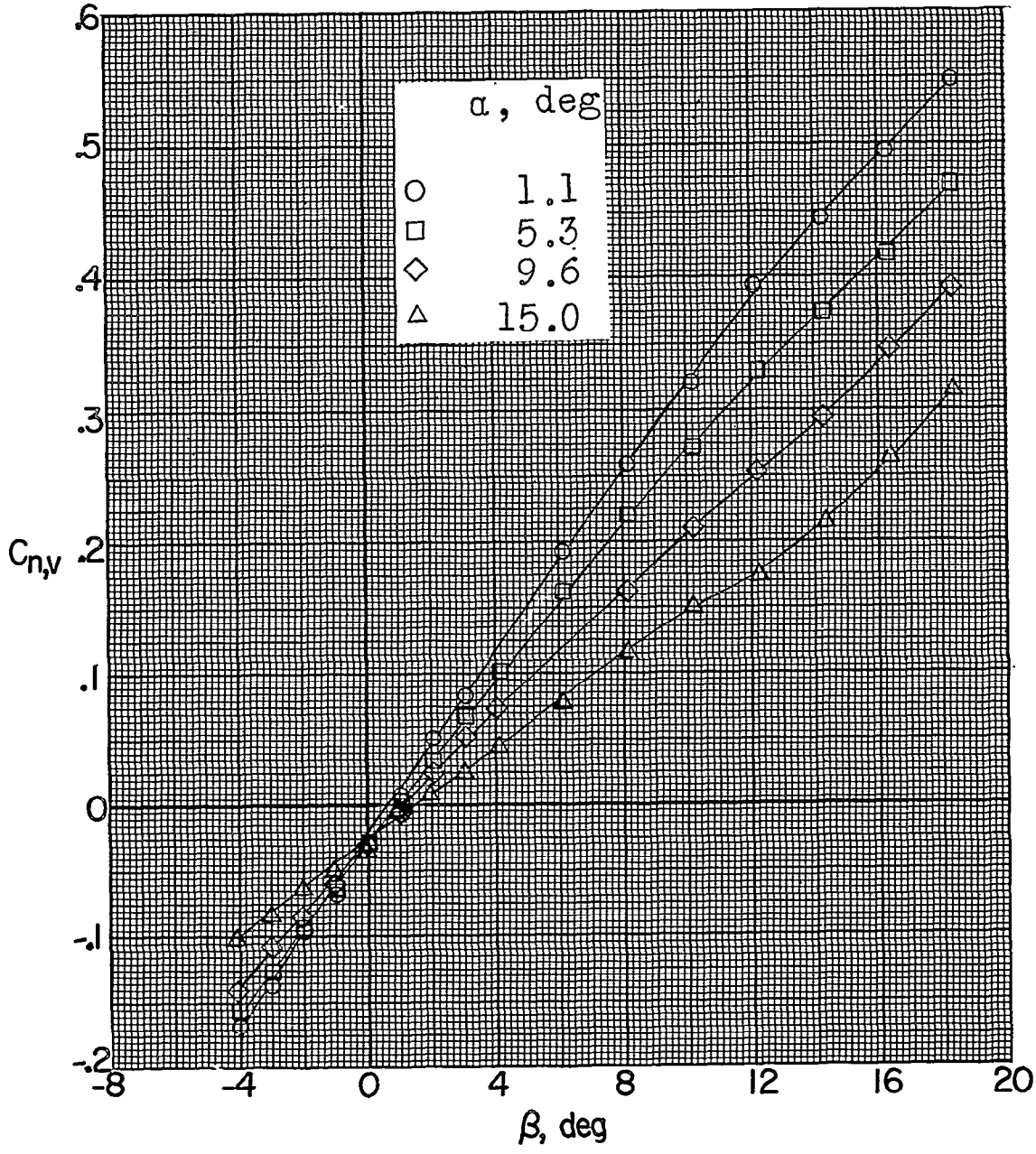

(c) Continued.

Figure 22.- Continued.

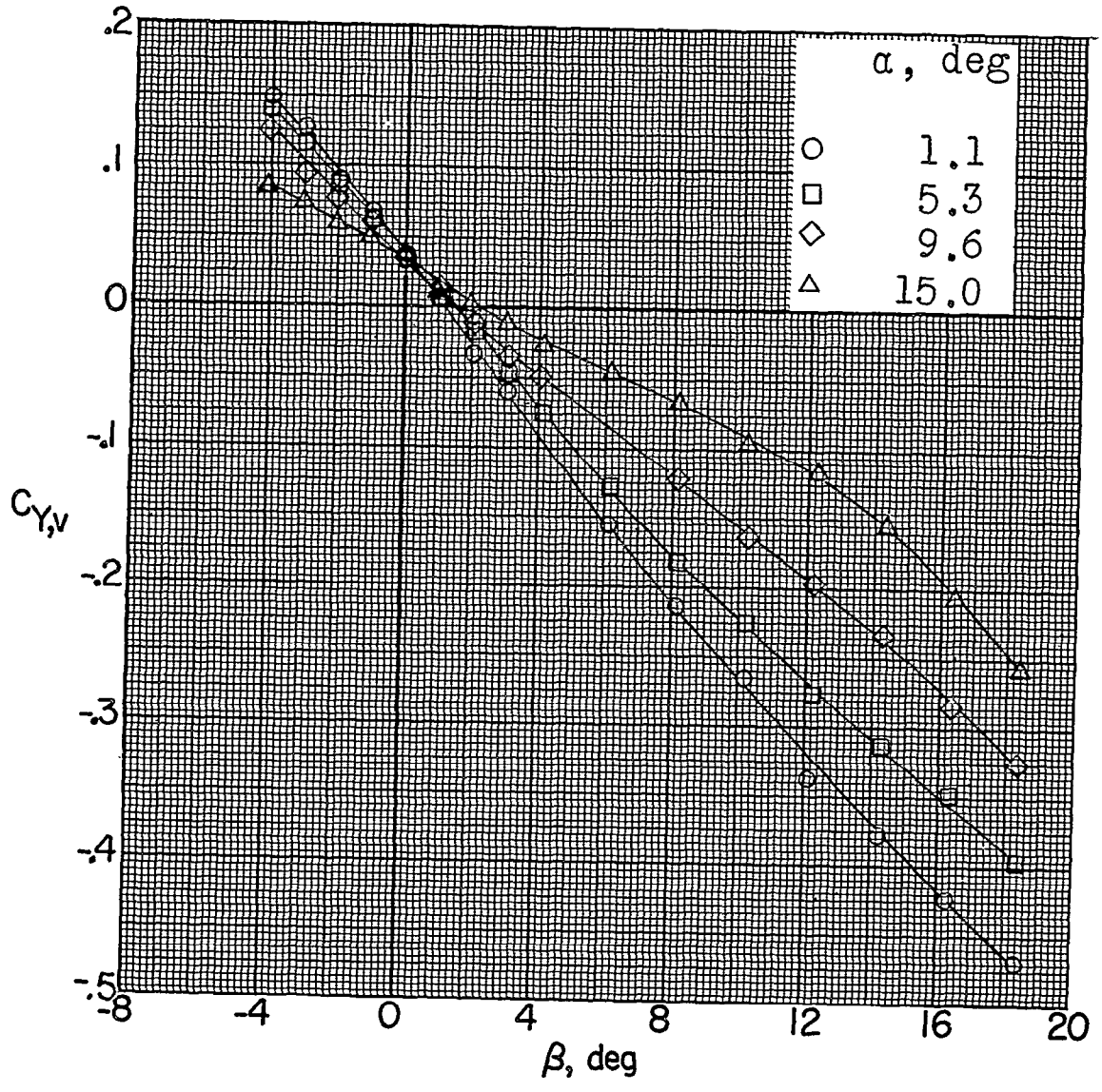

(c) Concluded.

Figure 22.- Concluded.

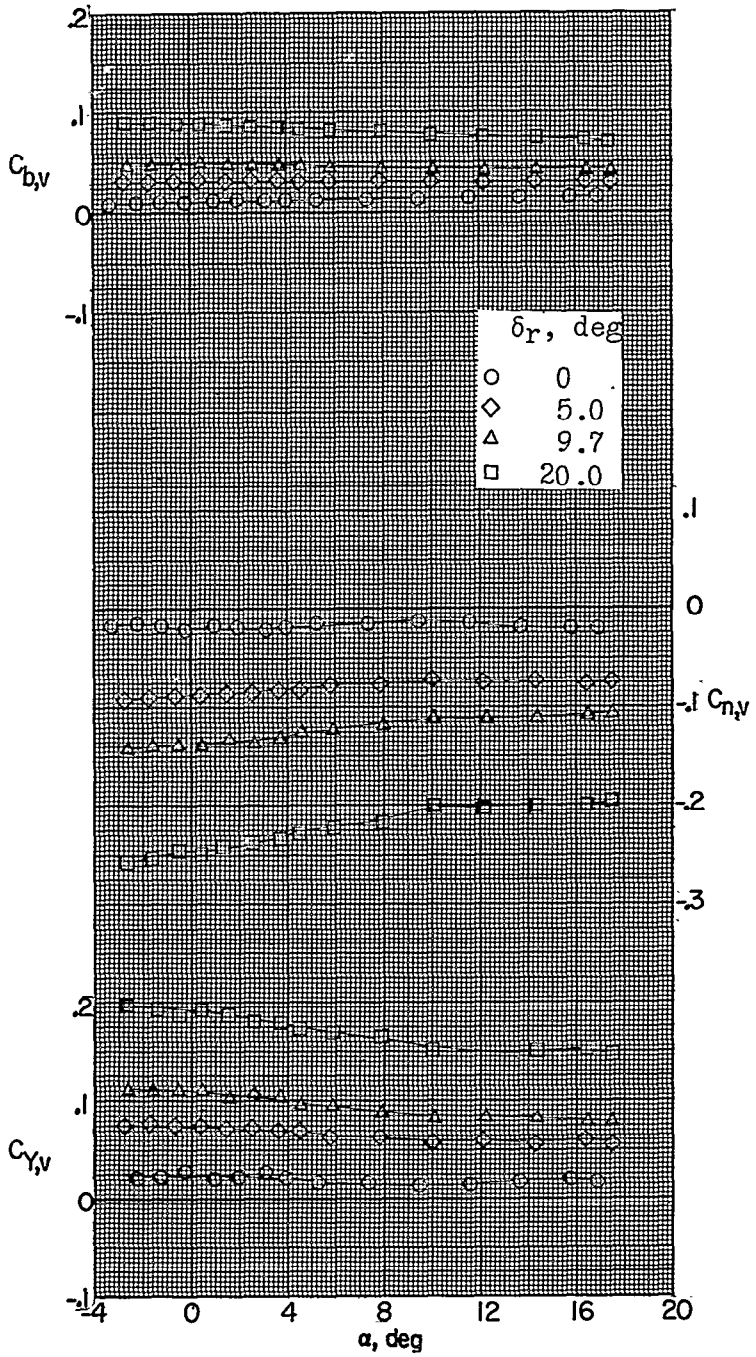

(a) M = 1.60.

Figure 23.- Effect of rudder deflection on aerodynamic characteristics of vertical-tail loads.

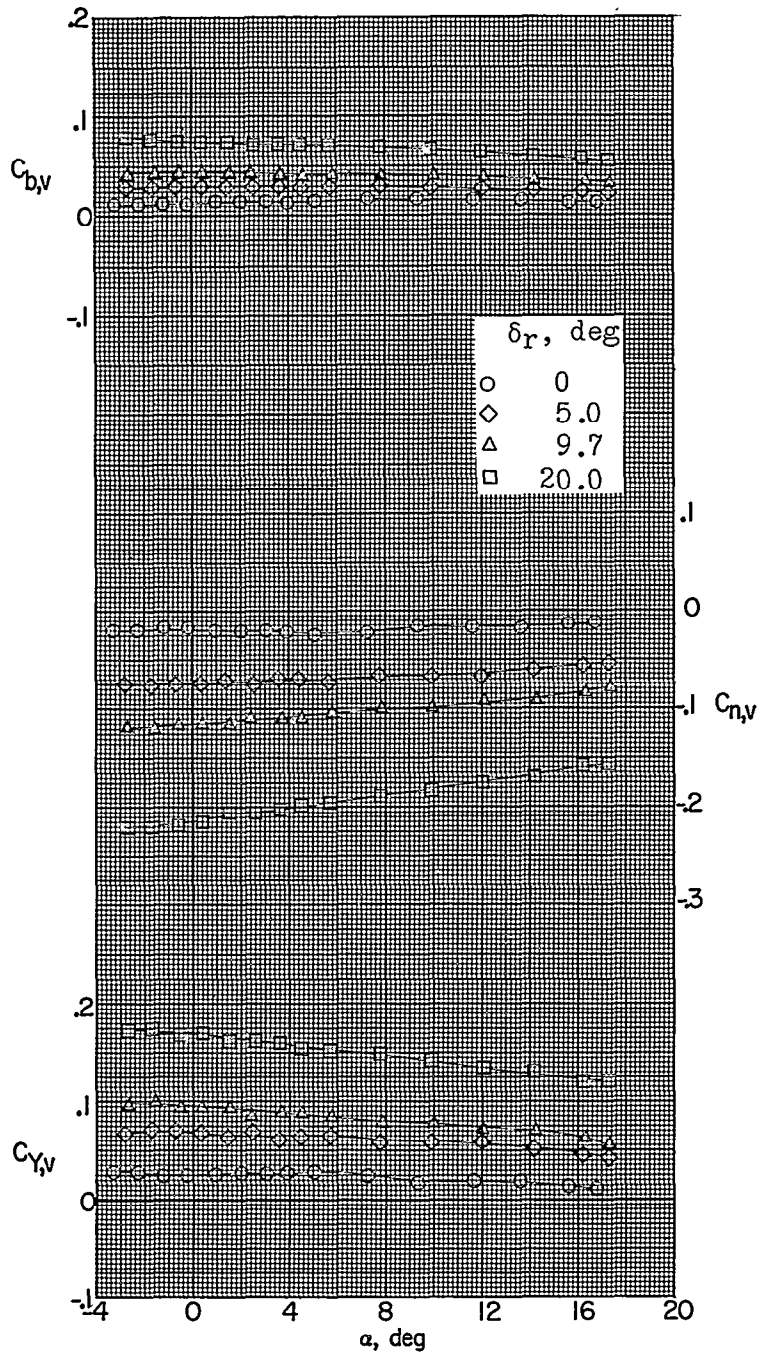

(b) M = 1.80.

Figure 23.- Continued.

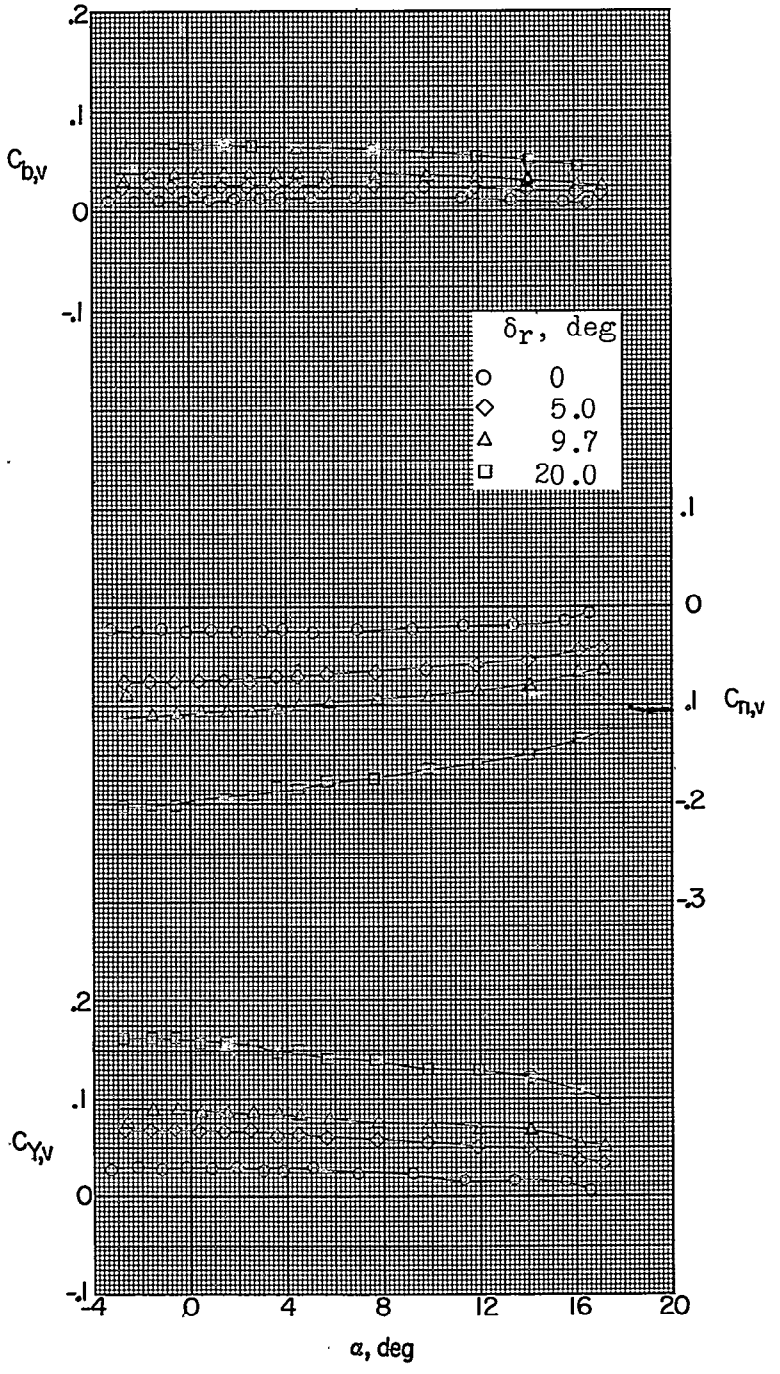

(c) M = 2.00.

Figure 23.- Concluded.

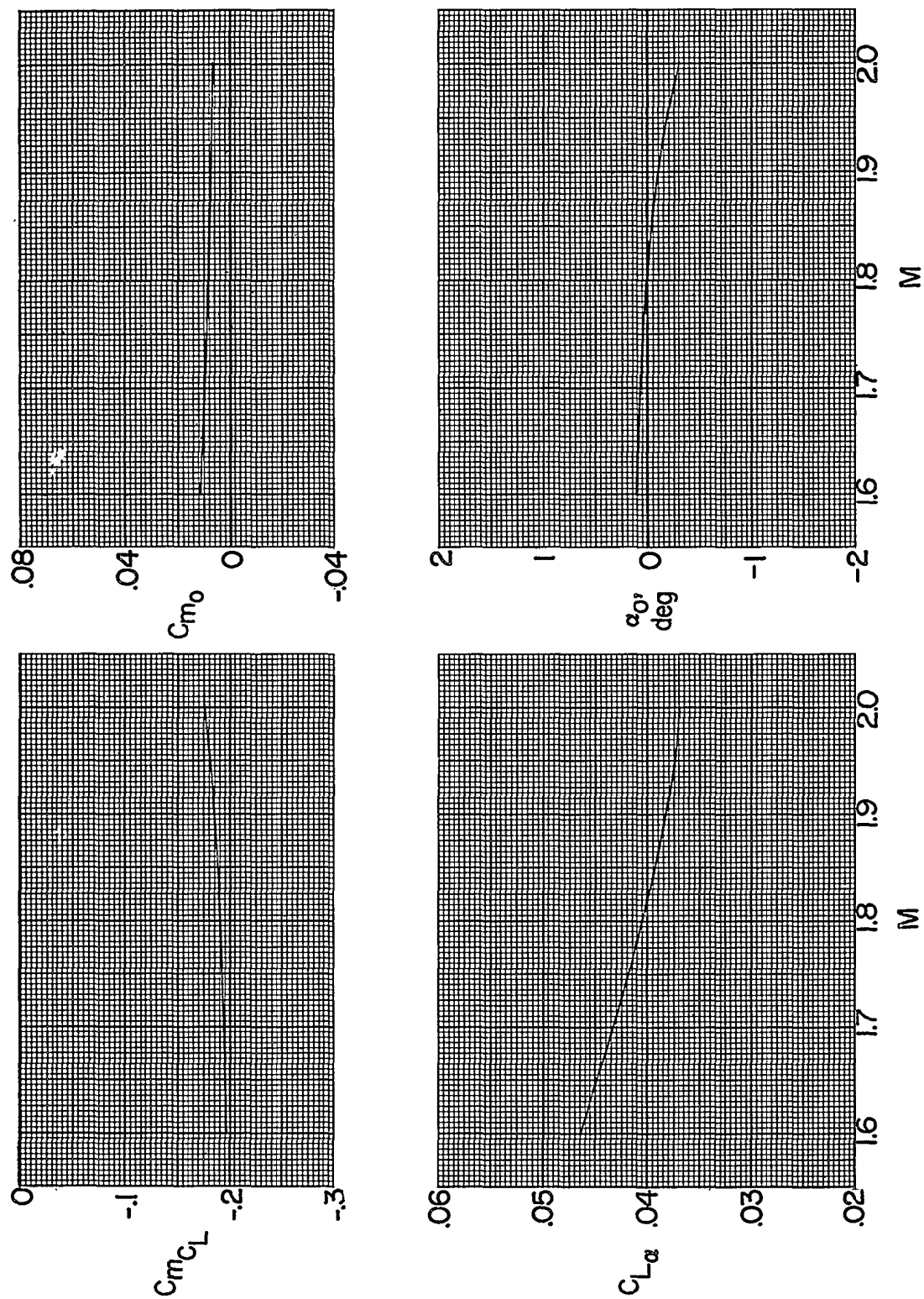

Figure 24.- Summary of longitudinal stability characteristics of test model.

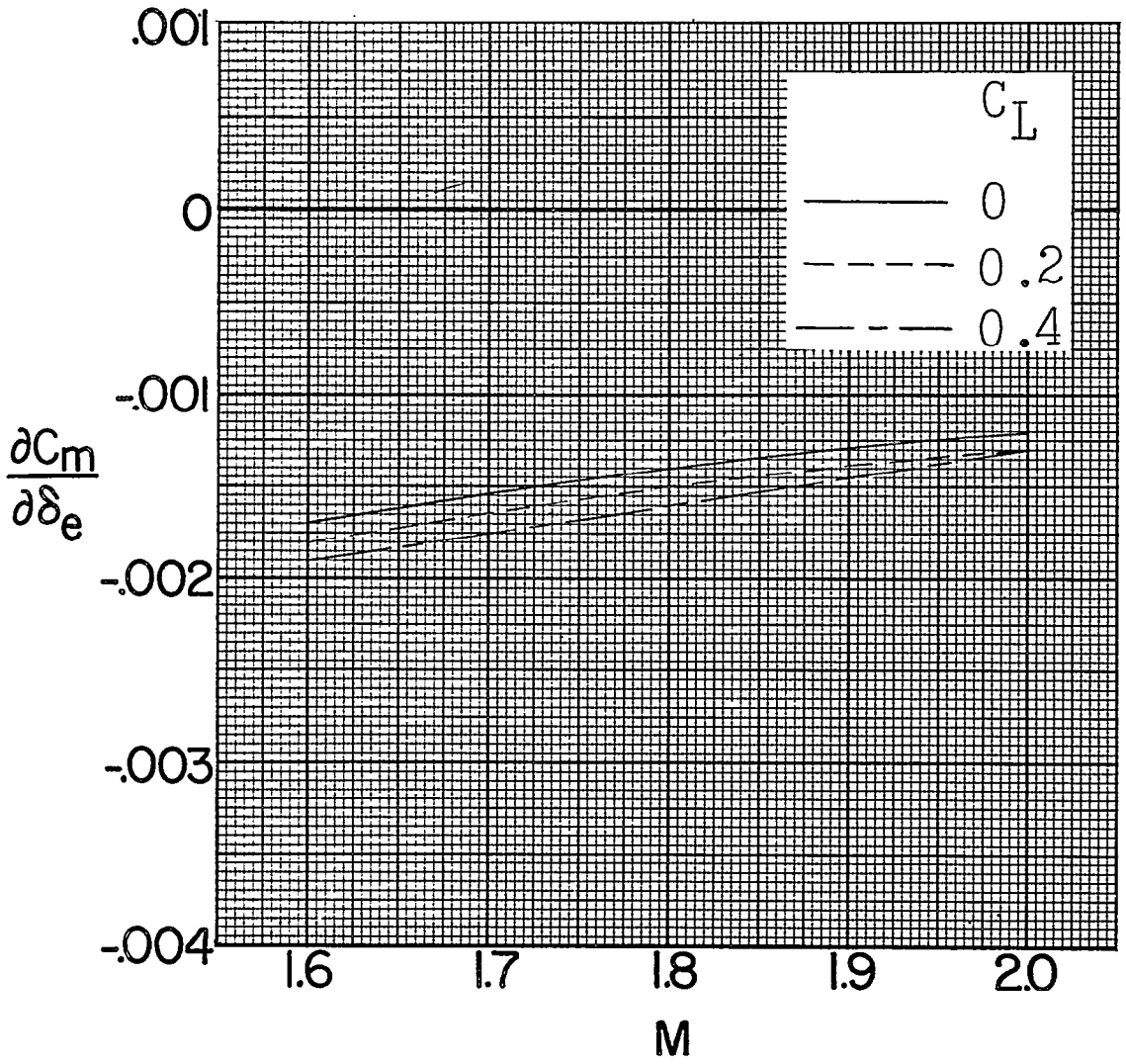

Figure 25.- Summary of longitudinal control effectiveness of test model.

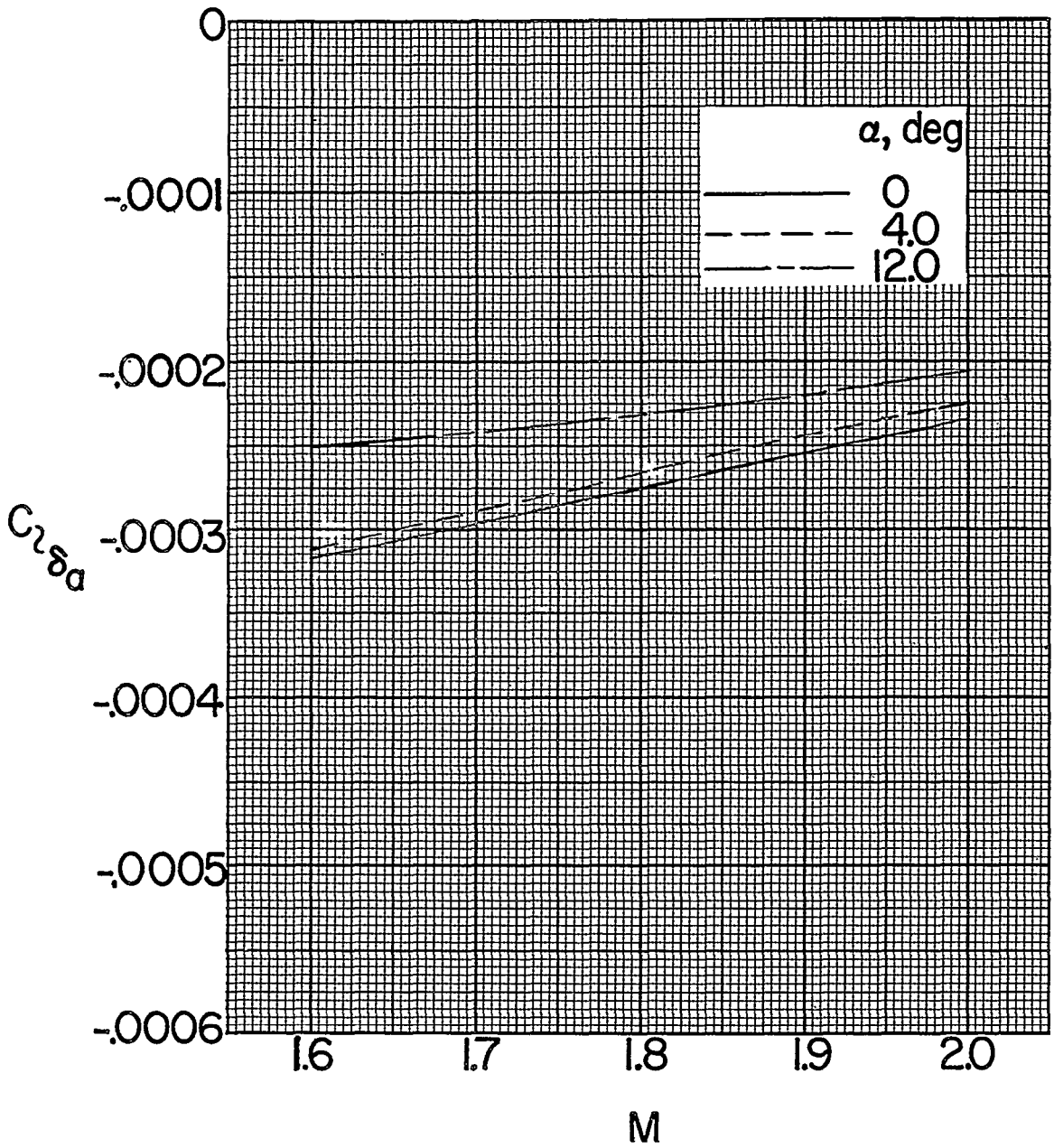

Figure 26.- Summary of aileron control effectiveness of test model.

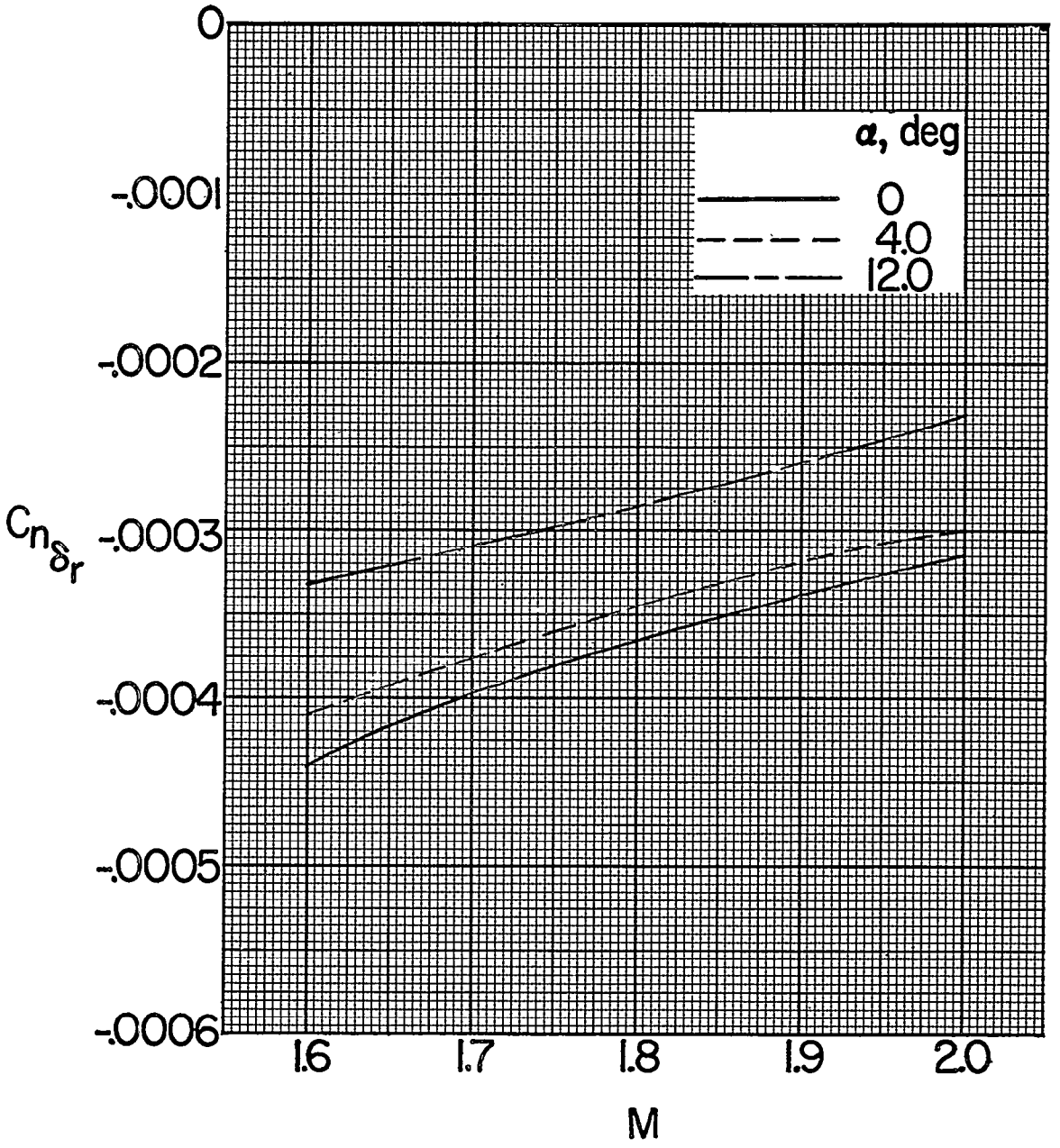

Figure 27.- Summary of rudder control effectiveness of test model.

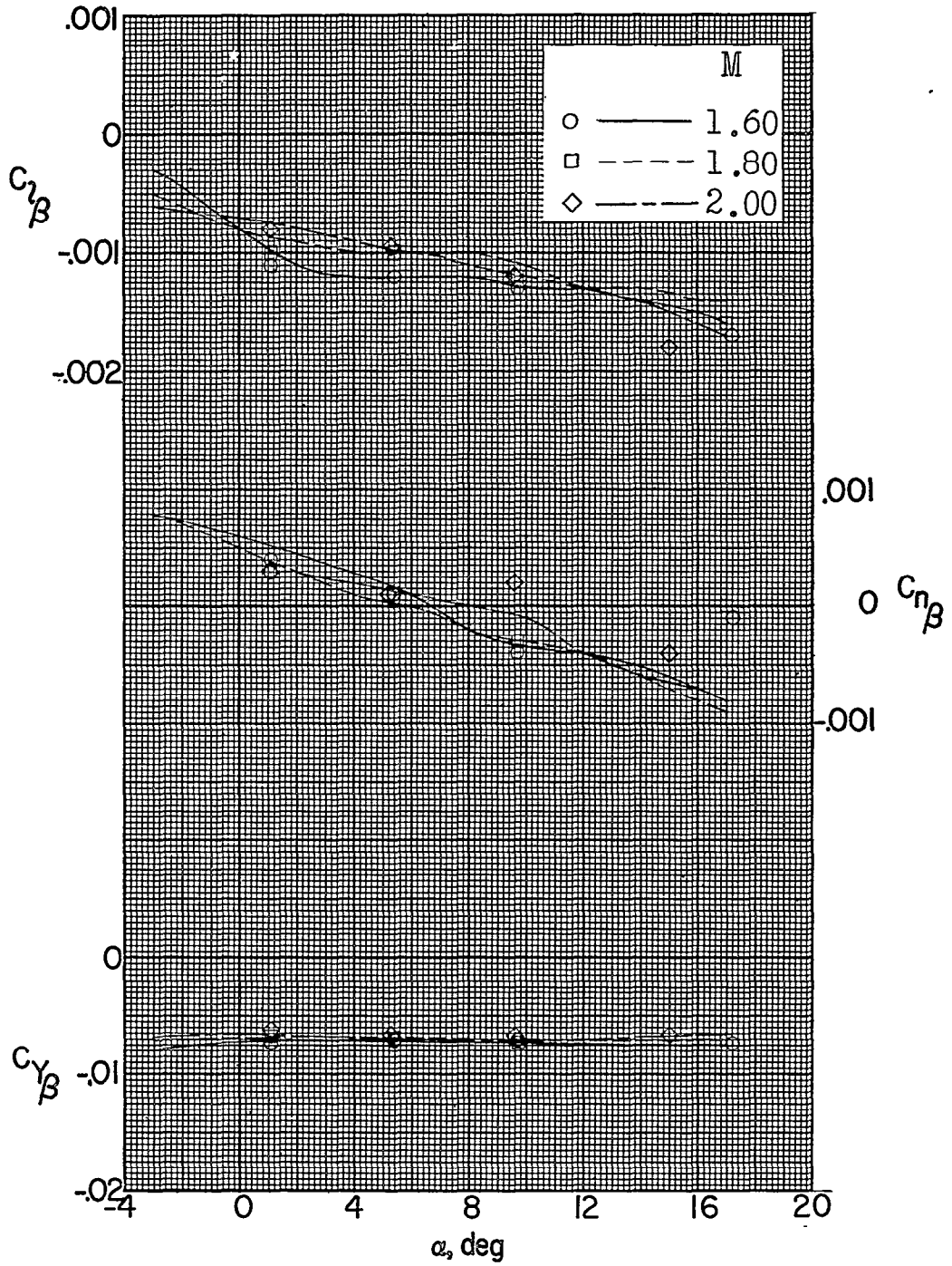

(a) Vertical-tail on.

Figure 28.- Summary of lateral stability parameters with variation of angle of attack of test model.

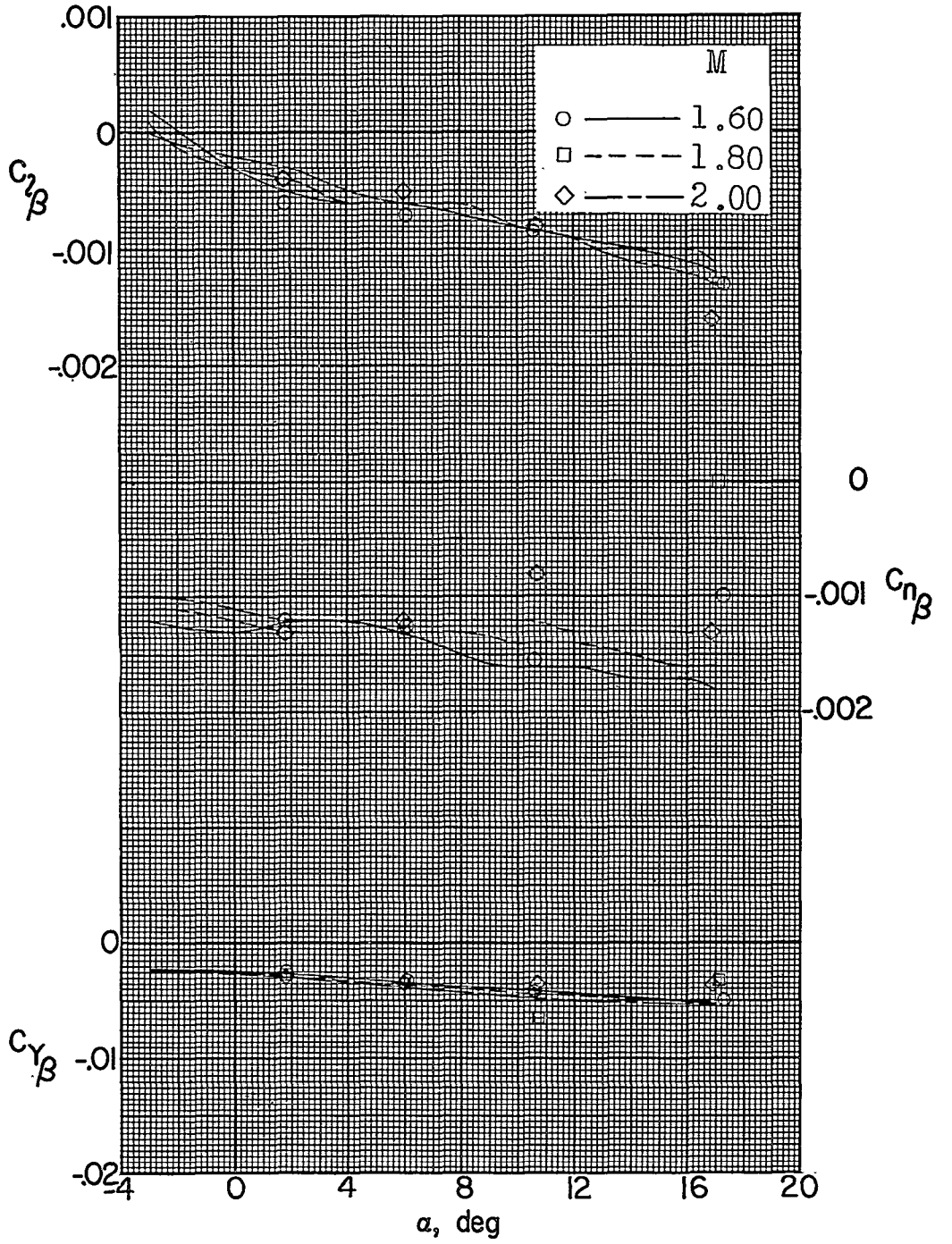

(b) Vertical tail off.

Figure 28.- Concluded.

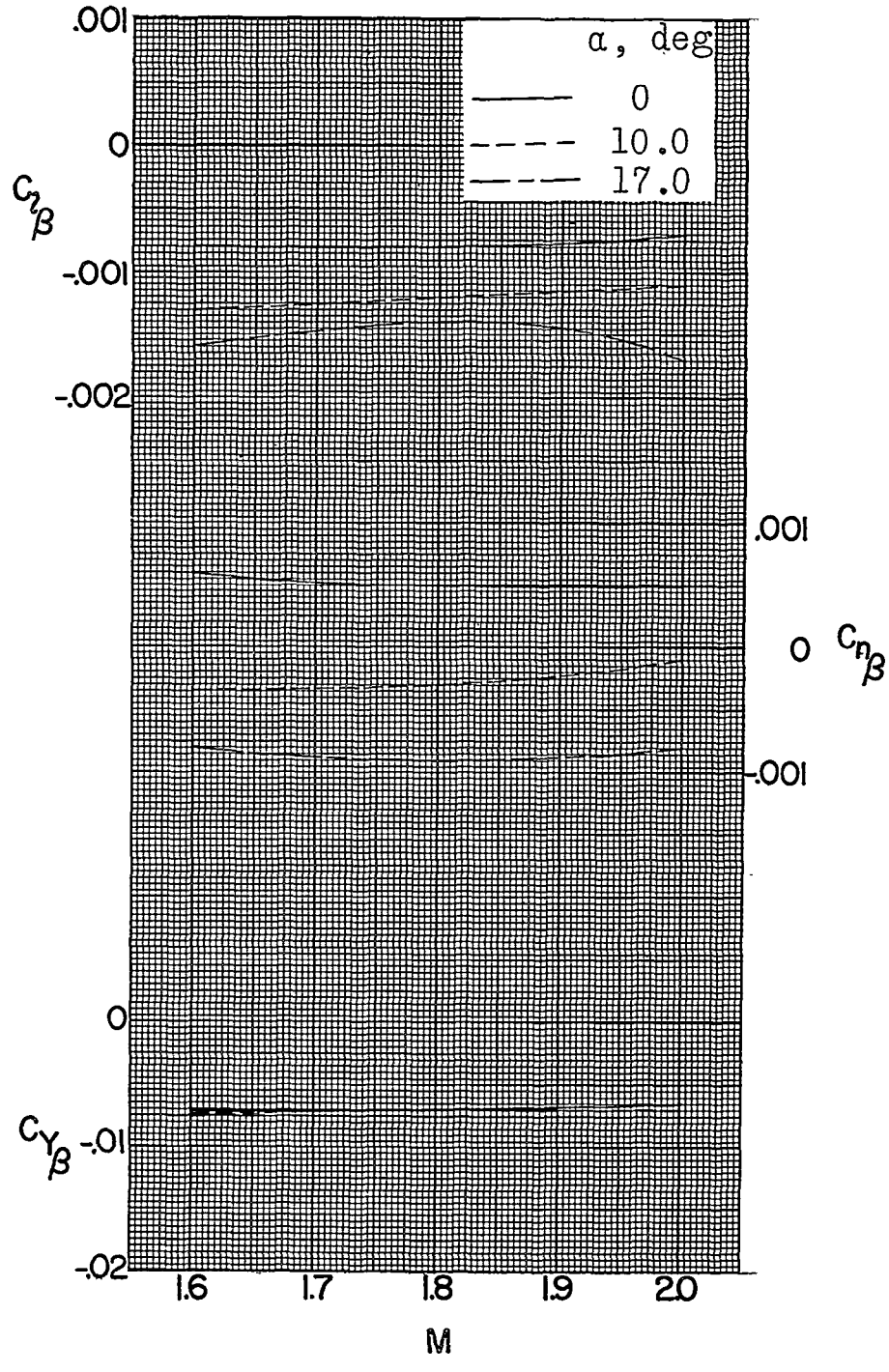

(a) Vertical tail on.

Figure 29.- Summary of lateral stability parameters with variation of Mach number of test model.

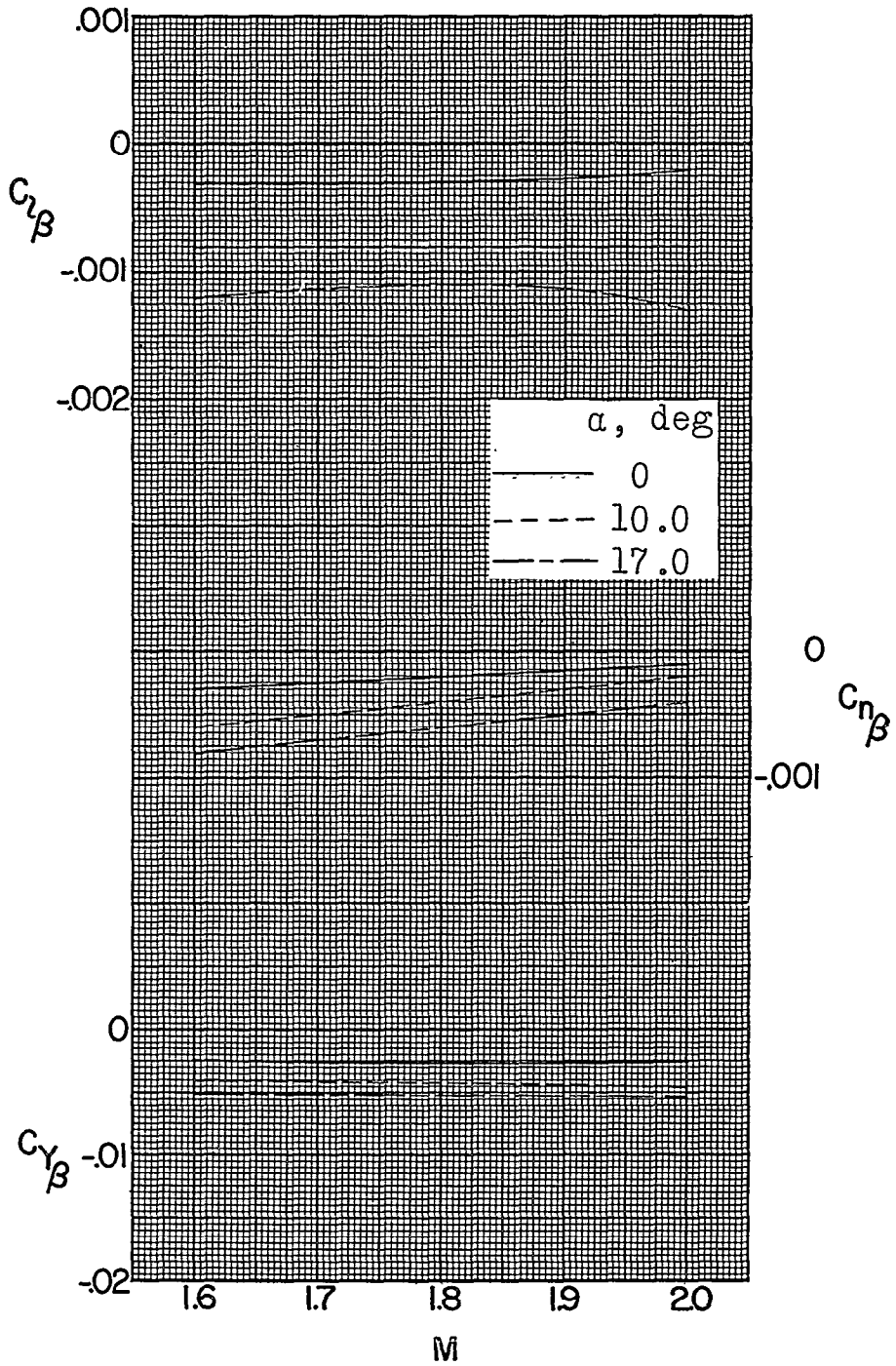

(b) Vertical tail off.

Figure 29.- Concluded.

LONGITUDINAL AND LATERAL STABILITY AND CONTROL CHARACTERISTICS AND VERTICAL-TAIL-LOAD MEASUREMENTS FOR A 0.03-SCALE MODEL OF THE AVRO CF-105 AIRPLANE AT MACH NUMBERS OF 1.60, 1.80, AND 2.00*

By H. Norman Silvers, Roger H. Fournier, and Jane S. Wills

ABSTRACT

The model had a 3.5-percent-thick modified delta wing with a leading-edge sweep of 61.4°, an aspect ratio of 2.04, and a taper ratio of 0.089. Results were obtained through an angle-of-attack range from approximately -4° to 18° and through an angle-of-sideslip range from approximately -4° to 18° at several angles of attack. In addition to six-component force and moment results on the complete model and vertical-tail loads, hinge moments were measured for the elevator, rudder, and aileron.

INDEX HEADINGS

Stability, Longitudinal - Static	1.8.1.1.1
Stability, Directional - Static	1.8.1.1.3
Control, Longitudinal	1.8.2.1
Control, Lateral	1.8.2.2
Control, Directional	1.8.2.3
Control, Hinge Moments	1.8.2.5
Loads, Steady - Tail	4.1.1.2.1

*Title, Confidential.

LONGITUDINAL AND LATERAL STABILITY AND CONTROL CHARACTERISTICS AND VERTICAL-TAIL-LOAD MEASUREMENTS FOR A 0.03-SCALE MODEL OF THE AVRO CF-105 AIRPLANE AT MACH NUMBERS OF 1.60, 1.80, AND 2.00

H. Norman Silvers

Roger H. Fournier

Jane S. Wills

Approved:

for Herbert A. Wilson, Jr.
Chief of Unitary Plan Wind Tunnel Division
Langley Aeronautical Laboratory

rh
(7/15/58)